

Major Project -II

EFFECT OF AREA RATIO AND CASING ANGLE ON THE PERFORMANCE OF AXIAL ANNULAR DIFFUSER

Submitted to **Delhi Technological University**
in partial fulfilment of the requirement for the award of the Degree of

Master of Technology

In

Thermal Engineering

By

ISHAN UDHAORAO MESHAM
(2K12/THR/11)

UNDER THE SUPERVISION OF

Dr. B. B. ARORA

Associate Professor

Mechanical Engineering Department



**Delhi Technological University,
Shahabad Daulatpur**

Bawana Road, Delhi-110042, INDIA

July, 2014

DECLARATION

I, hereby declare that the work embodied in the dissertation entitled “**EFFECT OF AREA RATIO AND CASING ANGLE ON THE PERFORMANCE OF AXIAL ANNULAR DIFFUSER**” in partial fulfilment for the award of degree of MASTER of TECHNOLOGY in “THERMAL ENGINEERING”, is an original piece of work carried out by me under the supervision of Dr. B. B. ARORA, Mechanical Engineering Department, Delhi Technological University. The matter of this work either full or in part have not been submitted to any other institution or University for the award of any other Diploma or Degree or any other purpose what so ever.

ISHAN UDHAORAO MESHARAM

M.Tech (Thermal Engineering)

Roll No.: 2K12/THR/11

CERTIFICATE

This is to certify that the work embodied in the dissertation entitled “**EFFECT OF AREA RATIO AND CASING ANGLE ON THE PERFORMANCE OF AXIAL ANNULAR DIFFUSER**” by **ISHAN UDHAORAO MESHARAM**, (Roll No.-**2K12/THR/11**) in partial fulfilment of requirements for the award of **Degree of Master of Technology in Thermal Engineering**, is an authentic record of student’s own work carried by him under my supervision.

This is also certified that this work has not been submitted to any other Institute or University for the award of any other diploma or degree.

Dr. B. B. ARORA

Associate Professor

Mechanical Engineering Department

Delhi Technological University

Delhi- 110042.

ACKNOWLEDGEMENT

It is a pleasure to acknowledge our gratitude to all the people involved, directly or indirectly in the completion of this project. I would like to thank our project guide **Dr. B. B. ARORA** who devoted valuable hours for this assignment and providing the motivational guidance during the entire preparation of this project, answering the number of technical queries despite his busy schedule. His valuable suggestions, constructive criticism and timely help proved extremely fruitful.

I am thankful to Sh. Deepak, and other project staff of computational fluid mechanics lab for all assistance during execution of this project work. I am also thankful to my fellow friends and colleagues at CFD lab who were always there to lend a helping hand in the hour of need.

ISHAN UDHAORAO MESHRAM

M.TECH (Thermal Engineering)

Roll No.-2K12/THR/11

ABSTRACT

A diffuser is a device for converting the kinetic energy of an incoming fluid into pressure. As the flow proceeds through the diffuser there is continuous retardation of the flow resulting in conversion of kinetic energy into pressure energy. Diffuser forms an important part in flow machinery and structures. The present study involves the CFD analysis of effect of area ratio and varying casing angle on axial annular diffuser performance using fluent and also the prediction of flow characteristics using various mathematical models. The axial annular diffuser considered in the present case has the hub angle keeping constant as 0° and casings are diverging with 6° and 8° angles. The geometries of the diffusers are calculated for different area ratio i.e. 2, 3, 4 and varying casing angle 6° , 8° . Swirl angle of 0° , 7.5° , 12° , 17° , 25° are introduced to predict the reversal of flow and separation of flow from the wall and to visualize the effect of area ratio, casing angle and inlet swirl. The variation in parameter i.e. longitudinal velocity, Swirl Velocity and Pressure Co-efficient along the various sections and flow patterns have been studying. In the present study RNG turbulence models are studied.

CONTENTS

		Page No.
Declaration		ii
Certificate		iii
Acknowledgments		iv
Abstract		v
Contents		vi-viii
List of Figures		ix-xiv
Nomenclature		xv-xvi
CHAPTER 1	INTRODUCTION	1-12
1.1	Axial diffuser	2
1.2	Radial diffuser	3
1.3	Curved wall diffuser	3
1.4	Annular diffuser	3
1.5	Principal for diffuser design	4
1.6	Diffuser Performance parameter	5-7
1.6.1	Geometric parameters	5
1.6.2	Aerodynamic blockage	6
1.6.3	Reynolds number:	6
1.6.4	Inlet Mach number	6
1.6.5	Inlet Turbulence intensity	6
1.6.6	Effect of Compressibility	7
1.6.7	Effect of Compressibility on Wall Design	7
1.7	Design Performance Parameters	8
1.7.1	Static Pressure Recovery Coefficient	8
1.7.2	Diffuser Effectiveness	8
1.7.3	Total Pressure Loss Coefficient	8
1.8	Swirling flows	10-11
1.8.1	Physics of Swirling and Rotating Flows	10
1.8.2	Method of swirl generation	11
1.9	Motivations	11

CHAPTER 2	LITRETURE REVIEW	13-25
2.1	Geometric Parameters	14-19
2.1.1	Effect of Geometric Parameters	16
2.1.2	Passage Divergence and Length	16
2.1.3	Wall Contouring	18
2.2	Effects of flow Parameters	19-24
2.2.1	Aerodynamic Blockage	19
2.2.2	Inlet Swirl	20
2.2.3	Inlet Turbulence	21
2.2.4	Mach number Influence	23
2.2.5	Reynolds Number Influence	23
2.3	Boundary Layer Parameter	24-25
2.3.1	Boundary Layer Suction	24
2.3.2	Blowing and Injection	25
CHAPTER 3	MATHEMATICAL MODELLING	26-36
3.1	Conservation Principals	26-28
3.1.1	Mass Conservation Equation (Continuity Equation)	27
3.1.2	Momentum Conservation Equations	27
3.2	Turbulence Modelling	28-30
3.2.1	Choosing a Turbulence Model	29
3.3	The STANDARD, RNG, and REALIZABLE k- ϵ	30-36
3.3.1	The Standard k- ϵ Model	30
3.3.2	Transport Equations for the Standard k- ϵ Model	31
3.3.3	Modelling the Turbulent Viscosity	31
3.3.4	The model constants	31
3.3.5	The RNG k- ϵ Model	32
3.3.6	Transport Equations for the RNG k- ϵ Model	32
3.3.7	Modelling the Effective Viscosity	33
3.3.8	The Realizable k- ϵ Model	34
3.3.9	Transport Equations for the Realizable k- ϵ Model	34
3.3.10	Modelling the Turbulent Viscosity	35
3.3.11	Model Constants	36
3.4	Turbulence Modelling in swirling flows	36

CHAPTER 4	CFD ANALYSIS	37-43
4.1	Program Capabilities	37
4.2	Planning CFD Analysis	38-39
4.2.1	Definition of the Modelling Goals	38
4.2.2	Grid Generation and its Independence	39
4.2.3	Choice of the Computational Model	39
4.2.4	Choice of Physical Models	39
4.2.5	Determination of the Solution Procedure	39
4.3	Discretization	39
4.4	Convergence criteria	41
4.5	Implementation of boundary conditions	41-42
4.5.1	Inlet boundary condition	41
4.5.2	Outlet boundary condition	42
4.5.3	Wall boundary condition	42
4.6	Simulation Procedure	42
CHAPTER 5	VALIDATION	44-48
5.1	Grid Independence	44
5.1.1	Validation with Experimental results	44
5.2	Turbulence model validation	44
5.2.1	Validation with Experimental results	45
CHAPTER 6	RESULT AND DISCUSSION	49-54
Case 1	Hub parallel and casing diverging at angle 6°	49
Case 2	Hub parallel and casing diverging at angle 8°	51
CHAPTER 7	RECOMMENDATIONS FOR FUTURE WORK	55
REFERENCES		56-61
FIGURES		62-96
APPENDIX		100

List of figures

Figure 5.1: Longitudinal Velocity (0°) Exp10/10, AR 2	46
Figure 5.2: Longitudinal Velocity (0°), Exp10/10, AR 2	47
Figure 5.3: Longitudinal Velocity (12°), Exp10/10, AR 2	47
Figure 5.4: Swirl Velocity (12°), Exp10/10, AR 2	48

List of Color Maps of Pressure and Velocity

Fig. 1 AR2, Casing Wall Angle= 6° , Swirl Angle= 0° , Velocity=60 m/s	62
Fig. 2 AR2, Casing Wall Angle= 6° , Swirl Angle= 7.5° , Velocity=60 m/s	62
Fig. 3 AR2, Casing Wall Angle= 6° , Swirl Angle= 12° , Velocity=60 m/s	62
Fig. 4 AR2, Casing Wall Angle= 6° , Swirl Angle= 17° , Velocity=60 m/s	62
Fig. 5 AR2, Casing Wall Angle= 6° , Swirl Angle= 25° , Velocity=60 m/s	63
Fig. 6 AR3, Casing Wall Angle= 6° , Swirl Angle= 0° , Velocity=60 m/s	63
Fig. 7 AR3, Casing Wall Angle= 6° , Swirl Angle= 7.5° , Velocity=60 m/s	63
Fig. 8 AR3, Casing Wall Angle= 6° , Swirl Angle= 12° , Velocity=60 m/s	63
Fig. 9 AR3, Casing Wall Angle= 6° , Swirl Angle= 17° , Velocity=60 m/s	64
Fig. 10 AR3, Casing Wall Angle= 6° , Swirl Angle= 25° , Velocity=60 m/s	64
Fig. 11 AR4, Casing Wall Angle= 6° , Swirl Angle= 0° , Velocity=60 m/s	64
Fig. 12 AR4, Casing Wall Angle= 6° , Swirl Angle= 7.5° , Velocity=60 m/s	64
Fig. 13 AR4, Casing Wall Angle= 6° , Swirl Angle= 12° , Velocity=60 m/s	65
Fig. 14 AR4, Casing Wall Angle= 6° , Swirl Angle= 17° , Velocity=60 m/s	65
Fig. 15 AR4, Casing Wall Angle= 6° , Swirl Angle= 25° , Velocity=60 m/s	65

Fig. 16 AR2, Casing Wall Angle=8°, Swirl Angle=0°, Velocity=60 m/s	65
Fig. 17 AR2, Casing Wall Angle=8°, Swirl Angle=7.5°, Velocity=60 m/s	66
Fig. 18 AR2, Casing Wall Angle=8°, Swirl Angle=12°, Velocity=60 m/s	66
Fig. 19 AR2, Casing Wall Angle=8°, Swirl Angle=17°, Velocity=60 m/s	66
Fig. 20 AR2, Casing Wall Angle=8°, Swirl Angle=25°, Velocity=60 m/s	66
Fig. 21 AR3, Casing Wall Angle=8°, Swirl Angle=0°, Velocity=60 m/s	67
Fig. 22 AR3, Casing Wall Angle=8°, Swirl Angle=7.5°, Velocity=60 m/s	67
Fig. 23 AR3, Casing Wall Angle=8°, Swirl Angle=12°, Velocity=60 m/s	67
Fig. 24 AR3, Casing Wall Angle=8°, Swirl Angle=17°, Velocity=60 m/s	67
Fig. 25 AR3, Casing Wall Angle=8°, Swirl Angle=25°, Velocity=60 m/s	68
Fig. 26 AR4, Casing Wall Angle=8°, Swirl Angle=0°, Velocity=60 m/s	68
Fig. 27 AR4, Casing Wall Angle=8°, Swirl Angle=7.5°, Velocity=60 m/s	68
Fig. 28 AR4, Casing Wall Angle=8°, Swirl Angle=12°, Velocity=60 m/s	68
Fig. 29 AR4, Casing Wall Angle=8°, Swirl Angle=17°, Velocity=60 m/s	69
Fig. 30 AR4, Casing Wall Angle=8°, Swirl Angle=25°, Velocity=60 m/s	69

List of pressure coefficient graphs

Fig. 31 AR=2, Pressure coefficient, Casing wall angle=6°, Velocity=60m/s (0°)	70
Fig. 32 AR=2, Pressure coefficient, Casing wall angle=6°, Velocity=60m/s (7.5°)	70
Fig. 33 AR=2, Pressure coefficient, Casing wall angle=6°, Velocity=60m/s (12°)	70
Fig. 34 AR=2, Pressure coefficient, Casing wall angle=6°, Velocity=60m/s (17°)	71
Fig. 35 AR=2, Pressure coefficient, Casing wall angle=6°, Velocity=60m/s (25°)	71

Fig. 36 AR=3, Pressure coefficient, Casing wall angle=6°, Velocity=60m/s (0°)	71
Fig. 37 AR=3, Pressure coefficient, Casing wall angle=6°, Velocity=60m/s (7.5°)	72
Fig. 38 AR=3, Pressure coefficient, Casing wall angle=6°, Velocity=60m/s (12°)	72
Fig. 39 AR=3, Pressure coefficient, Casing wall angle=6°, Velocity=60m/s (17°)	72
Fig. 40 AR=3, Pressure coefficient, Casing wall angle=6°, Velocity=60m/s (25°)	73
Fig. 41 AR=4, Pressure coefficient, Casing wall angle=6°, Velocity=60m/s (0°)	73
Fig. 42 AR=4, Pressure coefficient, Casing wall angle=6°, Velocity=60m/s (7.5°)	73
Fig. 43 AR=4, Pressure coefficient, Casing wall angle=6°, Velocity=60m/s (12°)	74
Fig. 44 AR=4, Pressure coefficient, Casing wall angle=6°, Velocity=60m/s (17°)	74
Fig. 45 AR=4, Pressure coefficient, Casing wall angle=6°, Velocity=60m/s (25°)	74
Fig. 46 AR=2, Pressure coefficient, Casing wall angle=8°, Velocity=60m/s (0°)	75
Fig. 47 AR=2, Pressure coefficient, Casing wall angle=8°, Velocity=60m/s (7.5°)	75
Fig. 48 AR=2, Pressure coefficient, Casing wall angle=8°, Velocity=60m/s (12°)	75
Fig. 49 AR=2, Pressure coefficient, Casing wall angle=8°, Velocity=60m/s (17°)	76
Fig. 50 AR=2, Pressure coefficient, Casing wall angle=8°, Velocity=60m/s (25°)	76
Fig. 51 AR=3, Pressure coefficient, Casing wall angle=8°, Velocity=60m/s (0°)	76
Fig. 52 AR=3, Pressure coefficient, Casing wall angle=8°, Velocity=60m/s (7.5°)	77
Fig. 53 AR=3, Pressure coefficient, Casing wall angle=8°, Velocity=60m/s (12°)	77
Fig. 54 AR=3, Pressure coefficient, Casing wall angle=8°, Velocity=60m/s (17°)	77
Fig. 55 AR=3, Pressure coefficient, Casing wall angle=8°, Velocity=60m/s (25°)	78
Fig. 56 AR=4, Pressure coefficient, Casing wall angle=8°, Velocity=60m/s (0°)	78
Fig. 57 AR=4, Pressure coefficient, Casing wall angle=8°, Velocity=60m/s (7.5°)	78

Fig. 58 AR=4, Pressure coefficient, Casing wall angle=8°, Velocity=60m/s (12°)	79
Fig. 59 AR=4, Pressure coefficient, Casing wall angle=8°, Velocity=60m/s (17°)	79
Fig. 60 AR=4, Pressure coefficient, Casing wall angle=8°, Velocity=60m/s (25°)	79

List of longitudinal and swirl velocity graphs

Fig.61 AR=2, Casing wall angle=6°, Velocity=60m/s (0°L)	80
Fig.62 AR=2, Casing wall angle=6°, Velocity=60m/s (7.5°L)	80
Fig.63 AR=2, Casing wall angle=6°, Velocity=60m/s (7.5°S)	80
Fig.64 AR=2, Casing wall angle=6°, Velocity=60m/s (12°L)	81
Fig.65 AR=2, Casing wall angle=6°, Velocity=60m/s (12°S)	81
Fig.66 AR=2, Casing wall angle=6°, Velocity=60m/s (17°L)	81
Fig.67 AR=2, Casing wall angle=6°, Velocity=60m/s (17°S)	82
Fig.68 AR=2, Casing wall angle=6°, Velocity=60m/s (25°L)	82
Fig.69 AR=2, Casing wall angle=6°, Velocity=60m/s (25°S)	82
Fig.70 AR=3, Casing wall angle=6°, Velocity=60m/s (0°L)	83
Fig.71 AR=3, Casing wall angle=6°, Velocity=60m/s (7.5°S)	83
Fig.72 AR=2, Casing wall angle=6°, Velocity=60m/s (12°L)	83
Fig.73 AR=3, Casing wall angle=6°, Velocity=60m/s (12°S)	84
Fig.74 AR=3, Casing wall angle=6°, Velocity=60m/s (17°L)	84
Fig.75 AR=3, Casing wall angle=6°, Velocity=60m/s (17°S)	84
Fig.76 AR=3, Casing wall angle=6°, Velocity=60m/s (25°S)	85
Fig.77 AR=4, Casing wall angle=6°, Velocity=60m/s (0°L)	85
Fig.78 AR=4, Casing wall angle=6°, Velocity=60m/s (7.5°L)	85

Fig.79 AR=4, Casing wall angle=6°, Velocity=60m/s (7.5°S)	86
Fig.80 AR=4, Casing wall angle=6°, Velocity=60m/s (12°L)	86
Fig.81 AR=4, Casing wall angle=6°, Velocity=60m/s (17°L)	86
Fig.82 AR=4, Casing wall angle=6°, Velocity=60m/s (17°S)	87
Fig.83 AR=4, Casing wall angle=6°, Velocity=60m/s (25°L)	87
Fig.84 AR=4, Casing wall angle=6°, Velocity=60m/s (25°S)	87
Fig.85 AR=2, Casing wall angle=8°, Velocity=60m/s (0°L)	88
Fig.86 AR=2, Casing wall angle=8°, Velocity=60m/s (7.5°L)	88
Fig.87 AR=2, Casing wall angle=8°, Velocity=60m/s (7.5°S)	88
Fig.88 AR=2, Casing wall angle=8°, Velocity=60m/s (12°L)	89
Fig.89 AR=2, Casing wall angle=8°, Velocity=60m/s (12°S)	89
Fig.90 AR=2, Casing wall angle=8°, Velocity=60m/s (17°L)	89
Fig.91 AR=2, Casing wall angle=8°, Velocity=60m/s (17°S)	90
Fig.92 AR=2, Casing wall angle=8°, Velocity=60m/s (25°S)	90
Fig.93 AR=3, Casing wall angle=8°, Velocity=60m/s (0°L)	90
Fig.94 AR=3, Casing wall angle=8°, Velocity=60m/s (7.5°L)	91
Fig.95 AR=3, Casing wall angle=8°, Velocity=60m/s (7.5°S)	91
Fig.96 AR=3, Casing wall angle=8°, Velocity=60m/s (12°L)	91
Fig.97 AR=3, Casing wall angle=8°, Velocity=60m/s (12°S)	92
Fig.98 AR=3, Casing wall angle=8°, Velocity=60m/s (17°L)	92
Fig.99 AR=3, Casing wall angle=8°, Velocity=60m/s (17°S)	92
Fig.100 AR=3, Casing wall angle=8°, Velocity=60m/s (25°L)	93

Fig.101 AR=3, Casing wall angle=8°, Velocity=60m/s (25°S)	93
Fig.102 AR=4, Casing wall angle=8°, Velocity=60m/s (0°L)	93
Fig.103 AR=4, Casing wall angle=8°, Velocity=60m/s (7.5°L)	94
Fig.104 AR=4, Casing wall angle=8°, Velocity=60m/s (7.5°S)	94
Fig.105 AR=4, Casing wall angle=8°, Velocity=60m/s (12°L)	94
Fig.106 AR=4, Casing wall angle=8°, Velocity=60m/s (12°S)	95
Fig.107 AR=4, Casing wall angle=8°, Velocity=60m/s (17°L)	95
Fig.108 AR=4, Casing wall angle=8°, Velocity=60m/s (17°S)	95
Fig.109 AR=4, Casing wall angle=8°, Velocity=60m/s (25°L)	96
Fig.110 AR=4, Casing wall angle=8°, Velocity=60m/s (25°S)	96

NOMENCLATURE

A	Area
AR	Area ratio
B	blockage factor
C	Constants
C_P	Pressure recovery co-efficient
C_{PI}	Ideal pressure recovery co-efficient
D	Diameter
G	generation of turbulence kinetic energy
g	acceleration due to gravity
K	Total pressure loss co-efficient
k	Turbulent kinetic energy
P	Static pressure
P_t	Total pressure
Re	Reynolds number
S	Swirl Number of flow
S_m	Mass added
U	Velocity
w	Swirl velocity
x, y, z	Cartesian coordinate system

Y_M fluctuating dilatation in compressible turbulence.

Symbols

$\bar{\bar{\tau}}$	Stress tensor
μ	laminar viscosity
μ_t	turbulent viscosity
2θ	Equivalent cone angle
Γ	Circulation
ε	Turbulent kinetic energy dissipation rate
η	Diffuser effectiveness
θ	Wall angle
ν	Kinematics viscosity
ξ	Total pressure loss co-efficient
ρ	Density
Σ	Turbulent Prandtl no.

CHAPTER 1

INTRODUCTION

Diffusers are one of the standard challenges in fluid mechanics. The task of a diffuser is to decelerate the flow and to regain total pressure. It is more difficult to arrange for an efficient deceleration of flow than it is to obtain an efficient acceleration. There is a natural tendency in a diffusing process for the flow to break away from the walls of the diverging passage, reverse its direction, and flow back in direction of the pressure gradient. If the divergence is too rapid, this may result in the formation of eddies with consequent transfer of some kinetic energy into internal energy and a reduction in useful pressure rise. A small angle of divergence, however, implies a long diffuser and a high value of skin friction loss. Usually, flow separation in a diffuser is sought to be avoided due to the invoked additional pressure loss. Other than in many strongly separated flows, such as the flow over a backward facing step, the point of flow separation, in diffuser, is not defined by the geometry but entirely by the pressure gradient. Hence, diffuser flows are very sensitive and are difficult to predict with numerical means. Diffusers have been studied extensively in the past, since this is a very common flow configuration. Apart from the characterization of diffusers, these flows are used to study fundamental physics of pressure-driven flow separations.

Diffusers are extensively used in centrifugal compressors, axial flow compressors, ram jets, combustion chambers, inlet portions of jet engines etc. The energy transfer in these turbo machineries involves the exchange of significant levels of kinetic energy in order to accomplish the intended purpose. As a consequence, very large levels of residual kinetic energy frequently accompany the work input and work extraction processes, sometime as much as 50% of the total energy transferred. A small change in pressure recovery can increase the efficiency significantly. Therefore diffusers are absolutely

essential for good turbo machinery performance. The flow in the diffuser is governed by the behaviour of the boundary layers at the diffuser walls. The deceleration of the flow through the diffuser produces a pressure rise in the stream wise direction. The wall shear layers are therefore subjected to a positive or adverse pressure gradient. As is well known, adverse pressure gradients cause the boundary layer thicken and possibly separate from the diffuser walls, forming areas of back flow in diffusers. The net result of thickening of the wall boundary layers or the formation of region of back-flow is the blockage of the flow area which reduces the effective area available to the flow. Reduction the effective flow area in turn results in a reduced pressure rise through the diffuser. The interaction of wall shear layers and or separated zone with the core flow in diffusers is very complicated; therefore diffuser design and performance estimation is largely based on experimental data and empiricism.

1.1 AXIAL DIFFUSER

In axial diffusers, fluid flows along the axis of diffusers and there is continuous retardation of the flow. Analysis of the velocity field of the turbulent flow in an axially rotating diffuser is based on several studies of fluid flowing through a stationary diffuser and on investigations of the swirl flow, which develops in axially rotating straight pipes.

Axial diffuser is divided in to the following categories-

- Conical diffuser
- Channel diffuser
- Annular diffuser

The main problem of stationary diffusers consists in their divergence angle. Large diffuser divergence angles ($>12^\circ$) cause separation of the boundary layer, which in turn deteriorates

the diffuser efficiency. On the other hand diffusers with small divergence angles have to be very long to provide enough pressure rises at considerably high friction losses.

1.2 RADIAL DIFFUSER

In radial diffusers fluid flows in radially outward direction in confined space between the two boundaries. Diffuser used in radial turbo machinery fall under this category. They may be vane less and vanned types. Unlike the axial diffuser, this type of diffuser may convert kinetic energy into static pressure rise by one or two principles an increases in flow passage area in order to bring about a reduction in the average velocity; a change in the mean flow path radius to bring about a recovery in angular velocity according to the conservation of angular momentum.

1.3 CURVED WALL DIFFUSER

In recent time most of the aircrafts use curved wall diffuser. In aircraft engines several modifications may introduce non-uniformities and higher level of turbulence in flow field entering the diffuser. In addition mechanical and structural requirement place limits on the length of the passage. Curved wall diffuser is useful in this case and compatible with downstream requirement of flow besides it, these diffuser are also of fundamental and practical interest for various other applications like gas turbine system.

1.4 ANNULAR DIFFUSER

Annular diffusers are used in axial-flow compressors and turbines to convert the kinetic energy of the exhaust flow into pressure. This makes the diffuser a critical element in the performance of the turbine, which is often neglected.

The essential variables to define the geometry of annular diffuser are two wall angles, area ratio, non-dimensional length and inlet radius ratio. As the number of variables

increases, geometry becomes more complex. This has not been economically possible by experiments and hence led to the development of computational fluid dynamic methods to analyse the performance characteristics of annular diffuser *Arora et. al.* [2005].

1.5 PRINCIPLE FOR DIFFUSER DESIGN

Since flow in diffusers are subjected to an adverse pressure gradient there is potential danger for flow separation to occur which leads to loss in performance and damage of downstream equipment. The aim of design is to keep the adverse pressure gradient as high as possible, but below a critical limit, by controlling the length versus area-ratio of the diffuser.

The design requirements for a good diffuser are as following:-

Convey the flow efficiently by transferring a portion of the kinetic energy into a static pressure rise.

1. It must accept a variety of inlet conditions including extreme swirl, blockage and Mach number.
2. Deliver the fluid with reasonable velocity and angle profiles without separated regions.
3. Wall curvature must not have a deleterious effect upon passage performance.
4. Pressure recovery achieved over a short axial length.

While obtaining the best possible design, some limitations are imposed on a diffuser.

1. Limited length
2. Specified area ratio
3. Specified cross- sectional shape
4. Maximum static pressure recovery
5. Minimum stagnation pressure loss

1.6 DIFFUSER PERFORMANCE PARAMETER

1.6.1 Geometric parameters

Any diffuser geometry with increasing area in the stream wise direction constitutes subsonic diffuser geometry. Therefore, the number of different diffusers geometries that can be conceived is infinite. However in practice adequate design data are available for limited numbers of geometries. These are:

1. Rectangular cross section plan diffusers
2. Conical diffuser
3. Annular diffuser

These geometric parameters can be consolidated to few non dimensional parameters that are found to be important in terms of diffuser performance.

- The first is area ratio (AR). The area ratio is measure of theoretical diffusion of pressure recovery expected.
- The second important parameter is the ratio of the length of the diffuser to the inlet throat half-width (l/d), may be used as the key parameters for the design of the diffuser.
- The third geometric parameter commonly used in displaying diffuser performance is the wall divergence angle $2D$ for planar and conical diffusers.

Area ratio and non-dimensional length tells the overall diffusion and pressure gradient respectively, which is the main factor in boundary layer development. *Markland et. al.* [1986] found that a variation in the AR from 2.5 to 8.0 has a small effect on the loss coefficients of the 2-D diffuser. *Sharan* [1972] reported that for a constant AR the performance of diffuser deteriorates with the increase in diffusion angle. *Reneau et. al.* [1974] concluded that for two dimensional straight diffusers the maximum pressure recovery at a constant area ratio occurs in the range of diffuser angle equal to 6-8deg.

1.6.2 Aerodynamic blockage

Thin inlet boundary layers tends to be beneficial to high diffuser recovery and those longer diffusers necessary to achieve high levels of recovery as the inlet boundary thickness increases as stated by *Hoadley D et.al.* [1969, 1970]. The blockage is the fraction or percentage of the inlet passage area which is occluded the boundary layer displacement thickness on all walls. The displacement thickness is taken as equal on all surfaces and then the following relationships ensue:

$B = 2\delta/h$ for annular diffusers where h is annular height at inlet.

$B = 2\delta/D_1$ for conical diffusers with uniform inlet boundary layers.

1.6.3 Reynolds number

Viscosity is an important parameter in any fluid dynamic process and normally appears in the form of a Reynolds number. Diffusers are characterizes by Reynolds number based on an inlet hydraulic diameter. *Shaanan et. al.* [1975] studies reported in this field suggest that the Reynolds number is a comparatively weak parameter as long as the flow is fully turbulent regime.

1.6.4 Inlet Mach number

The Mach number at the inlet to the diffuser was thought to be important at values as low as approximately 0.7 and performance to fall off past this point. No significance on Mach number develops at throat for Mach numbers of less than 1.0 is studied by *Thayer E B et. al.* [1971].

1.6.5 Inlet Turbulence intensity

The turbulence intensity is most frequently defined as an RMS value:

$$Tu = \frac{\left[\frac{1}{3} (u'^2 + v'^2 + w'^2) \right]^{1/2}}{U}$$

This equation defines the parameter most frequently used to specify the overall level of inlet turbulence intensity is given by *Shaanan, et. al.* [1975].

1.6.6 Effect of Compressibility

With compressible flow both area A, and density ρ , increases with passage down the diffuser so that the reduction in velocity V, will be greater than in the case of incompressible flow where only the cross sectional area increases. It therefore follows that the pressure recovery coefficient should also be greater.

$$v = \frac{m}{\rho \cdot A}$$

The rate of increase in value of Cp is not rapid until Mach number of 0.6 have been exceeded and then the effect is most pronounced when area ratios are low. These low area ratios correspond to the diffuser inlet vision and flow separation would therefore occur here as a result of predicted increasing adverse pressure gradient caused by the higher subsonic inlet Mach number.

1.6.7 Effect of Compressibility on Wall Design

The design of diffuser walls is achieved by using a step by step or “ marching” method where small element of diffuser are considered in sequence it was recommended the length of each element, s, should be on the order of two percent of the hydraulic diameter when assessed diffuser inlet.

1.7 DESIGN PERFORMANCE PARAMETERS

Performance parameters are very helpful in designing and predicting the performance of diffusers. These parameters reveal that diffuser geometry will give the desired output or not. The following parameters are important to find out diffuser performance.

1.7.1 Static Pressure Recovery Coefficient:

A diffuser is generally used either to recover static pressure or to minimize total pressure loss in a pipe or in a duct. The performance of the diffuser can be expressed in terms of non-dimensional pressure recovery factor.

$$C_p^* = \frac{\Delta p}{\frac{1}{2} \rho v^2}$$

Where Δp represents the gain in static pressure, ρ indicates the density of the fluid and v denotes the inlet velocity of the fluid flow.

1.7.2 Diffuser Effectiveness:

The diffuser effectiveness is simply the relation between the actual recovery and the ideal pressure recovery.

$$\eta = \frac{C_p}{C_{pi}}$$

This is an excellent parameter for judging the probable level of performance when it is necessary to estimate the expected performance under unknown conditions, relative to available data.

1.7.3 Total Pressure Loss Coefficient

The total pressure loss coefficient reflects the efficiency of diffusion and drag of the system. The most common definition of loss coefficient is as the ratio of total pressure rise

to the diffuser inlet dynamic head.

$$K = \frac{\bar{P}_{01} - \bar{P}_{02}}{\frac{1}{2} \rho v_{av1}^2}$$

$$K = \frac{(\bar{u}_1^2 - \bar{u}_2^2)}{U_i^2} - C_p = \left(\alpha_1 - \alpha_2 / AR^2 \right) - C_p$$

Where \bar{P}_{02} is the total pressure in the core region at the exit, the over bar indicate the mass averaged quantity, and α_1 and α_2 are the kinetic energy parameters at the inlet and exit of the diffuser. For the case where the velocity profile at the inlet of diffuser is flat with a thin wall boundary layer, $\alpha_1=1$ However, due to the thickening of boundary layer through the diffuser, α_2 is generally greater than unity. Nonetheless, it is often assumed that kinetic energy coefficient is equal to unity, then

$$K = C_{pi} - C_p$$

Since flow in diffusers are subjected to an adverse pressure gradient there is a potential danger for flow separation to occur which could lead to loss in performance as well as damage of downstream equipment. The aim of design is to keep the adverse pressure gradient as high as possible, but below a critical limit, by controlling the length versus area-ratio of the diffuser. The design requirements for a good diffuser are as following:

1. Convey the flow efficiently transferring a portion of the kinetic energy into a static pressure rise.
2. It must accept a variety of inlet conditions including extreme swirl, blockage and Mach number.
3. Deliver the fluid with reasonable velocity and angle profiles without separated regions.
4. Wall curvature must not have a deleterious effect upon passage performance.
5. Pressure recovery achieved over a short axial length.

While obtaining the best possible design, some limitations are imposed on a diffuser:

1. Limited length
2. Specified area ratio
3. Specified cross- sectional shape
4. Maximum static pressure recovery
5. Minimum stagnation pressure loss

It is not hard to appreciate that the performance of the diffuser directly and often strongly influences the overall efficiency of the turbo machine. Thus the detailed processes which occur in diffusing elements must be carefully understood and thoroughly optimized if good turbo machinery performance is to be obtained

1.8 SWIRLING FLOWS

1.8.1 Physics of Swirling and Rotating Flows:

In swirling flows, conservation of angular momentum ($r\omega$ or $r^2\Omega = \text{constant}$) tends to create a free vortex flow, in which the circumferential velocity, ω , increases sharply as the radius, r , decreases (with ω finally decaying to zero near $r = 0$ as viscous forces begin to dominate). A tornado is one example of a free vortex. Figure depicts the radial distribution of ω in a typical free vortex.



Typical Radial Distribution of ω in a Free Vortex

It can be shown that for an ideal free vortex flow, the centrifugal forces created by the circumferential motion are in equilibrium with the radial pressure gradient:

$$\frac{\partial p}{\partial r} = \frac{\rho\omega^2}{r}$$

As the distribution of angular momentum in a non-ideal vortex evolves, the form of this radial pressure gradient also changes, driving radial and axial flows in response to the highly non-uniform pressures that result. Thus, as you compute the distribution of swirl in your FLUENT model, you will also notice changes in the static pressure distribution and corresponding changes in the axial and radial flow velocities. It is this high degree of coupling between the swirl and the pressure field that makes the modeling of swirling flows complex.

In flows that are driven by wall rotation, the motion of the wall tends to impart a forced vortex motion to the fluid, wherein w/r or Ω is constant. An important characteristic of such flows is the tendency of fluid with high angular momentum (e.g., the flow near the wall) to be flung radially outward. This is often referred to as “radial pumping”, since the rotating wall is pumping the fluid radially outward.

1.8.2 Method of swirl generation

Methods of including rotation in a stream of fluid can be divided into three principle category:

- Tangential entry of the fluid stream, or a part of it, into the cylindrical duct.
- The use of guide vanes in axial tube flow.
- Rotation of mechanical devices which impart swirling motion to the fluid passing through them. This includes rotating vanes or grids and rotating tubes.

1.9 MOTIVATIONS

The purpose of this study is to investigate the level of knowledge and in certain important areas the lack thereof, concerning the performance of annular diffusers. For decades investigators have conducted individual studies without a careful consideration of how all the studies may be interwoven. A pattern of consistent behaviour among the database elements for annular diffusers is established in this investigation. However, it may be of even greater significance that the investigation reveals areas where critical design

knowledge is missing. It will be observed that conducting individual investigations of annular diffuser performance has blinded most investigators from seeing the larger picture and the critical interactions between the different variables which have been discussed in the literature. This study begins by looking at historical data, then proceeds to investigate the parametric dependence, resulting in the development of a preliminary design set of equations and then finally by careful examination of further investigations which are needed` before the annular diffuser design problem will be well understood.

LITERATURE REVIEW

Flow through a diffuser is accompanied by reduction of mean kinetic energy and a consequent increase in pressure. It is more difficult to arrange for an efficient deceleration of flow than it is to obtain an efficient acceleration. There is a natural tendency in a diffusing process for the flow to break away from the walls of the diverging passage, reverse its direction, and flow back in direction of the pressure gradient. If the divergence is too rapid, this may result in the formation of eddies with consequent transfer of some kinetic energy into internal energy and a reduction in useful pressure rise. A small angle of divergence, however, implies a long diffuser and a high value of skin friction loss. Usually, flow separation in a diffuser is sought to be avoided due to the invoked additional pressure loss. Other than in many strongly separated flows, such as the flow over a backward facing step, the point of flow separation, in diffuser, is not defined by the geometry but entirely by the pressure gradient. Hence, diffuser flows are very sensitive and are difficult to predict with numerical means. Diffusers have been studied extensively in the past, since this is a very common flow configuration. Apart from the characterization of diffusers, these flows are used to study fundamental physics of pressure-driven flow separations. Much of the extant data covering annular diffusers comes from the period from the 1950s through the 1980s. In this period of time, a considerable amount of research was done in the experimental laboratory to uncover some of the unusual performance characteristics of annular diffusers. By the late 1980s, however, the experimental research had reduced substantially due to a lack of government funding in a number of countries where the work had previously been extensive. It is, therefore, useful to review the data which has been made available and to look for patterns within this data. It is also necessary to determine how this data may best be used in future design studies and where it needs to be further improved. Much of the original data was taken in order to support studies of axial

compressor discharge diffusion as flow leaves a compressor and enters a combustion chamber. Other work was done for exhaust diffusers of hydroelectric turbines, small gas turbines, and turbochargers. While these topics are still important today and there are important unresolved questions, the level of activity has reduced. Now important research topics must be carefully selected for the more limited studies possible in future years.

Many persons have done a lot of tests on geometric parameter of diffuser *Sovran et. al.* [1967] who tested over one hundred different geometries, nearly all of which had conically diverging centre bodies with an inlet radius ratio $[R_i/R_o]$ of 0.55 to 0.70. The tests were carried out with a thin inlet boundary layer and the diffusers have free discharge. The tests were present as Contours of pressure recovery plotted against area ratio and non-dimensional length *Howard et. al.* [1967] also tested symmetrical annular diffusers with centre bodies of uniform diameter, using fully developed flow at inlet. The limits of the various flow regimes and the optimum performance lines were established. Besides it, some other researchers also contributed in the field of annular diffuser and concluded various important results. Much of the extent data covering the annular diffusers was done in the experimental laboratory to uncover some of the unusual performance characteristics of annular diffusers. But there are still some important unresolved questions. The reason for it is that the numbers of independent variables are large for annular diffusers. In the annular diffuser the flow take place between two boundary surfaces which can varies independently This chapter involves a systematic study of different geometric and flow parameters which influence the overall and internal performance of annular diffusers. In this regard the available literature has been examined with a view to make comments on the state of the art and to recognize the scope of further research on the subject.

2.1 GEOMETRIC PARAMETERS

Any diffuser geometry with increasing area in the stream wise direction constitutes subsonic diffuser geometry .therefore, the number of different diffusers geometries that can

be conceived in infinite .however in practice adequate design data are available for limited numbers of geometries.

1. Rectangular cross section plan diffusers
2. Conical diffuser
3. Annular diffuser

These geometric parameters can be consolidated to few non dimensional parameters that are found to be important in terms of diffuser performance. The first is area ratio, AR the area ratio of diffuser exit to inlet areas .the area ratio is measure of theoretical diffusion of pressure recovery expected. *Manoj kumar et. al.* [2013] define the effect of area ratio on the performance annular diffuser. The second important parameter is the dimensionless diffuser length is define as N/W_i or L/W_i for planar diffusers, and $L/(R_i - R_h)$, for annular diffusers.

The third geometric parameter commonly used in displaying diffuser performance is the wall divergence angle 2θ for planar and conical diffusers. Area ratio and non dimensional length tells the overall diffusion and pressure gradient respectively, which is the main factor in boundary layer development. *Markland et. al.* [1986] found that a variation in the AR from 2.5 to 8.0 has a small effect on the loss coefficients of the 2-D diffuser. *Sharan* [1972] reported that for a constant AR the performance of diffuser deteriorates with the increase in diffusion angle. *Reneau et. al.* [1967] concluded that for two dimensional straight diffusers the maximum pressure recovery at a constant area ratio occurs in the range of diffuser angle equal to 6-8 degree. The research of extensive nature to define optimum geometrical characteristics of diffuser has been carried out by various researchers such as *Anderson M.G.* [2008], *Arora et. al.* [2010]. These investigators found improved diffuser performance with swirl up to ascertain point after that it deteriorated. The performance of an annular diffuser apart from swirl is dependent on a large number of geometrical and dynamical parameters. The effectiveness of annular axial diffusers

worsens with flow separation. The separation of the flow can be suppressed or shifted from one location to another with the help of swirl. The efforts have been made to design an annular diffuser for no flow separation *Stevens S. J et. al.* [1969, 1980], however little success has been achieved. Experimental studies on annular diffuser require sophisticated instrumentation and complicated time consuming procedures which is not economically viable and thus has limited the research activity in the field of annular diffusers *Awai T et.al.* [1984].

2.1.1 Effect of Geometric Parameters

In an annular diffuser, a number of different geometric variables can influence the variation of pressure recovery and inlet condition of flow. The basic equations of motion reveal the importance of both geometric and aerodynamic parameters on the ultimate performance of annular diffuser. The specification of a wide variety of geometric parameters is essential before the performance of diffuser is given. In this section, the various geometric parameters and their influence on diffuser performance is reviewed. Effect of geometry on the performance of annular diffuser governs by *Arora B.B. et. al.* [2005]. Numerical analysis of the impact of conical diffuser geometry change on velocity distribution in its outlet cross-section by *Krystyna prync-skotniczny* [2006]. Correlation of annular diffuser performance with geometry, swirl and blockage is given by *Japikse Dr. David* [2000].

2.1.2 Passage Divergence and Length

Area ratio and non-dimension length prescribes the overall diffusion and pressure-gradient respectively, which is the principle factor in boundary layer development. The study by *Henry et. al.* [1958] is useful to understand the subsonic annular diffuser. Two diffusers with area ratio 2.1 and divergence of 5° and 10° were tested at various Mach

number. It found by this study that most of data clusters around a line of constant Effectiveness. If a higher divergence had been used, then one might anticipate stall on the inner surface. An extensive study is carried out by *Kmonicek et. al.* [1974] in which, the pressure loss coefficient is found out on the basis of the work of compression required to meet the static pressure rise, the results are very interesting but difficult to understand due to use of unconventional terminology *Sovran and Klomp* [1967] and *Howard et. al.* [1967] produced the first widely used annular diffuser maps for channel diffusers. *Sovran and Klomp* [1967] conducted a large number of performance measurements which spanned a broad selection of geometric types of diffusers. The map is only a broad representation of the bulk of configurations tested in the vicinity of their best performance areas. The poorer diffusers are not well defined by the map. These maps also show optimal diffuser geometrics under different conditions and two optimum lines are established. The same results were found out by *Howard et. al.* [1967]. The important difference between this and the *Sovran and Klomp* [1967] map was that the latter was made for very low inlet aerodynamic blockage whereas the former study was carried out for fully developed inlet profiles, implying high aerodynamic blockage. Along the line of peak recovery there is fairly good agreement between the two maps but in the region of heavy transitory stall the maps disagree substantially.

Johnston I. H [1959] and *Johnston J. P* [1959] reported a study of four different annular diffusers. Three of the four agree tolerably well with the basics *Sovran and Klomp* [1967] map, one of them disagree substantially; the case a strong disagreement is probably in stall. *Srinath* [1968] studied four equiangular annular diffuser with $2\theta = 7^\circ, 10^\circ, 15^\circ$ and 20° respectively. Tests were reported with a variety of $L/\Delta r$ values. An extensive study of diffusers which, although annular, begin with a circular cross section was reported by *Ishikawa and Nakamura* [1989]. The author found that the performance of the diffuser differed significantly depending on whether it is parallel or diverging for L/r_1 greater than

about 2. When both types have the same non dimensional length and area ratio, the parallel diffuser has the higher CP. The lines of optimum performance are also drawn. *Ishikawa and Nakamura* [1989], also attempted to compare their results with those of *Sovran and Klomp* [1967], for a conventional annular diffuser for the same wall length and area ratio, their diffuser was superior, but since the inlet conditions were different in the two studies, this conclusion is only tentative. It was also found that the addition of a conical centre body improves the performance of simple conical diffusers with appreciable or large stall. The study carried out by *Moller E.S* [1965], who designed an axial to radial band with the intention of eliminating diffusion in the inlet region; found that the peak pressure recovery for the entire band and radial diffuser sections was 0.88 and 0.82 for the low blockage and high blockage cases, respectively. *Cockrell D.J and Markland* [1963], reported that a variation in the area ratio from 2.5 to 8.0 has a small effect on the loss coefficients of conical diffusers.

2.1.3 Wall Contouring

Several annular diffuser studies have been published in which contoured walls were an essential part of the design problem. *Thayer* [1971], reported that curved wall diffusers had pressure recovery as high as 0.61 to 0.65 for an area ratio of 2.15. An extensive study by *Stevens and Williams* [1980], reported that for curved wall diffuser, good pressure recovery was found for a loss significantly below the level which would be expected from pressure recovery loss correlation , but pressure recovery values were lower than those which would be expected from the *Sovran and Klomp* [1967], map. Upon careful examination, it was determined that the boundary layers in this diffuser are different from those which would be expected in most diffuser studies. *Takehira et. al.* [1977], presented extensive data for a large set of both straight annular diffusers and curved wall diffusers, and determined that the use of strong curvature at the exit of diffuser was not debilitating

but did produce a penalty compared to no curved diffusers or diffusers with curvature at the inlet.

An additional study by *Japikse* [2000] shows that wall contouring is an important parameter regarding pressure recovery. *Adkins et. al.* [1983], tested an annular diffuser of constant outer radius and a conical centre body with cones of different angles. In general the pressure recovery increases with decreasing cone angle for various area ratios, but the 132° and sometimes the 45°-cone angle produced lower pressure recoveries than an equivalent sudden expansion. This was attributed to a large and rapid separation at the base of the cone where the diffuser starts. Adding a radius to the base of the cone so that it smoothly blended into the upstream hub, was found to improve the performance.

2.2 EFFECTS OF FLOW PARAMETERS

2.2.1 Aerodynamic Blockage

The basic boundary layer equations reveal the importance of the displacement thickness as a characteristic length scale of the inlet boundary layer flow. *Startford et. al.* [1957, 1955] and (evidently) Bragg recognized the importance of the boundary layer displacement thickness to pressure recovery process .it is clear that thin inlet boundary layer should be beneficial to high diffuser recovery and that longer diffusers are necessary to achieve high level of recovery as the inlet boundary thickness increases. *Thayer* [1971], reported that curved wall diffusers had pressure recovery as high as 0.61 to 0.65 for an area ratio of 2.15. An extensive study by *Stevens and Williams* [1980], reported that for curved wall diffuser, good pressure recovery was found for a loss significantly below the level which would be expected from pressure recovery loss correlation , but pressure recovery values were lower then those which would be expected from the *Sovran and Klomp* [1967], map. *Klein* [1995] compared *Stevens and Williams* [1980] data with the result of

Sovern and Klomp [1967] for an inlet blockage of .02 and with predictions using the latter's method for diffuser performance at larger blockages. A comprehensive study on the influence of aerodynamic blockage on annular diffuser performance carried out by *Globel and Japikse* [1981]. similar measurements were made at 20° and 40° of inlet swirl. In all cases the data trend was in the direction of reduced pressure recovery for increased aerodynamic blockage. Upon careful examination, it was determined that the boundary layers in this diffuser are different *Mazumdar P.M. et. al.* [2003] done aerodynamic design optimization at cases. . First, the influence of inlet conditions on annular diffuser performance is more complicated than for channel and conical diffuser. In this case, both the hub and casing surfaces can develop boundary layers with significantly different histories. The two differing boundary layers will experience different growth processes as they pass through the diffuser. Furthermore, blockage on one wall has the effect of modifying the effective flow area and hence the core flow velocity, thereby influencing the growth of the boundary layer on the opposite wall. Hence complex interactions can develop within the diffuser.

2.2.2 Inlet Swirl

The method of swirl generation can itself influence the performance of an annular diffuser and, therefore, consideration must be given first to this question. Most investigators have chosen to generate swirl in a radial inflow plane in order to take advantage of the simple cascade design geometry. Others have preferred to use axial cascade which have the advantage that they more closely simulate specific turbo machinery flow condition and permit control of the spacing between the diffuser and the vanes in form that may be more typical of an actual turbo machine. On the other hand axial cascade invariably introduces tip and hub leakage since the cascades are of a variable geometry type, an effective sealing is impossible. In addition to inlet swirl, there may be

changes in inlet turbulence intensity, velocity or total pressure gradients, vorticity or wake shading, and inlet aerodynamic blockage may change indirectly as a function of the swirl angle as it is varied. In order for firm conclusion to be drawn, the effect of swirl variation must be deciphered from the performance data *Dovzhik et. al.* [1975] also reported by the same type of study that the best performance can be achieved between the ranges of 10° to 20° of inlet swirl angle. A study is presented by *Japikse and Pamprreen* [1979] of an exhaust diffuser and hood found that substantial recovery has been achieved even up to swirl angle in excess of 40°. *Steenbergen W. J. Voskamp* [1998]. The rate of decay of swirl in turbulent pipe flow.

He found that on increase of swirl number the rate of increase. Guo it seems that higher swirl level require fine grid. Numerical Investigation of Swirling Flow in Annular Diffusers With a Rotating Hub Installed at the Exit of Hydraulic Machines is done by *Kochevsky A.N.* [2000] Numerical investigation of swirl flow on conical diffuser was done by the *Walter Gyllenram* [2006]. *Najafi A.F.* [2004] have done Numerical analysis of turbulent swirling decay pipe flow The flow characteristics through a rotating honeycomb and resulting downstream swirling decay flow through a fixed pipe have been investigated in this research. The modeling of the rotating honeycomb is observed to be of major importance for the prediction of the downstream flow. Several methods are used and tested. The flow field properties obtained by the honeycomb tubes which are the annular cylinders in our axis-symmetric computations have a considerable effect on the downstream flow. *Ogor Buntia et. al.* [2006] give the An Adaptive Turbulence Model for Swirling Flow.

2.2.3 Inlet Turbulence

With long approach pipes diffuser performance rises as approach length increases. This was first noted in the *Cockrell and Markland* [1963] and attributed this to changes in

turbulence which enhances mixing transverse to flow directions, thus reducing the distortions. Indeed, the core turbulence intensity of developing pipe flow rises significantly from La/D is equal to 20 to 45 and then remains nearly constant. Two studies have been published which considered variation in inlet turbulence intensity or structure for their impact on annular diffuser performance. The data of *Coladieu et al.* [1974] have included both low and high inlet turbulence intensity levels, and this may be an explanation for the unusual measurements observed at different blockage. The second study is the work of *Williams and Stevens* [1969] and *Stevens and Fry* [1973], which showed that substantial improvements in radial momentum transport were achieved by turbulence producing grids and wall spoilers. Additional results by *Hestermann et al.* [1995], and *Klein* [1995] also show that increasing the level of turbulence to 6 – 8.5 % is beneficial in increasing the pressure recovery and, in one case of removing the separation of stalled diffuser. *Stefano Ubertini and Uberto Desideri* [2000] determined the flow development in terms of the mean and fluctuating components of the velocity and turbulence dissipating eddy length scales in annular exhaust diffuser. The K- ϵ and other turbulent models are evaluated with respect to their applicability in swirling flows by *Arora.B.B. et al.* [2005]. In most of the past numerical simulations, swirling air is introduced around this, in most cases perpendicular to the axis. In this configuration, it is straightforward to specify the inlet velocity profiles *Ogor Buntia et al.* [2006] give the An Adaptive Turbulence Model for Swirling Flow. *M.A. Leschziner* [2004] had done modelling turbulent separated flow in the context of aerodynamic applications. *Bajcar Tom et al.* [2006] Heat transfer influenced by turbulent airflow inside an axially rotating diffuser. *Olle Törnblom* [2006] give an Experimental and computational studies of turbulent separating internal flows The experimental investigation of the mean flow and turbulence properties revealed a flow with

several interesting characteristics: strong and suddenly imposed shearing, non-equilibrium turbulence, separation, reattachment and turbulence relaxation. The conclusion of above study is that the effect of increasing inlet turbulence intensity is to increase pressure recovery.

2.2.4 Mach number Influence

Most annular diffuser research has been carried out at low inlet mach numbers. However, several studies have shown measurement at different Mach number. The study by *Thayer* [1971], *Wood and Henry* [1958] and *Japikse and Pampreen* [1979] illustrate virtual independence of recovery with Mach number up to some critical level of approximately 0.80 to 1.1. The actual level depends on method of measurement and the type of inlet. *Wood and Henry* [1971] show that a shock structure must be presented before the performance begins to deteriorate, but the reference Mach number may have little to do with the actual shock location and shock structure. In most cases, the reduction of performance with Mach number is very slight but in a few cases there can be a degradation of five or ten point of performance recovery.

2.2.5 Reynolds Number Influence

Viscosity is an important parameter in any fluid dynamic process and normally appears in the form of a Reynolds number. Typically, diffusers are characterized by a Reynolds number based on an inlet hydraulic diameter. All studies reported that the Reynolds number is a comparatively weak parameter as long as the flow is in the fully turbulent regime. *Crockrell and Markland* [1963] state that a variation of the inlet Reynolds number has no significant effect on the diffuser performance if this variation is uncoupled from its effects on the inlet boundary layer parameters. For Reynolds number variation within the range of $2 \times 10^4 - 7 \times 10^5$, they also pointed out that the diffuser

performance would be practically independent of Reynolds number provided the inlet boundary parameters remain constant. *Sharan* [1972] reported that for thick boundary layers, there is no change in pressure recovery as the Reynolds number increases.

2.3 BOUNDARY LAYER PARAMETER

The flow in diffuser is governed by the behavior of the boundary layers at the diffuser walls. The deceleration of the flow through the diffuser produces a pressure rise in the stream wise direction. The wall shear layers are therefore subjected to a positive or adverse pressure gradient. As is well known, an adverse pressure gradients cause the wall boundary layers to thicken and possibly separate from the diffuser walls, forming areas of backflow in the diffuser. The net result of thickening of the wall boundary layers or the formation of regions of backflow is the blockage of flow area which reduces the effective area available to the flow. Reduction in effective flow area in turn results in a reduced pressure rise through the diffuser.

2.3.1 Boundary Layer Suction

The effect of suction consists in the removal of decelerated fluid particles from the boundary layer before they are given a chance to cause separation. *Stafford, W et. al.* [1957] investigated the suction phenomenon and found that a suction flow rate of 2.3% increased the static pressure rise by 25 – 60% and decreased the measured total pressure loss by 63%. In another study by *Stafford, W et. al.* [1955], it is shown that suction control is not efficient when applied in an extensive backflow region such as exists immediately downstream of an abruptly turned body. Experiments by *Juhasz* [1974], on short annular diffuser showed that the diffuser exit profiles could be shifted either towards the hub or towards the casing of annulus by bleeding off a small fraction of the flow through the inner and outer wall respectively. Boundary Layer Suction is also adopted by *Ackert* [1967], for both channel and conical diffuser with large divergence angle.

2.3.2 Blowing and Injection

Stafford, W et. al. [1955], found that at an injection rate of 3.4%, a 33% increase in the measured static pressure rise and a 50% decrease in the measured total pressure loss can be obtained. *Juhasz* [1974], have reported results of their investigations on the effect of injecting secondary fluid into wide angle conical diffusers through annular slot at inlet. Injection was found to result in considerable improvement in the uniformity of exit flow as well as in the magnitude of pressure recovery.

MATHEMATICAL MODELLING

The present study involves various models and basic laws of fluid mechanics to attain the results. FLUENT provides comprehensive modeling capabilities for a wide range of incompressible laminar and turbulent fluid problems. In FLUENT, a broad range of mathematical models for transport phenomena (like heat transfer swirl and chemical reactions) is combined with the ability to model complex geometries. The range of problems that can be addressed is very wide. The turbulence models provided have broad range of applicability without the need for fine tuning to a specific application.

FLUENT uses four equations to simulate a 2-D flow problem in addition to the turbulence modelling equations. These four equations are:

- Conservation Principle
 - Momentum equation
 - Continuity equation
- Velocity Equations
 - X- velocity equation
 - Y- velocity equation

3.1 CONSERVATION PRINCIPALS

Conservation laws can be derived considering a given quantity of matter or control mass and its extensive properties, such as mass, momentum and energy. This approach is used to study the dynamics of solid bodies. In fluid flows, however it is difficult to follow a parcel of matter. It is more convenient to deal with the flow within a certain spatial region we call a control volume, rather than a parcel of matter, which quickly passes through the region of interest. For all fluid flows the two extensive properties mass and momentum are solved. Flows involving heat and mass transfer or compressibility, an additional equation of energy conservation are solved. Additional flow transport equations

are solved when the flow is turbulent.

3.1.1 Mass Conservation Equation (Continuity Equation)

The equation for conservation of mass, or continuity equation, can be written as follows:

$$\frac{\partial \rho}{\partial t} + \nabla \cdot (\rho \vec{v}) = S_m$$

Equation is the general form of the mass conservation equation and is valid for incompressible as well as compressible flows. The source S_m is the mass added to the continuous phase from the dispersed second phase (e.g., due to vaporization of liquid droplets) and any user-defined sources.

For 2D ax symmetric geometries, the continuity equation is given by

$$\frac{\partial \rho}{\partial t} + \frac{\partial}{\partial x}(\rho v_x) + \frac{\partial}{\partial r}(\rho v_r) = S_m$$

Where x is the axial coordinate, r is the radial coordinate, v_x is the axial velocity, and v_r is the radial velocity.

3.1.2 Momentum Conservation Equations

Conservation of momentum in an inertial (non-accelerating) reference frame

$$\frac{\partial}{\partial t}(\rho \vec{v}) + \nabla \cdot (\rho \vec{v} \vec{v}) = -\nabla p + \nabla \cdot (\bar{\bar{\tau}}) + \rho \vec{g} + \vec{F}$$

Where p is the static pressure, τ is the stress tensor (described below), and $\rho \vec{g}$ and \vec{F} are the gravitational body force and external body forces (e.g., that arise from interaction with the dispersed phase), respectively. \vec{F} also contains other model-dependent source terms such as porous-media and user-defined sources.

The stress tensor τ is given by

$$\bar{\bar{\tau}} = \mu \left[\left(\nabla \vec{v} + \nabla \vec{v}^T \right) - \frac{2}{3} \nabla \cdot \vec{v} I \right]$$

Where μ is the molecular viscosity, I is the unit tensor, and the second term on the right

hand side is the effect of volume dilation.

For 2D axisymmetric geometries, the axial and radial momentum conservation equations are given by

$$\begin{aligned} \frac{\partial}{\partial t}(\rho v_x) + \frac{1}{r} \frac{\partial}{\partial x}(r \rho v_x v_x) + \frac{1}{r} \frac{\partial}{\partial r}(r \rho v_r v_x) = & -\frac{\partial p}{\partial x} + \frac{1}{r} \frac{\partial}{\partial x} \left[r \mu \left(2 \frac{\partial v_x}{\partial x} - \frac{2}{3} (\nabla \cdot \vec{v}) \right) \right] + \\ & \frac{1}{r} \frac{\partial}{\partial r} \left[r \mu \left(\frac{\partial v_x}{\partial r} + \frac{\partial v_r}{\partial x} \right) \right] + F_x \end{aligned}$$

And

$$\begin{aligned} \frac{\partial}{\partial t}(\rho v_r) + \frac{1}{r} \frac{\partial}{\partial x}(r \rho v_x v_r) + \frac{1}{r} \frac{\partial}{\partial r}(r \rho v_r v_r) = & -\frac{\partial p}{\partial r} + \frac{1}{r} \frac{\partial}{\partial x} \left[r \mu \left(\frac{\partial v_r}{\partial x} + \frac{\partial v_x}{\partial r} \right) \right] \\ & + \frac{1}{r} \frac{\partial}{\partial r} \left[r \mu \left(2 \frac{\partial v_r}{\partial r} - \frac{2}{3} (\nabla \cdot \vec{v}) \right) \right] - 2 \mu \frac{v_r}{r^2} + \frac{2}{3} \frac{\mu}{r} (\nabla \cdot \vec{v}) + \rho \frac{v_z^2}{r} + F_r \end{aligned}$$

Where

$$\nabla \cdot \vec{v} = \frac{\partial v_x}{\partial x} + \frac{\partial v_r}{\partial r} + \frac{v_z}{r}$$

And v_z is the swirl velocity

The tangential momentum equation for 2D swirling flows may be written as

$$\begin{aligned} \frac{\partial}{\partial t}(\rho v_z) + \frac{1}{r} \frac{\partial}{\partial x}(r \rho v_x v_z) + \frac{1}{r} \frac{\partial}{\partial r}(r \rho v_r v_z) = & \frac{1}{r} \frac{\partial}{\partial x} \left[r \mu \frac{\partial v_z}{\partial x} \right] - \rho \frac{v_r v_z}{r} \\ & + \frac{1}{r^2} \frac{\partial}{\partial r} \left[r^3 \mu \frac{\partial}{\partial r} \left(\frac{v_z}{r} \right) \right] \end{aligned}$$

3.2 TURBULENCE MODELLING

Turbulent flows are characterized by fluctuating velocity fields. These fluctuations mix with transported quantities such as momentum, energy, and species concentration, and cause the transported quantities to fluctuate as well. Since these fluctuations can be of small scale and high frequency, they are too computationally expensive to simulate directly

in practical engineering calculations. Instead, the instantaneous (exact) governing equations can be time-averaged, ensemble-averaged, or otherwise manipulated to remove the small scales, resulting in a modified set of equations that are computationally less expensive to solve. However, the modified equations contain additional unknown variables, and turbulence models are needed to determine these variables in terms of known quantities.

3.2.1 Choosing a Turbulence Model

It is an unfortunate fact that no single turbulence model is universally accepted as being superior for all classes of problems. The choice of turbulence model will depend on considerations such as the physics encompassed in the flow, the established practice for a specific class of problem, the level of accuracy required, the available computational resources, and the amount of time available for the simulation. To make the most appropriate choice of model for your application, one needs to understand the capabilities and limitations of the various options. The purpose of this section is to give an overview of issues related to the turbulence models provided in FLUENT. The computational effort and cost in terms of CPU time and memory of the individual models is discussed. While it is impossible to state categorically which model is best for a specific application, general guidelines are presented to help you choose the appropriate turbulence model for the flow you want to model.

FLUENT

Provides the following choices of turbulence models:

- Spalart-Allmaras model
- k- ϵ models
 - Standard k- ϵ model
 - Renormalization-group (RNG) k- ϵ model
 - Realizable k- ϵ model
- k- ω models

- Standard k - ω model
- Shear-stress transport (SST) k - ω model
- Reynolds stress model (RSM)
- Large eddy simulation (LES) model

3.3 THE STANDARD, RNG, AND REALIZABLE k - ϵ MODELS

All three models have similar forms, with transport equations for k and ϵ . The major differences in the models are as follows:

- the method of calculating turbulent viscosity
- the turbulent Prandtl numbers governing the turbulent diffusion of k and ϵ
- the generation and destruction terms in the ϵ equation

The transport equations, methods of calculating turbulent viscosity, and model constants are presented separately for each model.

3.3.1 The Standard k - ϵ Model

The simplest “complete models” of turbulence are two-equation models in which the solution of two separate transport equations allows the turbulent velocity and length scales to be independently determined. The standard k - ϵ model in FLUENT falls within this class of turbulence model and has become the workhorse of practical engineering flow calculations in the time since it was proposed by Launder and Spalding. Robustness, economy, and reasonable accuracy for a wide range of turbulent flows explain its popularity in industrial flow and heat transfer simulations. It is a semi-empirical model, and the derivation of the model equations relies on phenomenological considerations and empiricism.

The standard k - ϵ model is a semi-empirical model based on model transport equations for the turbulence kinetic energy (k) and its dissipation rate (ϵ). The model transport equation for k is derived from the exact equation, while the model transport equation for ϵ was obtained using physical reasoning and bears little resemblance to its

mathematically exact counterpart. For k-ε model, it was assumed that the flow is fully turbulent, and the effects of molecular viscosity are negligible, therefore valid only for fully turbulent flows.

3.3.2 Transport Equations for the Standard k-ε Model

The turbulence kinetic energy, k, and its rate of dissipation, ε, are obtained from the following transport equations:

$$\frac{\partial}{\partial t}(\rho k) + \frac{\partial}{\partial x_i}(\rho k u_i) = \frac{\partial}{\partial x_j} \left[\left(\mu + \frac{\mu_t}{\sigma_k} \right) \frac{\partial k}{\partial x_j} \right] + G_k + G_b - \rho \varepsilon - Y_M + S_k$$

And

$$\frac{\partial}{\partial t}(\rho \varepsilon) + \frac{\partial}{\partial x_i}(\rho \varepsilon u_i) = \frac{\partial}{\partial x_j} \left[\left(\mu + \frac{\mu_t}{\sigma_\varepsilon} \right) \frac{\partial \varepsilon}{\partial x_j} \right] + C_{1\varepsilon} \frac{\varepsilon}{k} (G_k + C_{3\varepsilon} G_b) - C_{2\varepsilon} \rho \frac{\varepsilon^2}{k} + S_\varepsilon$$

In these equations, G_k represents the generation of turbulence kinetic energy due to the mean velocity gradients. G_b is the generation of turbulence kinetic energy due to buoyancy. Y_M represents the contribution of the fluctuating dilatation in compressible turbulence to the overall dissipation rate. $C_{1\varepsilon}$, $C_{2\varepsilon}$, and $C_{3\varepsilon}$ are constants. σ_k and σ_ε are the turbulent Prandtl numbers for k and ε, respectively.

3.3.3 Modeling the Turbulent Viscosity

The turbulent (or eddy) viscosity, μ_t , is computed by combining k and ε as follows:

$$\mu_t = \rho C_\mu \frac{k^2}{\varepsilon} \quad \text{Where } C_\mu \text{ is a constant.}$$

3.3.4 The model constants

$C_{1\varepsilon}$, $C_{2\varepsilon}$, C_μ , σ_k , and σ_ε have the following default values:

$$C_{1\varepsilon} = 1.44, \quad C_{2\varepsilon} = 1.92, \quad C_\mu = 0.09, \quad \sigma_k = 1.0, \quad \sigma_\varepsilon = 1.3$$

These default values have been determined from experiments with air and water for fundamental turbulent shear flows including homogeneous shear flows and decaying isotropic grid turbulence. They have been found to work fairly well for a wide range of wall-bounded and free shear flows.

3.3.5 The RNG k-ε Model

The RNG-based k-ε turbulence model is derived from the instantaneous Navier-Stokes equations, using a mathematical technique called “renormalization group” (RNG) methods. It is similar in form to the standard k-ε model, but includes the following refinements:

- The RNG model has an additional term in its ε equation that significantly improves the accuracy for rapidly strained flows.
- The effect of swirl on turbulence is included in the RNG model, enhancing accuracy for swirling flows.
- The RNG theory provides an analytical formula for turbulent Prandtl numbers, while the standard k-ε model uses user-specified, constant values.
- While the standard k-ε model is a high-Reynolds-number model, the RNG theory provides an analytically-derived differential formula for effective viscosity that accounts for low-Reynolds-number effects. Effective use of this feature does, however, depend on an appropriate treatment of the near-wall region.

These features make the RNG k-ε model more accurate and reliable for a wider class of flows than the standard k-ε model.

3.3.6 Transport Equations for the RNG k-ε Model

The RNG k- ε model has a similar form to the standard k-ε model:

$$\frac{\partial}{\partial t}(\rho k) + \frac{\partial}{\partial x_i}(\rho k u_i) = \frac{\partial}{\partial x_j} \left[\alpha_k \mu_{eff} \frac{\partial k}{\partial x_j} \right] + G_k + G_b - \rho \varepsilon - Y_M + S_k$$

And

$$\frac{\partial}{\partial t}(\rho\varepsilon) + \frac{\partial}{\partial x_i}(\rho\varepsilon u_i) = \frac{\partial}{\partial x_j} \left[\alpha_k \mu_{eff} \frac{\partial \varepsilon}{\partial x_j} \right] + C_{1\varepsilon} \frac{\varepsilon}{k} (G_k + C_{3\varepsilon} G_b) - C_{2\varepsilon} \rho \frac{\varepsilon^2}{k} - R_\varepsilon + S_\varepsilon$$

In these equations, G_k represents the generation of turbulence kinetic energy due to the mean velocity gradients. G_b is the generation of turbulence kinetic energy due to buoyancy. Y_M represents the contribution of the fluctuating dilatation in compressible turbulence to the overall dissipation rate,. The quantities α_k and α_ε are the inverse effective Prandtl numbers for k and ε , respectively. S_k and S_ε are user-defined source terms.

3.3.7 Modeling the Effective Viscosity

The scale elimination procedure in RNG theory results in a differential equation for turbulent viscosity:

$$d \left(\frac{\rho^2 k}{\sqrt{\varepsilon \mu}} \right) = 1.72 \frac{\hat{\nu}}{\sqrt{\hat{\nu}^3 - 1 + C_\nu}}$$

Where

$$\hat{\nu} = \frac{\mu_{eff}}{\mu} \quad C_\nu \approx 100$$

Equation is integrated to obtain an accurate description of how the effective turbulent transport varies with the effective Reynolds number (or eddy scale), allowing the model to better handle low-Reynolds-number and near-wall flows.

In the high-Reynolds-number limit, Equation gives

$$\mu_t = \rho C_\mu \frac{k^2}{\varepsilon}$$

With $C_{\mu} = 0.0845$, derived using RNG theory. It is interesting to note that this value of C_{μ} is very close to the empirically-determined value of 0.09 used in the standard k- ϵ model.

3.3.8 The Realizable k- ϵ Model

The realizable k- ϵ model is a relatively recent development and differs from the standard k- ϵ model in two important ways:

- The realizable k- ϵ model contains a new formulation for the turbulent viscosity.
- A new transport equation for the dissipation rate, ϵ , has been derived from an exact equation for the transport of the mean-square vorticity fluctuation.

The term “realizable” means that the model satisfies certain mathematical constraints on the Reynolds stresses, consistent with the physics of turbulent flows. Neither the standard k- ϵ model nor the RNG k- ϵ model is realizable. An immediate benefit of the realizable k- ϵ model is that it more accurately predicts the spreading rate of both planar and round jets. It is also likely to provide superior performance for flows involving rotation, boundary layers under strong adverse pressure gradients, separation, and recirculation. Since the model is still relatively new, it is not clear in exactly which instances the realizable k- ϵ model consistently outperforms the RNG model. One limitation of the realizable k- ϵ model is that it produces non-physical turbulent viscosities in situations when the computational domain contains both rotating and stationary fluid zones (e.g., multiple reference frames, rotating sliding meshes). This is due to the fact that the realizable k- ϵ model includes the effects of mean rotation in the definition of the turbulent viscosity. This extra rotation effect has been tested on single rotating reference frame systems and showed superior behavior over the standard k- ϵ model.

3.3.9 Transport Equations for the Realizable k- ϵ Model

The modeled transport equations for k and ϵ in the realizable k- ϵ model are

$$\frac{\partial}{\partial t}(\rho k) + \frac{\partial}{\partial x_i}(\rho k u_i) = \frac{\partial}{\partial x_j} \left[\left(\mu + \frac{\mu_t}{\sigma_k} \right) \frac{\partial k}{\partial x_j} \right] + G_k + G_b - \rho \varepsilon - Y_M + S_k$$

And

$$\begin{aligned} \frac{\partial}{\partial t}(\rho \varepsilon) + \frac{\partial}{\partial x_i}(\rho \varepsilon u_i) = \frac{\partial}{\partial x_j} \left[\left(\mu + \frac{\mu_t}{\sigma_\varepsilon} \right) \frac{\partial \varepsilon}{\partial x_j} \right] + \rho C_1 S_\varepsilon + C_{1\varepsilon} \frac{\varepsilon}{k} (C_{3\varepsilon} G_b) \\ - C_2 \rho \frac{\varepsilon^2}{k + \sqrt{\nu \varepsilon}} + S_\varepsilon \end{aligned}$$

Where

$$C_1 = \max \left[0.43, \frac{\eta}{\eta + 5} \right] \quad \eta = S \frac{k}{\varepsilon}$$

3.3.10 Modeling the Turbulent Viscosity

As in other k-ε models, the eddy viscosity is computed from

$$\mu_t = \rho C_\mu \frac{k^2}{\varepsilon}$$

The difference between the realizable k-ε model and the standard and RNG k-ε models is that C_μ is no longer constant. It is computed from

$$C_\mu = \frac{1}{A_0 + A_s \frac{k U^*}{\varepsilon}}$$

Where

$$U^* = \sqrt{S_{ij} S_{ij} + \tilde{\Omega}_{ij} \tilde{\Omega}_{ij}}$$

And

$$\tilde{\Omega}_{ij} = \Omega_{ij} - 2\varepsilon_{ijk}\omega_k$$

$$\tilde{\bar{\Omega}}_{ij} = \bar{\Omega}_{ij} - \varepsilon_{ijk}\omega_k$$

3.3.11 Model Constants

The model constants C_2 , σ_k , and σ_ε have been established to ensure that the model performs well for certain canonical flows. The model constants are

$$C_{1\varepsilon} = 1.44; \quad C_2 = 1.9; \quad \sigma_k = 1.0; \quad \sigma_\varepsilon = 1.2$$

3.4 TURBULENCE MODELING IN SWIRLING FLOWS

If you are modeling turbulent flow with a significant amount of swirl (e.g., cyclone flows, swirling jets), you should consider using one of FLUENT's advanced turbulence models: the RNG k- ε model, realizable k- ε model, or Reynolds stress model. The appropriate choice depends on the strength of the swirl, which can be gauged by the swirl number. The swirl number is defined as the ratio of the axial flux of angular momentum to the axial flux of axial momentum:

$$S = \frac{\int r\omega\vec{v}.d\vec{A}}{R\int u\vec{v}.d\vec{A}}$$

Where R is the hydraulic radius.

For swirling flows encountered in devices such as cyclone separators and swirl combustors, near-wall turbulence modeling is quite often a secondary issue at most. The fidelity of the predictions in these cases is mainly determined by the accuracy of the turbulence model in the core region. However, in cases where walls actively participate in the generation of swirl (i.e., where the secondary flows and vertical flows are generated by pressure gradients), non-equilibrium wall functions can often improve the predictions since they use a law of the wall for mean velocity sensitized to pressure gradients.

FLUENT is a state-of-the-art computer program for modeling fluid flow and heat transfer in complex geometries. FLUENT provides complete mesh flexibility, solving your flow problems with unstructured meshes that can be generated about complex geometries with relative ease. Supported mesh types include 2D triangular/quadrilateral, 3D tetrahedral/hexahedral/pyramid/wedge, and mixed (hybrid) meshes. FLUENT also refine or coarsen grid based on the flow solution.

4.1 PROGRAM CAPABILITIES

The FLUENT solver has the following modeling capabilities:

- 2D planar, 2D axisymmetric, 2D axisymmetric with swirl (rotationally symmetric), and 3D flows
- Quadrilateral, triangular, hexahedral (brick), tetrahedral, prism (wedge), pyramid, polyhedral, and mixed element meshes
- Steady-state or transient flows
- Incompressible or compressible flows, including all speed regimes (low subsonic, transonic, supersonic, and hypersonic flows)
- Inviscid, laminar, and turbulent flows
- Newtonian or non-Newtonian flows
- Heat transfer, including forced, natural, and mixed convection, conjugate (solid/fluid) heat transfer, and radiation
- Chemical species mixing and reaction, including homogeneous and heterogeneous combustion models and surface deposition/reaction models

- Free surface and multiphase models for gas-liquid, gas-solid, and liquid-solid flows
- Lagrangian trajectory calculation for dispersed phase (particles/droplets/bubbles), including coupling with continuous phase and spray modeling
- Cavitation model
- Phase change model for melting/solidification applications
- Porous media with non-isotropic permeability, inertial resistance, solid heat conduction, and porous-face pressure jump conditions
- Lumped parameter models for fans, pumps, radiators, and heat exchangers
- Acoustic models for predicting flow-induced noise
- Inertial (stationary) or non-inertial (rotating or accelerating) reference frames
- Multiple reference frame (MRF) and sliding mesh options for modeling multiple moving frames
- Mixing-plane model for modeling rotor-stator interactions, torque converters, and similar turbo-machinery applications with options for mass conservation and swirl conservation
- Volumetric sources of mass, momentum, heat, and chemical species

FLUENT is ideally suited for incompressible and compressible fluid-flow simulations in complex geometries.

4.2 PLANNING CFD ANALYSIS

The following consideration should be taken while planning CFD analysis:

4.2.1 Definition of the Modeling Goals:

What specific results are required from the CFD model and how will they be used? What degree of accuracy is required from the model?

4.2.2 Grid Generation and its Independence:

What type of element will be used? What size of the mesh should be kept so as to optimize between accuracy and time and resources being consumed?

4.2.3 Choice of the Computational Model:

How will you isolate a piece of the complete physical system to be modeled? Where will the computational domain begin and end? What boundary conditions will be used at the boundaries of the model? Can the problem be modeled in two dimensions or is a three-dimensional model required? What type of grid topology is best suited for this problem?

4.2.4 Choice of Physical Models:

Is the flow in viscous, laminar, or turbulent? Is the flow unsteady or steady? Is heat transfer important? Will you treat the fluid as incompressible or compressible? Are there other physical models that should be applied?

4.2.5 Determination of the Solution Procedure:

Can the problem be solved simply, using the default solver formulation and solution parameters? Can convergence be accelerated with a more judicious solution procedure? Will the problem fit within the memory constraints of your computer, including the use of multigrain? How long will the problem take to converge on your computer?

Careful consideration of these issues before beginning CFD analysis will contribute significantly to the success of modeling effort.

4.3 DISCRETIZATION

The governing equations are converted into algebraic equations with the help of the finite volume technique that can be solved numerically. This control volume technique consists of integrating the governing equations about each control volume, yielding discrete equations

that conserve each quantity on a control-volume basis.

Discretization of the governing equations can be illustrated most easily by considering the steady-state conservation equation for transport of a scalar quantity ϕ . This is demonstrated by the following equation written in integral form for an arbitrary control volume V as follows:

$$\oint \rho \phi \vec{v} \cdot d\vec{A} = \oint \Gamma_{\phi} \nabla \phi \cdot d\vec{A} + \int_V S_{\phi} dV$$

Where

ρ = density

\vec{v} = velocity vector \vec{A} = surface area vector

Γ_{ϕ} = diffusion co-efficient for ϕ

$\nabla \phi$ = gradient of ϕ

S_{ϕ} = source of ϕ per unit volume

Above equation is applied to each control volume, or cell, in the computational domain.

Discretization of Equation on a given cell yields

$$\sum_f^{N_{faces}} \rho_f \vec{v}_f \phi_f \cdot \vec{A}_f = \sum_f^{N_{faces}} \Gamma_{\phi} (\nabla \phi)_n \cdot \vec{A}_f + S_{\phi} V$$

Where

N_{faces} = number of faces enclosing cell

ϕ_f = value of ϕ convected through face f

$\rho_f \vec{v}_f \cdot \vec{A}_f$ = mass flux through the face

A_f = area of face f , $|A_f|$

$(\nabla \phi)_n$ = magnitude of $\nabla \phi$ normal to face f

V = cell volume

The equations take the same general form as the one given above and apply readily to multi-dimensional, unstructured meshes composed of arbitrary polyhedral, the discrete values of the

scalar ϕ at the cell centers. However, face values ϕ_f is required for the convection terms in Equation and must be interpolated from the cell center values. This is accomplished using an upwind scheme.

Up winding means that the face value ϕ_f is derived from quantities in the cell upstream, or “upwind,” relative to the direction of the normal velocity v_n .

4.4 CONVERGENCE CRITERIA

Finally, one needs to set the convergence criteria for the iterative method. Usually, there are two levels of iterations, within which the linear equations are solved and outer iteration that deal with the non-linearity and coupling of the equations. Deciding when to stop the iterative process on each level is important, from both the efficiency and accuracy point of view. A numerical is said to be convergent if the solution of the discretized equations tend to exact the solution of the differential as the grid spacing tends to be zero. For convergence criteria around 10^{-6} for X velocity variable, the results are stable in the present problem.

4.5 IMPLEMENTATION OF BOUNDARY CONDITIONS

Each CV provides one algebraic equation. Volume integrals are calculated for every control volume, but flux through Cv faces coinciding with the domain boundary requires special treatment. These boundary fluxes must be known, or be expressed as a combination of interior values and boundary data. Two types of boundary conditions need to be specified.

4.5.1 Inlet boundary condition

The present analysis involves the velocity with and without swirl. The incorporation of velocity without swirl can be specified by any one of the velocity specification methods described in FLUENT. Turbulence intensity is specified as

$$I = 0.16(\text{Re}_{\text{DH}})^{-1/8} \times 100$$

The inlet based on the Reynolds number with respect to equivalent flow diameter.

Where, Re_{DH} is the Reynolds number based on the hydraulic diameter.

For specifying the velocity in case of flow with swirl, tangential component of velocity will also have to be defined along with axial component. Inlet velocity of 60 m/s with flat profile is considered for both the cases.

4.5.2 Outlet boundary condition

Atmospheric pressure condition is applied at the outlet boundary condition and set a “back flow” conditions is also specified if the flow reverses direction at the pressure outlet boundary during the solution process. In the “back flow” condition turbulence intensity is specified based on the equivalent flow diameter.

4.5.3 Wall boundary condition

Wall boundary conditions are used to bind fluid and solid regions. In viscous flows the no slip boundary condition is enforced at the walls. Wall roughness affects the drag (resistance) and heat and mass transfer on the walls. Hence roughness effects were considered for the present analysis and a specified roughness based on law of wall modified for roughness is considered. Two inputs to be specified are the physical roughness height and the roughness constant. And the default roughness constant (0.5) is assigned which indicates the uniform sand grain roughness.

4.6 SIMULATION PROCEDURE

(STEP 1) Modeling (In Gambit):

- Diffuser geometry is created
- Stabilizing length equal to D was attached at inlet.

- Boundary layer was attached to both the hub and casing wall with growth factor 1.1 and 10 rows.
- The model has been meshed with quadratic-mesh. Fine meshing with spacing 0.07 was done and mesh elements range from 12000 – 75000 elements.
- Boundary conditions taken were for velocity at inlet, pressure at outlet and wall type for both the hub and casing.
- Fluid was specified as air for the continuum type and the mesh was exported to Fluent for post processing.

(STEP 2) Post Processing (In Fluent):

- Grid was checked and scaled.
- 2D axisymmetric solver and segregated solution method was chosen.
- Air was chosen as the fluid for flow, and its properties were selected.
- K- ϵ RNG models is selected.
- At air inlet section, the inlet velocity of 60 m/s with different swirl intensity was specified.
- Turbulence intensity of 3% based on inlet flow diameter was specified. At the exit section, the pressure was specified being equal to atmospheric pressure.
- Second order upwind scheme was selected to solve continuity and momentum equations.
- Convergence criteria of 10^{-6} were taken.
- Solution was initialized at inlet and made to iterate until it converges.

Once solution is converged, various data for pressure and velocity were obtained and graphs were plotted.

5.1 GRID INDEPENDENCE

The grid independence is studied for the k- ϵ RNG model employing four sizes of grids to examine the sensitivity of grid. As we decrease the mesh size we get a more fine mesh and better results, but due to more numbers of nodes the computation time increases. So we have to optimize the grid size with the accuracy required. We took the following mesh sizes:

	Element Type	Mesh Size	No. of Cells	No. of Face	No. of Nodes	Computation Time (hrs)
Coarse mesh	Quad.	0.09	37076	74812	37737	3.5
Fine mesh	Quad.	0.08	45024	90787	45764	6.1
Finer mesh	Quad.	0.07	56064	112969	56906	12.2
Finer mesh	Quad.	0.06	73554	148087	74534	19.9

5.1.1 Validation with experimental results [5]:-

Velocity Graph:

- Figure 5.2 shows with k- ϵ RNG model the results of mesh size of 0.08 and 0.09 cm shows deviation in their values, thus need to go for more finer mesh.
- The results of mesh size 0.06 and 0.07 remain almost same, thus mesh size of 0.07 cm is considered optimum for the CFD modeling of diffuser.

5.2 TURBULENCE MODEL VALIDATION:

FLUENT provide many models to model the turbulence in the flow. But the following turbulence models and were test against experimental results [5]:

- k- ϵ models
 - Standard k- ϵ model
 - Renormalization-group (RNG) k- ϵ model
 - Realizable k- ϵ model

- Reynolds stress model (RSM)

These models were tested against an experimental profile with hub is parallel and casing diverging at angle of 10° with swirl of 0° and 12° separately. At a velocity profile of 60m/s.

5.2.1 Validation with Experimental results [5]:

Longitudinal velocity Graph with velocity of 60m/s and no swirl (0°):

Figure 5.1 shows that k- ϵ RNG model most nearer to the experimental Results [5].

- At $x = 0.3L$: RNG and Realizable are very near to the experimental results.
- At $x = 0.5L$: RNG and Realizable are very near to the experimental results, but Realizable start deviating from experimental results.
- At $x = 0.7L$: Only RNG model is in accordance to the experimental results.
- At $x = 0.9L$: Only RNG model has least variation from experimental results.

Longitudinal and Swirl velocity graph with velocity of 60m/s and swirl (12°):

Figure 5.3 and 5.4: shows that k- ϵ RNG model most nearer to the experimental results [5].

- At $x = 0.3L$: Almost every model varies from experimental results.
- At $x = 0.5L$: RNG and Reynolds Stress model are near to the experimental results.
- At $x = 0.7L$: Only RNG model is in accordance to the experimental results.
- At $x = 0.9L$: Only RNG model results are nearer to the experimental results.

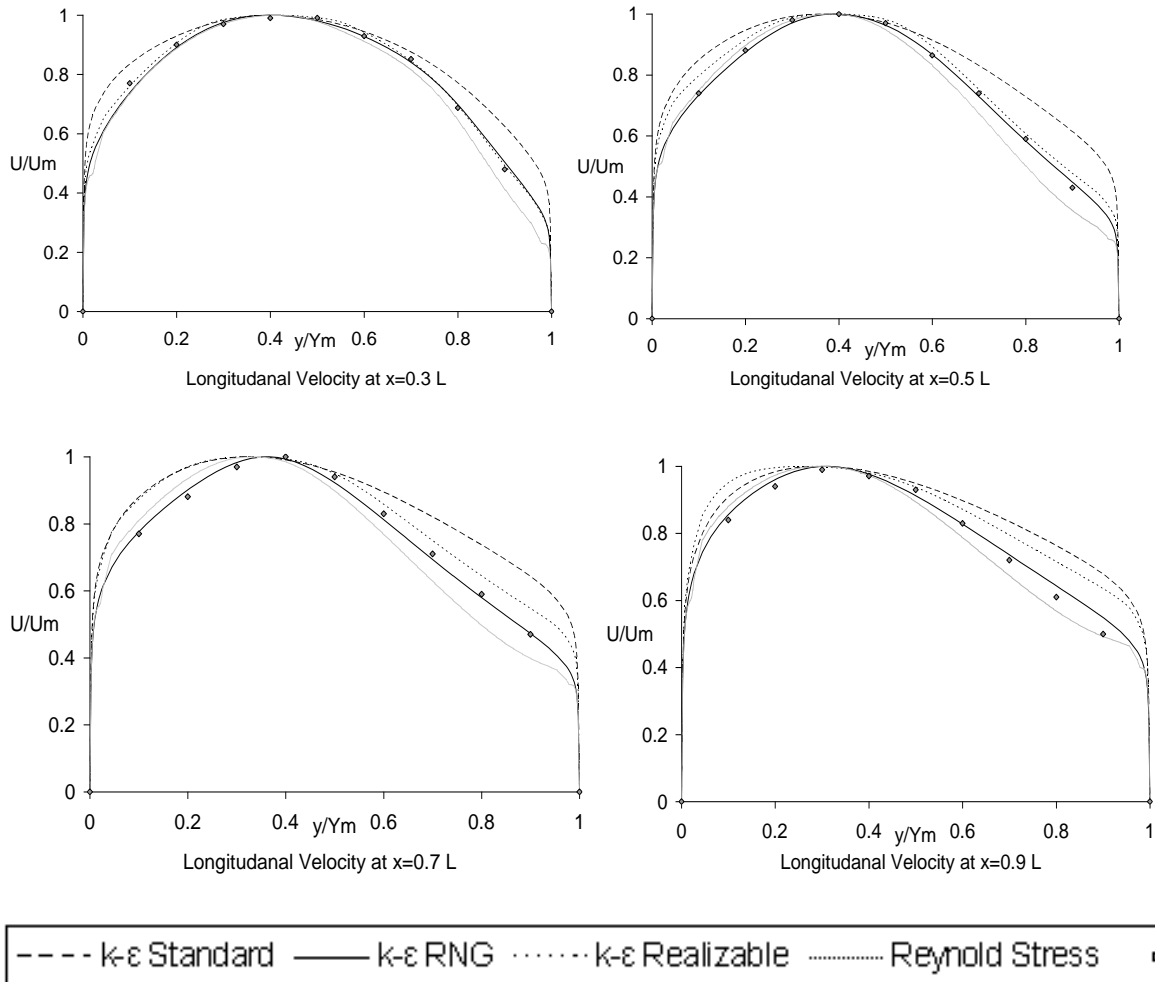
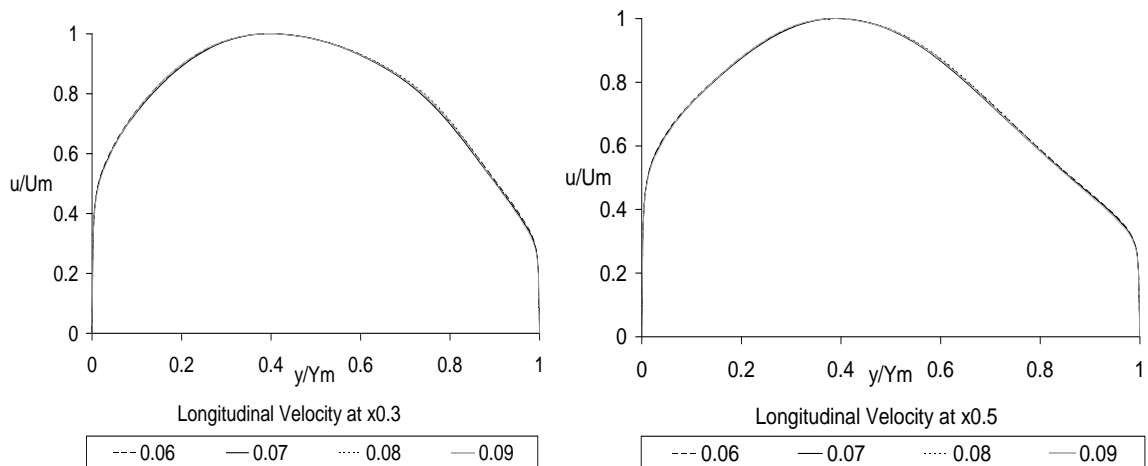


Figure 5.1: Longitudinal Velocity (0°) Exp10/10, AR 2



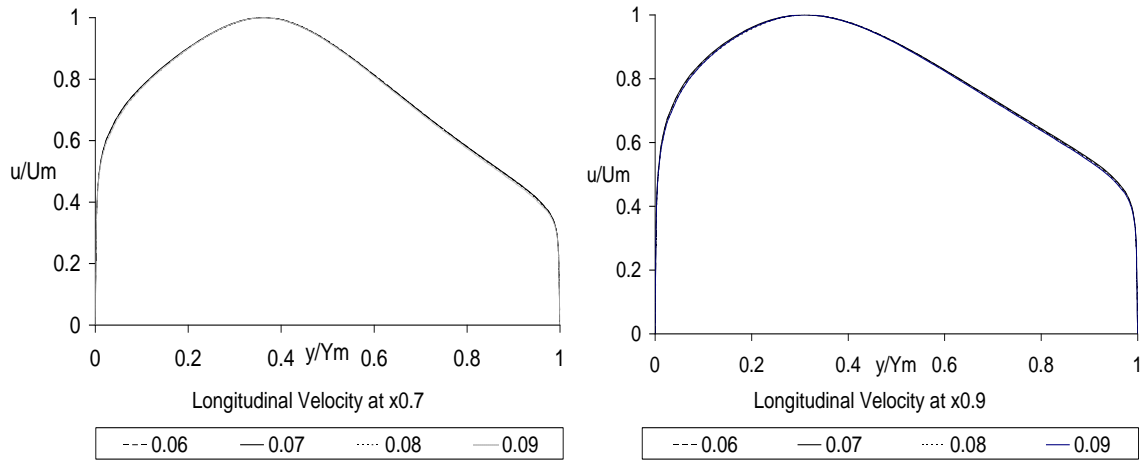


Figure 5.2: Longitudinal Velocity (0°), AR 2

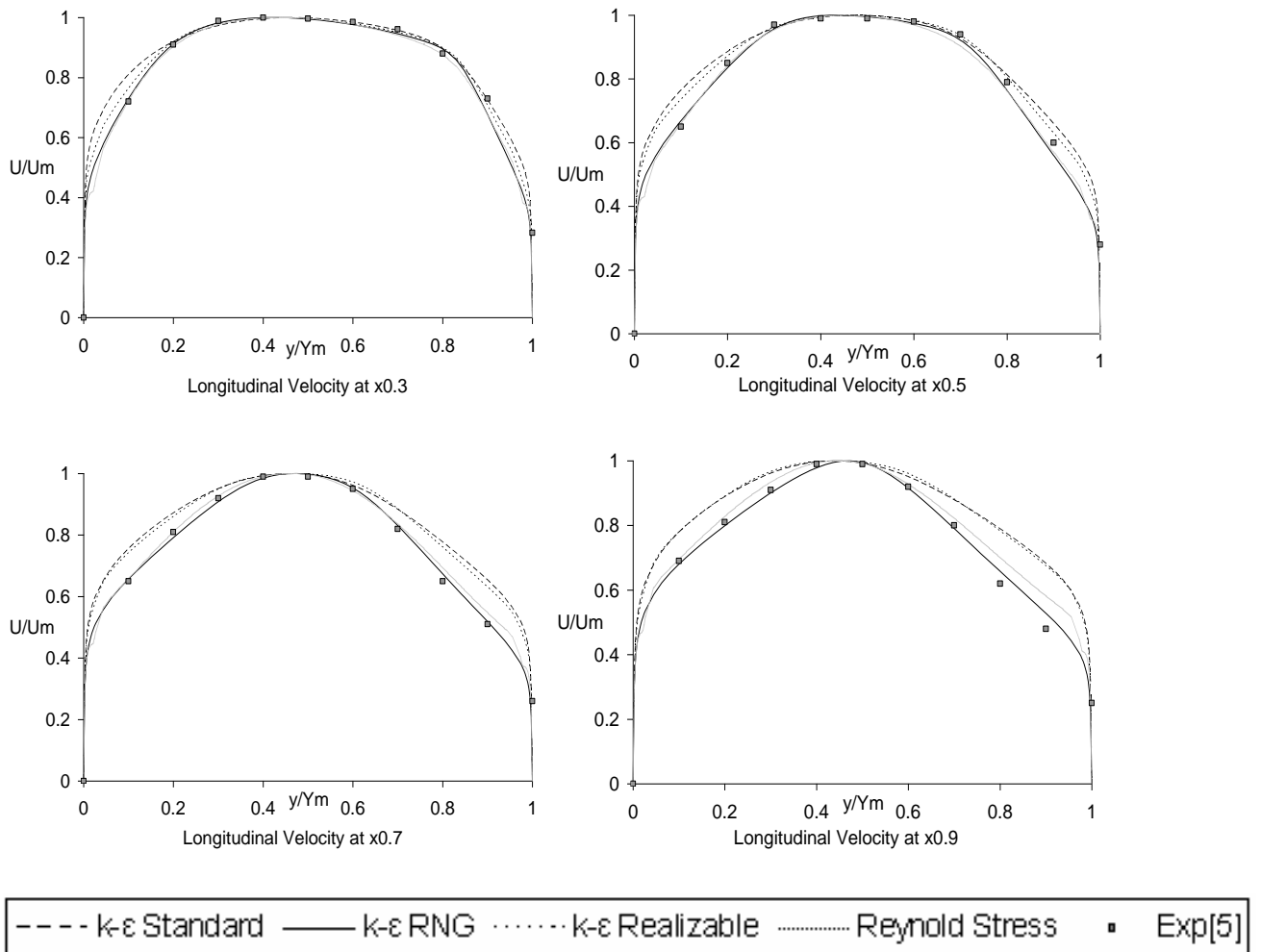


Figure 5.3: Longitudinal Velocity (12°), AR 2

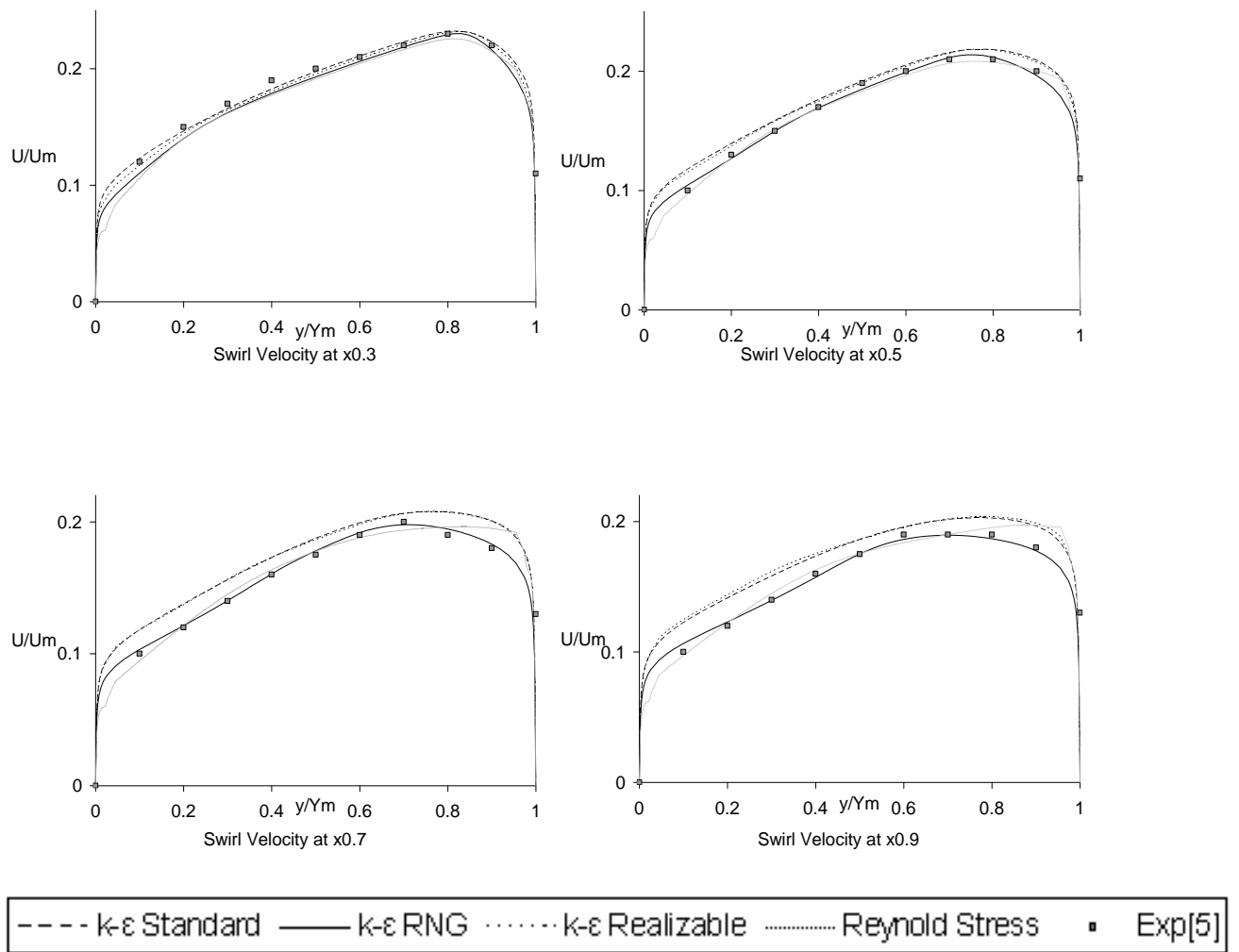


Figure 5.4: Swirl Velocity (12°), AR 2

RESULT AND DISCUSSION

In the present thesis subsonic turbulent flows inside the different type of axial annular diffusers with the help of GAMBIT and FLUENT. In different type of diffuser also varying area ratio and casing angle. Analysis gives the effect of geometry on the pressure recovery coefficient. The following conclusions can be drawn from the results.

Fig 1-30 show the results generated by FLUENT. In these figures fluid characteristics like a pressure coefficient, velocity magnitude and velocity vectors are shown by different colors. A particular color does not give a single value of these characteristics but shows a range of these values. If the value of a characteristic at a particular point falls in this range, there will be color of that range

CASE 1: HUB PARALLEL AND CASING DIVERGING AT ANGLE 6°

1. In the straight core annular diffuser for area ratio 2 and 0 degree inlet swirl, in the section $x=0.1$ the maximum Tangential velocity is found at $y/Y_m=0.466$. Further from the section $x =0.3, 0.5, 0.7, 0.9$ it transfer towards the hub side at point $y/Y_m =0.453, 0.447, 0.441, 0.428$. In this case there is no separation found at hub or casing. And static pressure first rapidly, then slowly increasing at casing. And it is maximum at $x/L=1$. At hub it is continuously increasing and found maximum at $x/L=1$. This is shown in Fig. 31, 61.
2. At fix area ratio and increasing the swirl 7.5 degree. There for we find that the maximum tangential velocity found at $y/Y_m=0.428$ in the section $x=0.1$, then it is continuously decreasing and sifted towards the hub side. And maximum swirl velocity is also found at casing at point $y/Y_m=0.913$ then it is decreases from casing to hub. In this case very slightly separation is found at casing. And the static pressure is also increases. And found maximum at $x/L=1$. It can be seen in Fig. 32, 63, 62.

3. On increasing the swirl angle 12, 17, and 25 we find that the separation is also increasing. And the static pressure at hub is decreasing and at casing it is increasing. Refer Fig. 33, 34, 35, 64, 65, 66, 67, 68, 69.
4. In the straight core annular diffuser for area ratio 3 and 0 degree inlet swirl, in the section $x=0.1$ the maximum Tangential velocity is found at $y/Y_m=0.457$. Further from the section $x =0.3, 0.5, 0.7, 0.9$ it transfer towards the casing side at point $y/Y_m =0.448, 0.434, 0.410, 0.391$. In this case there is slightly separation found at casing. And static pressure first rapidly, then slowly increasing at casing. And it is maximum at $x/L=1$. At hub it is continuously increasing and found maximum at $x/L=1$. This is given in Fig. 70, 36.
5. In this case we find that at swirl angle 0 and 7.5 the separation occur at casing. And the swirl velocity sifted from casing to hub. That means the separation position become change. It may be occur due to the reverse flow. Refer Fig. 71
6. But on increasing the swirl angle 12, 17, and 25 we find that the separation at hub side. The maximum tangential velocity transfer from casing side to hub. And the swirl velocity is decreases from hub to casing side. And the static pressure at hub is decreasing and at casing it is increasing. This is shown in Fig. 72, 73, 74, 75, 76, 38, 39, 40.
7. In the straight core annular diffuser for area ratio 4 and 0 degree inlet swirl, in the section $x=0.1$ the maximum Tangential velocity is found at $y/Y_m=0.456$. And the maximum tangential velocity shifted from casing to hub side. Further from the section $x =0.3, 0.5, 0.7, 0.9$ it transfer towards the casing side at point $y/Y_m =0.436, 0.411, 0.387, 0.343$. In this case there is slightly separation found at casing. And static pressure first rapidly, then slowly increasing at casing. And it is maximum at

$x/L=1$. At hub it is continuously increasing and found maximum at $x/L=1$. Refer Fig. 77, 41.

8. At area ratio 4 and increasing the swirl 7.5 degree. There for we find that the maximum tangential velocity found at $y/Y_m=0.421$ in the section $x=0.1$, then it is continuously decreasing and sifted towards the hub side. And maximum swirl velocity is also found at casing at point $y/Y_m=0.867$ then it is decreases from casing to hub. In this case separation is found at casing. And the static pressure is also increases. And found maximum at $x/L=1$. This can be observed from Fig. 78, 79, 42.
9. But on increasing the swirl angle 12, 17, and 25 the separation occur at hub side. The maximum tangential velocity transfer from casing side to hub. And the swirl velocity is decreases from hub to casing side. And the static pressure at hub is decreasing and at casing it is increasing. Refer fig. 80, 81, 82, 83, 84, 43, 44, 45.

CASE 2: HUB PARALLEL AND CASING DIVERGING AT ANGLE 8°

1. In the straight core annular diffuser for area ratio 2 and 0 degree inlet swirl, in the section $x=0.1$ the maximum Tangential velocity is found at $y/Y_m=0.466$. Further from the section $x =0.3, 0.5, 0.7, 0.9$ it transfer towards the hub side at point $y/Y_m =0.441, 0.422, 0.410, 391$. In this case there is no separation found at hub or casing. And static pressure first rapidly, then slowly increasing at casing. And it is maximum at $x/L=1$. At hub it is continuously increasing and found maximum at $x/L=1$. Refer Fig. 85, 46.
2. At fix area ratio and increasing the swirl 7.5 degree. There for we find that the maximum tangential velocity found at $y/Y_m=0.416$ in the section $x=0.1$, then it is continuously decreasing and sifted towards the hub side. And maximum swirl

- velocity is also found at casing at point $y/Y_m=0.882$ then it is decreases from casing to hub. In this case very slightly separation is found at casing. And the static pressure is also increases. And found maximum at $x/L=1$. It is shown in Fig. 86, 87, 47.
3. On increasing the swirl angle 12, 17, and 25 we find that the separation is also increasing. And the static pressure at hub is decreasing and at casing it is increasing. Refer Fig. 88, 89, 90, 91, 92, 48, 49, 50.
 4. In the straight core annular diffuser for area ratio 3 and 0 degree inlet swirl, in the section $x=0.1$ the maximum Tangential velocity is found at $y/Y_m=0.450$. Further from the section $x =0.3, 0.5, 0.7, 0.9$ it transfer towards the casing side at point $y/Y_m =0.426, 0.396, 0.366, 0.337$. In this case there is slightly separation found at casing. And static pressure first rapidly, then slowly increasing at casing. And it is maximum at $x/L=1$. At hub it is continuously increasing and found maximum at $x/L=1$. This is given in Fig. 93, 51.
 5. In this case we find that at swirl angle 0 and 7.5 the separation occur at casing. And the swirl velocity shifted from casing to hub. That means the separation position become change. It may be occur due to the reverse flow. Refer Fig. 94, 95.
 6. But on increasing the swirl angle 12, 17, and 25 we find that the separation at hub side. The maximum tangential velocity transfer from casing side to hub. And the swirl velocity is decreases from hub to casing side. And the static pressure at hub is decreasing and at casing it is increasing. This can be seen from Fig. 96, 97, 98, 99, 100, 101, 52, 53, 54, 55.
 7. In the straight core annular diffuser for area ratio 4 and 0 degree inlet swirl, in the section $x=0.1$ the maximum Tangential velocity is found at $y/Y_m=0.441$. And the maximum tangential velocity shifted from casing to hub side. Further from the

section $x = 0.3, 0.5, 0.7, 0.9$ it transfer towards the casing side at point $y/Y_m = 0.411, 0.372, 0.333, 0.303$. In this case there is slightly separation found at casing. And static pressure first rapidly, then slowly increasing at casing. And it is maximum at $x/L=1$. At hub it is continuously increasing and found maximum at $x/L=1$. This is given in Fig. 102, 56.

8. At area ratio 4 and increasing the swirl 7.5 degree. There for we find that the maximum tangential velocity found at $y/Y_m=0.402$ in the section $x=0.1$, then it is continuously decreasing and sifted towards the hub side. And maximum swirl velocity is also found at casing at point $y/Y_m=0.867$ then it is decreases from casing to hub. In this case separation is found at casing. And the static pressure is also increases. And found maximum at $x/L=1$. Please refer Fig. 103, 104, 57.
9. But on increasing the swirl angle 12, 17, and 25 the separation occur at hub side. The maximum tangential velocity transfer from casing side to hub. And the swirl velocity is decreases from hub to casing side. And the static pressure at hub is decreasing and at casing it is increasing. Refer Fig. 105, 106, 107, 108. 109, 110, 58, 59, 60.

CONCLUSION

On the basis of above results the following conclusion is withdrawn:

1. From the above discussion we can conclude that in the case of area ratio 3 and 4 the separation position change from hub to casing because of the reverse flow.
2. We also find that on increasing the area ratio the separation occur at 0 degree swirl.
3. As the angle of swirl is increased, the point of separation of flow shifts towards the hub of the diffuser.
4. On increasing the swirl angle the separation is also increases in every case.

5. It is observed from this work that in both the casing angles at area ratio 2 and swirl angle 7.5 degree, there is no separation found. This seems to be the best flow observed from all swirl angle and area ratio.

RECOMMENDATIONS FOR FUTURE WORK

1. Annular diffuser with parallel hub is considered in the present study. Future work can be done on other diffusers i.e. conical, rectangular, radial type diffusers, etc.
2. The present work was done for sub-sonic flow incompressible flow only. The further scope of work can be extended to compressible, sonic flows and hypersonic flows.
3. The present analysis is done for a diverging portion of diffuser. As the geometry is an important parameter, which indicates the overall diffusion and hence varying the geometry type, we can further extend studies.
4. The analysis is basically performed with an advanced k- ϵ RNG model for swirling flows. Using higher order discretization schemes and better turbulence models can be used for better results in case of swirling flows
5. The present analysis is done for stationary hub and casing. Further studies can be done on rotating hub and casing diffuser.
6. Modeling of the geometry can be modified by attaching a tailpipe at the exit to recover some of the excess kinetic energy of a non-uniform diffuser exit profile in to pressure energy.

REFERENCES

1. Ackert, J. 1967. "Aspect of Internal Flow. Fluid Mechanics of Internal Flow" Ed. Sovaran G., Elsevier Amsterdam, ppl.
2. Adkins R.C, Jacobsen OH, Chevealier P, 1983, "A Premilary Study of Annular Diffuser with Constant Diameter Outer Wall" ASIVIE paper no. 83-GT-218.
3. Adkins R.C., 1983. "A simple Method for Design Optimum Annular Diffusers" ASTVE Paper No. 83-GT-42.
4. Awai T., Nakagawa T., Sakai T., 1986. "Study of Axially Curved Mixed Flow Vaneless Diffuser". Bull JSME 29, 1759-1764.
5. Arora, B.B., 2007, "Aerodynamic Analysis of Diffuser", PhD Thesis, 2007, DU, Delhi.
6. Arora, B.B, Pathak, B.D. 2005 "Flow characteristics of parallel hub diverging casing axial annular diffusers". ISME publication pp 794-798.
7. Cockrell, D.J., Markland, E., 1963. "A Review of Incompressible Diffuser Flow" Aircraft Engg. Volume 35, pp 286.
8. Coladipietro R., Schneider, J.M., Sridhar, K.1974. "Effects of Inlet Flow Conditions on the Performance of Equiangular Annular Diffusers," Trans. CSME 3 (2): pp. 75-82.
9. Dovzhik, S.A., Kartavenko, V.M., 1975. "Measurement of the Effect of Flow Swirl on the Efficiency of Annular Ducts and exhaust Nozzles of Axial Turbo-machines," Fluid Mechanics/Soviet Research 4(4): 156-172.
10. Goebel J. H., Japikse D., 1981. "The Performance of an Annular Diffuser Subject to Various Inlet Blockage and Rotor Discharge Effects ". Consortium Final Report, Creare TN-325.

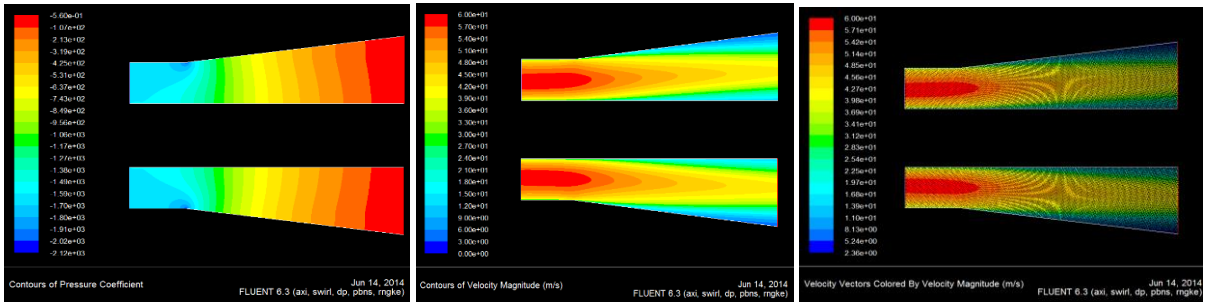
11. Hesterman R., Kim S., Ban Khalid A., Witting S., 1995. "Flow Field and Performances Characteristics of Combustor Diffusers". ASME Journal Engineering for Gas Turbine and Power 117, pp 686-694.
12. Hoadley D., 1970. "Three Dimensional Turbulent Boundary Layers in an Annular Diffuser ". Ph.D. Thesis University of Cambridge.
13. Hoadley D., Hughes D .W, 1969. "Swirling Flow in an Annular Diffuser". University of Cambridge, Department of Engineering, Report CUED/ATurbo/TR5.
14. Howard J. H. G., Thornton, Trump A. B., Henseler H. J., 1967. "Performance and Flow Regime for Annular Diffusers ". ASME Paper No. 67-WA/FE-2 1.
15. Ishkawa K. Nakamura I, 1989. "An Experimental Study on the Performance of Mixed Flow Type Conical Wall Annular Diffuser", ASIVIE FED-69.
16. Markland, 1986. "A New Diffuser Mapping Technique — Studies in Component Performance: Part 1," ASIVIE Paper No. 84-GT-237, Amsterdam, June 1984; also, Journal of Fluids Engineering, Vol. 108, No. 2. pp. 148-156.
17. Japikse, D., and Pampreen, R., 1978. "Annular Diffuser Performance for an Automotive Gas Turbine," ASIVIE Publication 78-GT-147.
18. Japikse, D., 1980. "The Influence of Inlet Turbulence on Diffuser Performance," Concepts ETI, Inc., Design Data Sheet No. 1.
19. Japikse, D., 2000. "Performance of Annular Diffusers Subject to Inlet Flow Field Variations and Exit Distortion," Presented at the ISROMAC conference in Honolulu, Hawaii, March 26-30.
20. Johanston I.H., 1959. "Effect of Inlet Conditions on the Flow in Annular Diffusers." National Gas Turbine Establishment Memo No. 167, Cp No.178.
21. Johnston J. P., 1959. "Summary of Results of Test on Short Conical Diffuser with Flow Control Inserts": as of June 1, 1959.Ingersoll —Rand TN No. 71.

22. Juhasz. A. J. 1974. "Performance Of An Asymmetric Annular Diffuser With Non Diverging Inner Wall Using Suction", NASA TN -7575.
23. Kamonicek V., Hibs M., 1974. "Results of Experimental and Theoretical Investigation of Annular Diffuser." CSIRO, Division of Mechanical Engg.
24. Klein, A., 1995. "Characteristics of Combustor Diffusers." Program Aerospace Science 31: 171-271.
25. Mahalakshmi N.V., Krithiga G., Sandhya S., Vikraman J., Ganesan V., 2007, "Experimental investigations of flow through conical diffusers with and without wake type velocity distortions at inlet" Experimental Thermal and Fluid Science, 2007.
26. Moller E.S, 1965. "Radial Diffuser Using Incompressible Flow between Disks." ASIVIE paper no. 65-FE-12.
27. Moller E.S., 1965. "Radial Flow without Swirl between Parallel Disks Having both Supersonic and Subsonic Regions." ASME Paper No. 65-FE-li.
28. Shaalan, M.R.A., Shabaka, I.M.M., 1975. "An Experimental Investigation of the Swirling Flow Performance of an Annular Diffuser at Low Speed," ASIVIE Paper No. 75-WA/FE-17.
29. Sharan V. K, 1972. "Diffuser Performance Co-Relations". JASI, Volume 24, pp 415.
30. Sovran, G., Klomp, E.D., 1967. "Experimentally Determined Optimum Geometries for Rectilinear Diffusers with Rectangular, Conical or Annular Cross- Section," Fluid Dynamics of Internal Flow, Elsevier Publishing Company.
31. Srinath T, 1968, "An Investigation of the Effects of Swirl on the Flow Regimes and Performance of Annular Diffuser with Equal Inner and Outer Cone Angles". M.A. Science Thesis, University of Waterloo Canada.

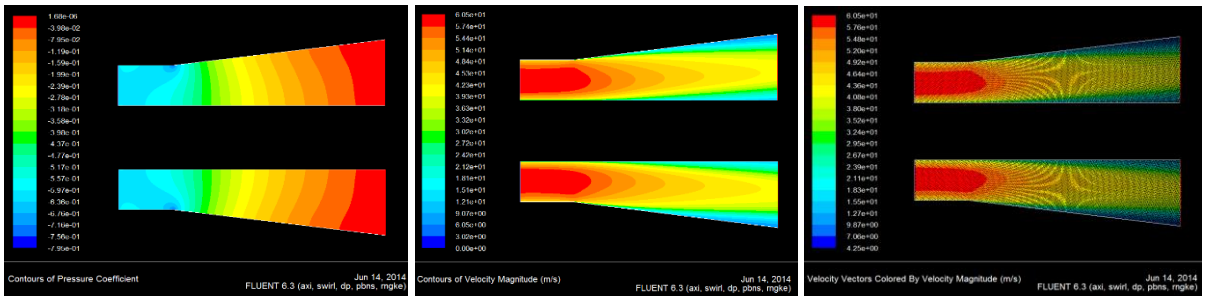
32. Stafford W. Wilbur, James T.H. 1957. "Investigation of Short Annular Diffuser Configuration Utilizing Suction as a Means of Boundary Layer Control", NACA TN-3996.
33. Stafford, W. Wilbur, James T. Higginbotham, 1955. "Investigation of Two Short Annular Diffuser Configurations Utilizing Suction and Injection as Means of Boundary Layer Control". NACA RI\4 L54K18.
34. Stevan S. J., Williams G.J., 1980. "The Influence of Inlet Conditions on the Performance of Annular Diffuser." Trans. ASIVIE Journal Fluids Engg. 2002, 357-363.
35. Stevens S. J., Fry P., 1973. "Measurements of the Boundary Layer Growth in Annular Diffusers". Journal Aircraft Feb., pp 73-89.
36. Stevens S. J., Williams G. J., 1969. "Performance of Annular Diffusers" Gas Turbine Collaboration Committee Report No. 299.
37. Stevens S. J., Williams G. J., 1980. "The Influence of Inlet Conditions on the Performance of Annular Diffuser". Trans. ASME Journal Fluids Egg. 102, 357-363.
38. Takehira A., 1977. "An Experimental Study of the Annular Diffusers in Axial-Flow Compressors and Turbines" Japan Society of Mechanical Engineers, Paper No.39, 1977.
39. Thayer E B, 1971 "Evaluation of Curved Wall Annular Diffuser" ASIVIE paper no .71 -WA/FE-3 5.
40. Wood, C .C. Henry, JR., 1958. "Effects of Shock Boundary Layer Interaction on the Long and Short Subsonic Annular Diffuser", NACA RIVI L58A3 1.
41. Anderson M. G, 2008 "FLUENT CFD versus Sovran & Klomp Diffuser Data Benchmark study" 46th AIAA Aerospace Sciences Meeting and Exhibit 7-10 January 2008, Reno, Nevada at American Institute of Aeronautics and Astronautics pp 1-26.

42. Arora B.B, Manoj Kumar and Subhashish Mazi, 2010. "Analysis of Flow Separation in Wide Angle Annular Diffusers". International Journal of Applied Engineering Research ISSN 0973-4562 Volume 5 Number 20 (2010) pp. 3419-3428.
43. Arora B.B, Manoj Kumar and Subhashish Mazi, 2010. " A Study of Inlet Conditions on Diffuser Performance" Journal International Journal of Theoretical and Applied Mechanics" ISSN 0973-6085 Volume 5 Number 2(2010) pp. 201-221.
44. BB Arora, BD Pathak, 2009. "Effect of Geometry on the Performance of Annular Diffuser". International Journal of Applied Engineering Research, volume 4.
45. BB Arora, 2014. "Performance analysis of parallel hub diverging casing axial annular diffuser with 20° equivalent cone angle" Australian Journal of Mechanical Engineering Volume 12.
46. Manoj kumar, BB Arora, S Maji, 2013. "The effect of area ratio on the performance annular diffuser" International Journal of Applied Engineering Research, volume 7.
47. Walter Gyllenram, 2006 "Analytical and numerical investigation of steady and unsteady turbulent swirling flow in diffuser" thesis for licentiate of engineering no. 2006:05 ISSN 1652-8565
48. Najafi, A. F., 2004. "Investigation of Internal Turbulent Swirling Flow, Single Phase and Two Phase Flow", Ph. D. dissertation, Sharif University of Technology, 24–30.
49. Kochevsky A.N., 2000. "Numerical Investigation of Swirling Flow in Annular Diffusers with a Rotating Hub Installed at the Exit of Hydraulic Machines" J. Fluids Eng. 123(3), 484-489.
50. Steenbergen, W., and Voskamp, J., 1998. "The rate of decay of swirl in turbulent pipe flow". Flow Measurements and Instrumentations, 9, pp. 67–78

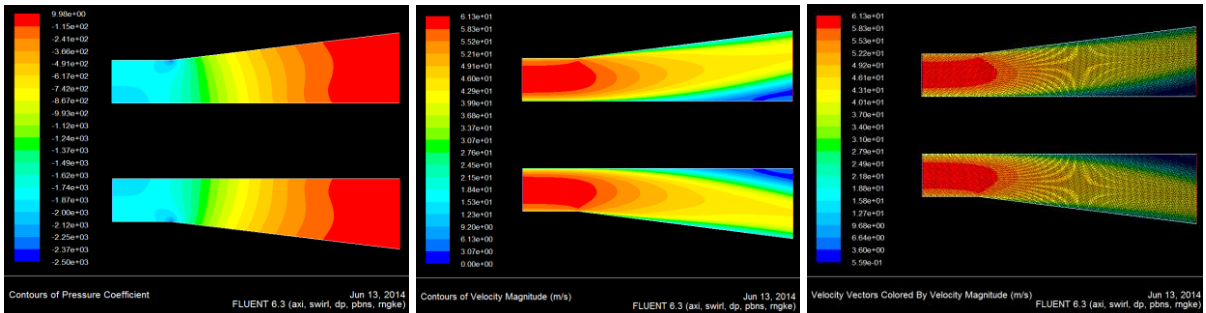
51. Krystyna prync-skotniczny, 2006. "Numerical analysis of the impact of the conical diffuser geometry change on velocity distribution in its outlet cross section". Mechanics Vol 25 no. 2.
52. Stefano Ubertini and Uberto Desideri, 2000. "Experimental Performance Analysis of an Annular Diffuser With and Without Struts", Experimental Thermal and Fluid Science, Vol. 22, pp.183-195.
53. Stefano Ubertini and Uberto Desideri, 2000. "Flow Development and Turbulence Length Scales within an Annular Gas Turbine Exhaust Diffuser", Experimental Thermal and Fluid Science, Vol. 22, pp.55-70.
54. M.A. Leschziner, 2004. "Modelling turbulent separated flow in the context of aerodynamic applications" Fluid Dynamics Research 38 (2004) 174 – 210
55. Tom Bajcar & Brane Širok & Marko Hočevvar & Ferdinand Trenc, 2006. "Heat Transfer Influenced by Turbulent Airflow inside an Axially Rotating Diffuser". Flow Turbulence Combust (2006) 80:3–19
56. Olle Törnblom, 2006 "Experimental and computational studies of turbulent separating internal flows". ISBN 91-7178-416-0.
57. Ivana Buntic-Ogor, Walter Gyllenram, Eugene Ohlberg, Håkan Nilsson & Albert Ruprecht, 2006. "An Adaptive Turbulence Model for Swirling Flow" Conference on Turbulence and Interactions TI2006, May 29 – June 2.



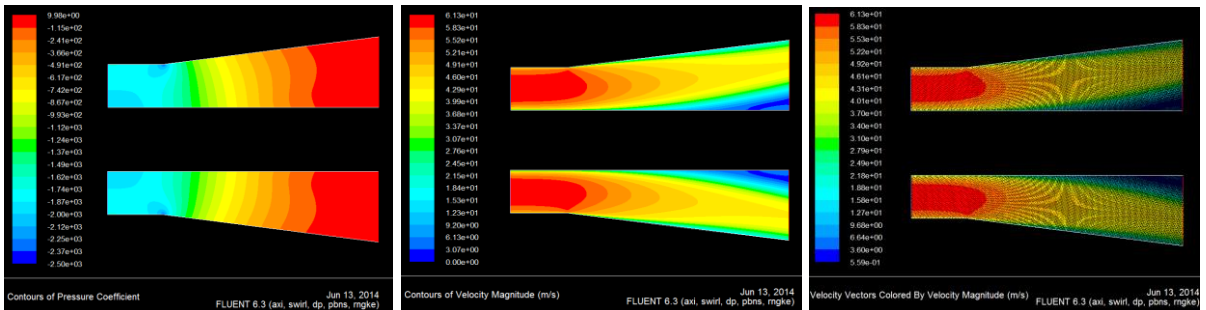
Pressure Coefficient Contours Velocity Magnitude Contours Velocity Vectors
Fig.1 AR2, Casing Wall Angle=6°, Swirl Angle=0°, Velocity=60 m/s



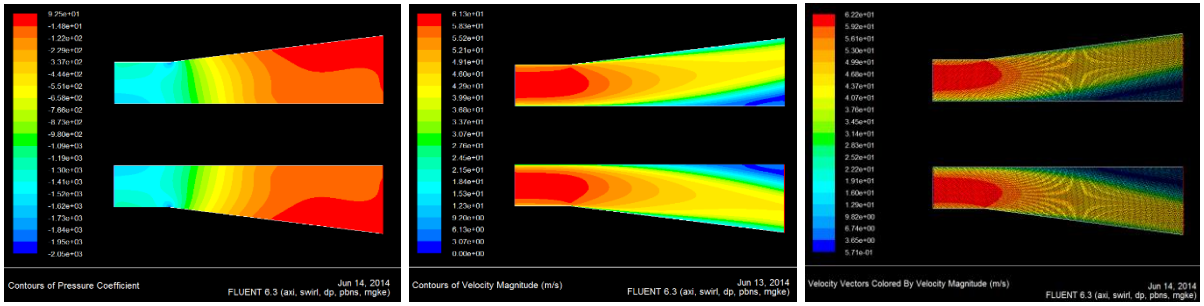
Pressure Coefficient Contours Velocity Magnitude Contours Velocity Vectors
Fig. 2 AR2, Casing Wall Angle=6°, Swirl Angle=7.5°, Velocity=60 m/s



Pressure Coefficient Contours Velocity Magnitude Contours Velocity Vectors
Fig. 3 AR2, Casing Wall Angle=6°, Swirl Angle=12°, Velocity=60 m/s

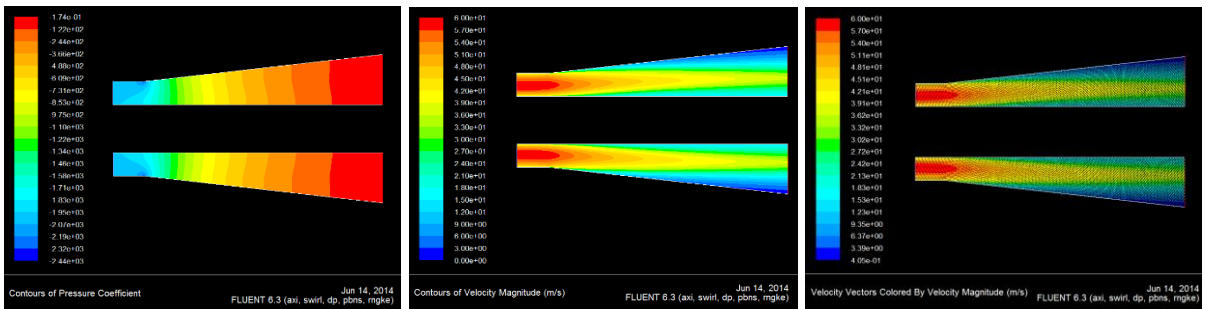


Pressure Coefficient Contours Velocity Magnitude Contours Velocity Vectors
Fig. 4 AR2, Casing Wall Angle=6°, Swirl Angle=17°, Velocity=60 m/s



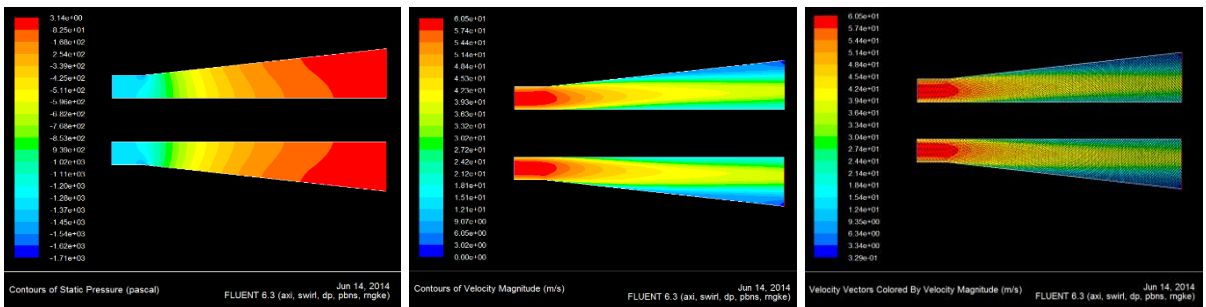
Pressure Coefficient Contours Velocity Magnitude Contours Velocity Vectors

Fig. 5 AR2, Casing Wall Angle=6°, Swirl Angle=25°, Velocity=60 m/s



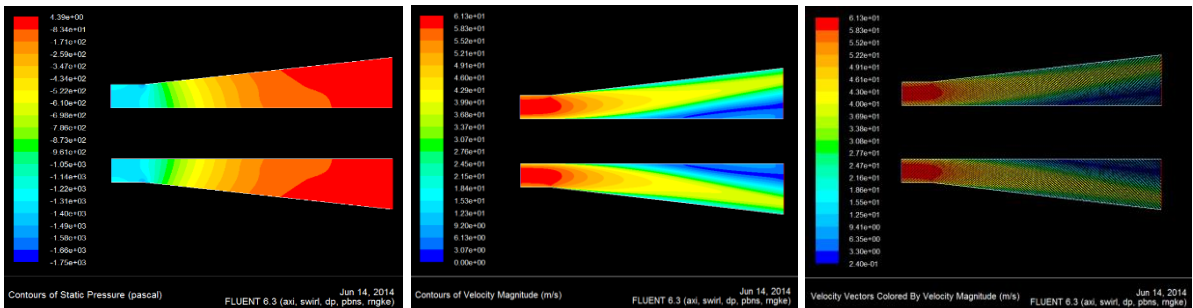
Pressure Coefficient Contours Velocity Magnitude Contours Velocity Vectors

Fig. 6 AR3, Casing Wall Angle=6°, Swirl Angle=0°, Velocity=60 m/s



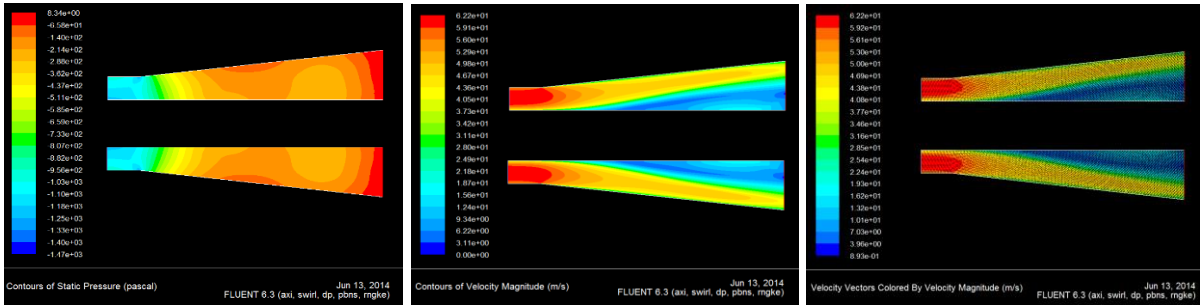
Pressure Coefficient Contours Velocity Magnitude Contours Velocity Vectors

Fig. 7 AR3, Casing Wall Angle=6°, Swirl Angle=7.5°, Velocity=60 m/s



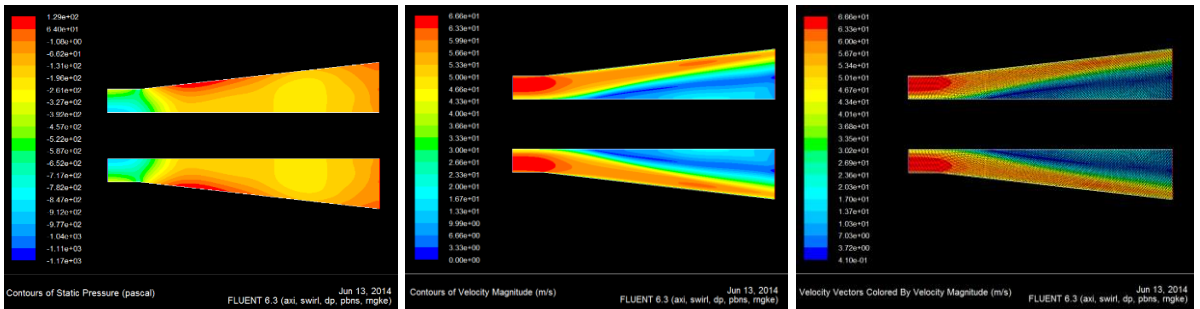
Pressure Coefficient Contours Velocity Magnitude Contours Velocity Vectors

Fig. 8 AR3, Casing Wall Angle=6°, Swirl Angle=12°, Velocity=60 m/s



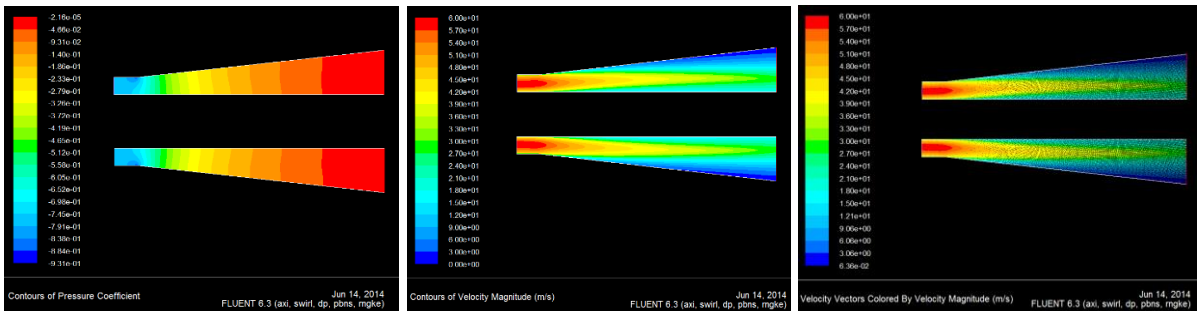
Pressure Coefficient Contours Velocity Magnitude Contours Velocity Vectors

Fig. 9 AR3, Casing Wall Angle=6°, Swirl Angle=17°, Velocity=60 m/s



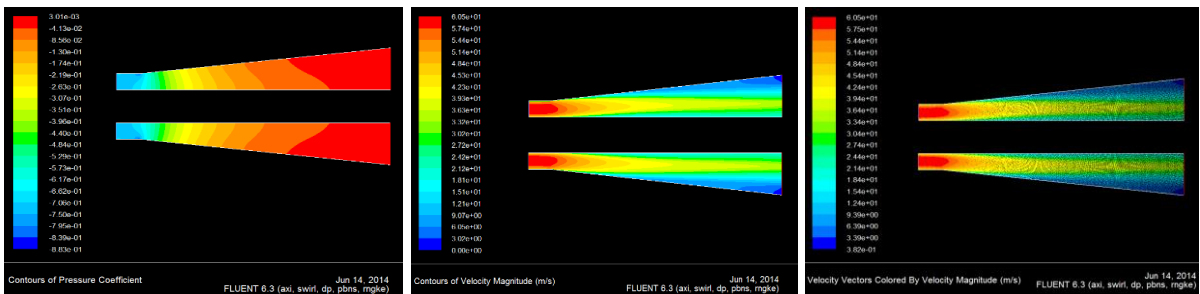
Pressure Coefficient Contours Velocity Magnitude Contours Velocity Vectors

Fig. 10 AR3, Casing Wall Angle=6°, Swirl Angle=25°, Velocity=60 m/s



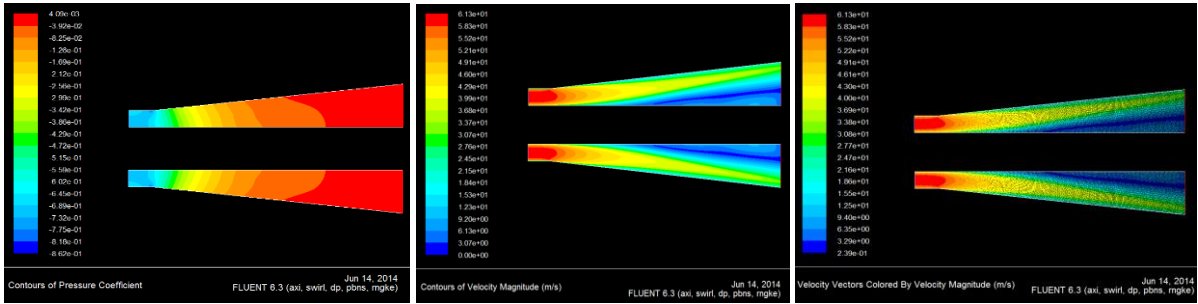
Pressure Coefficient Contours Velocity Magnitude Contours Velocity Vectors

Fig. 11 AR4, Casing Wall Angle=6°, Swirl Angle=0°, Velocity=60 m/s



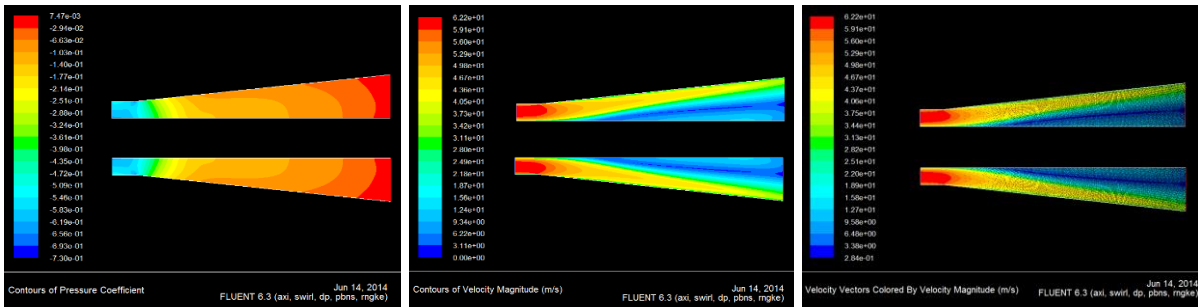
Pressure Coefficient Contours Velocity Magnitude Contours Velocity Vectors

Fig. 12 AR4, Casing Wall Angle=6°, Swirl Angle=7.5°, Velocity=60 m/s



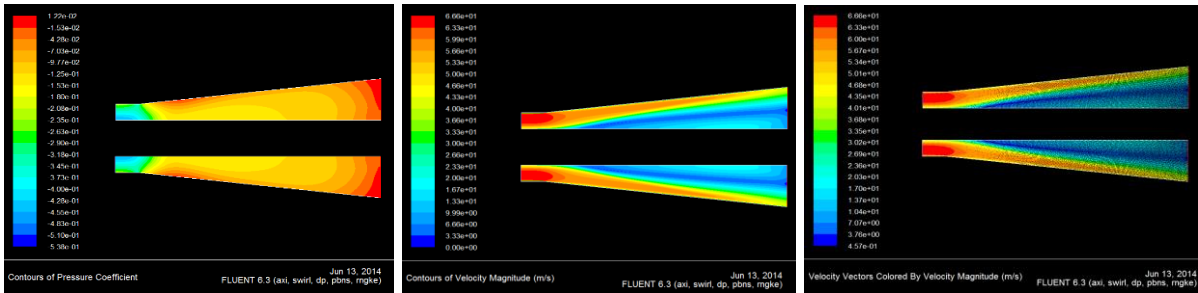
Pressure Coefficient Contours Velocity Magnitude Contours Velocity Vectors

Fig. 13 AR4, Casing Wall Angle=6°, Swirl Angle=12°, Velocity=60 m/s



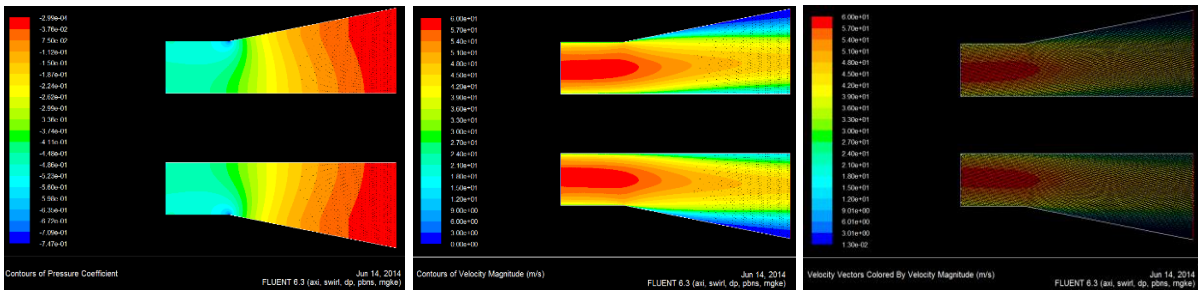
Pressure Coefficient Contours Velocity Magnitude Contours Velocity Vectors

Fig. 14 AR4, Casing Wall Angle=6°, Swirl Angle=17°, Velocity=60 m/s



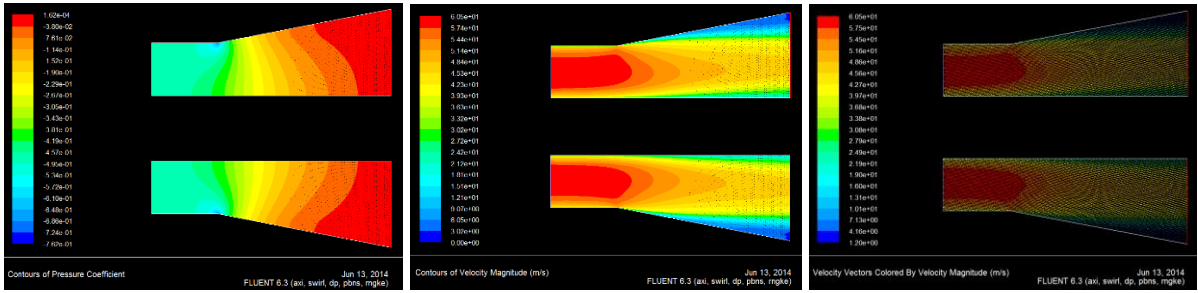
Pressure Coefficient Contours Velocity Magnitude Contours Velocity Vectors

Fig. 15 AR4, Casing Wall Angle=6°, Swirl Angle=25°, Velocity=60 m/s



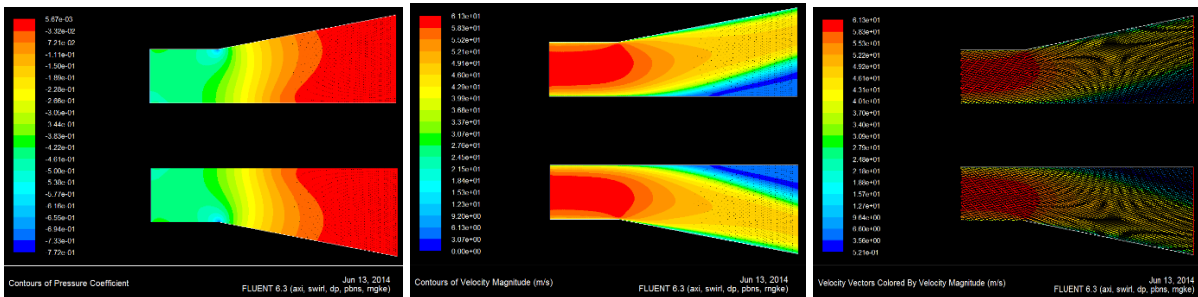
Pressure Coefficient Contours Velocity Magnitude Contours Velocity Vectors

Fig. 16 AR2, Casing Wall Angle=8°, Swirl Angle=0°, Velocity=60 m/s



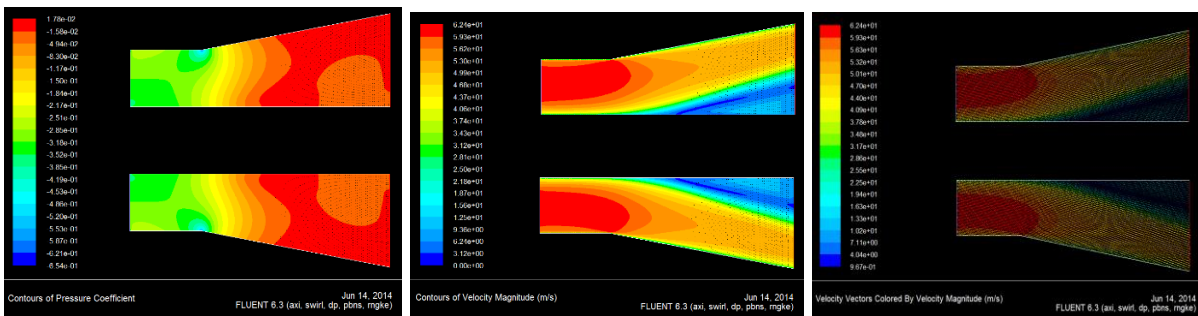
Pressure Coefficient Contours Velocity Magnitude Contours Velocity Vectors

Fig. 17 AR2, Casing Wall Angle=8°, Swirl Angle=7.5°, Velocity=60 m/s



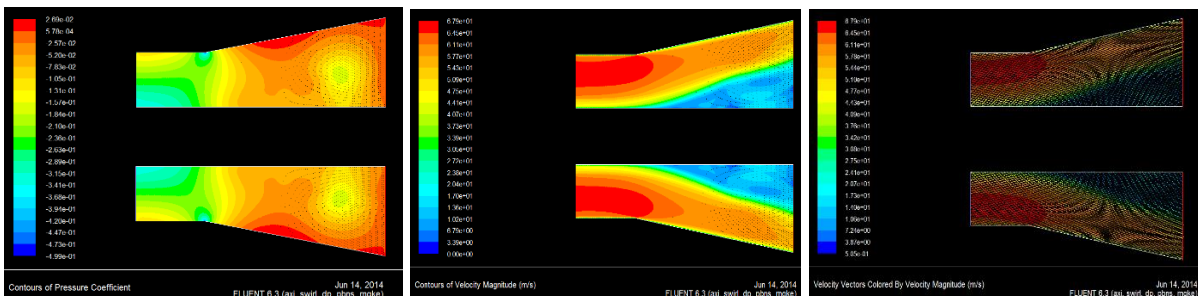
Pressure Coefficient Contours Velocity Magnitude Contours Velocity Vectors

Fig. 18 AR2, Casing Wall Angle=8°, Swirl Angle=12°, Velocity=60 m/s



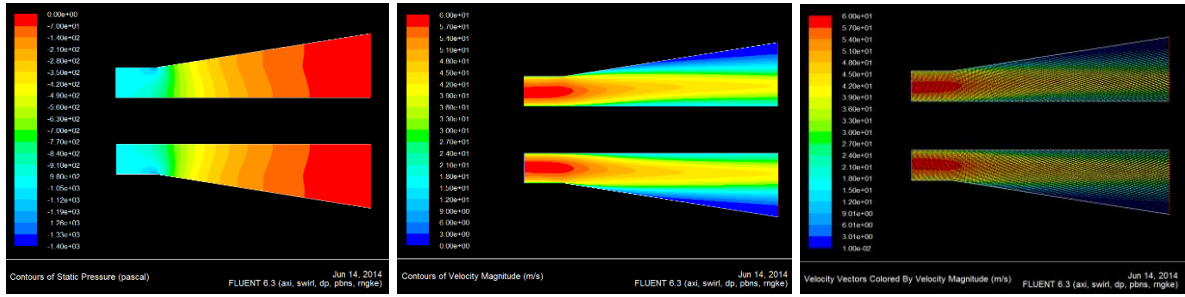
Pressure Coefficient Contours Velocity Magnitude Contours Velocity Vectors

Fig. 19 AR2, Casing Wall Angle=8°, Swirl Angle=17°, Velocity=60 m/s



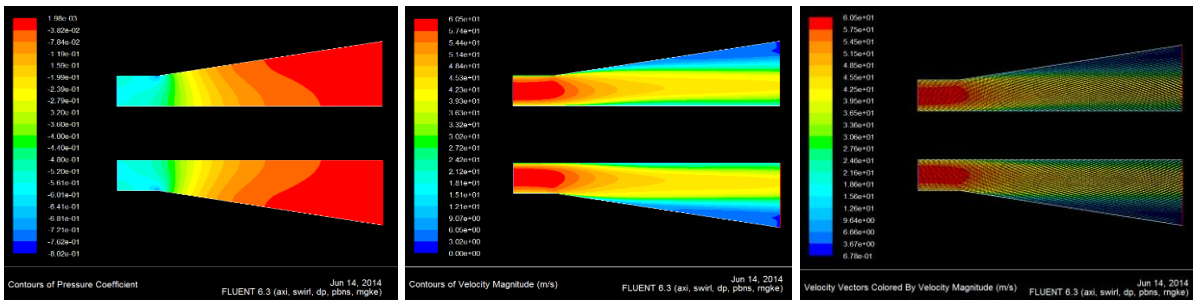
Pressure Coefficient Contours Velocity Magnitude Contours Velocity Vectors

Fig. 20 AR2, Casing Wall Angle=8°, Swirl Angle=25°, Velocity=60 m/s



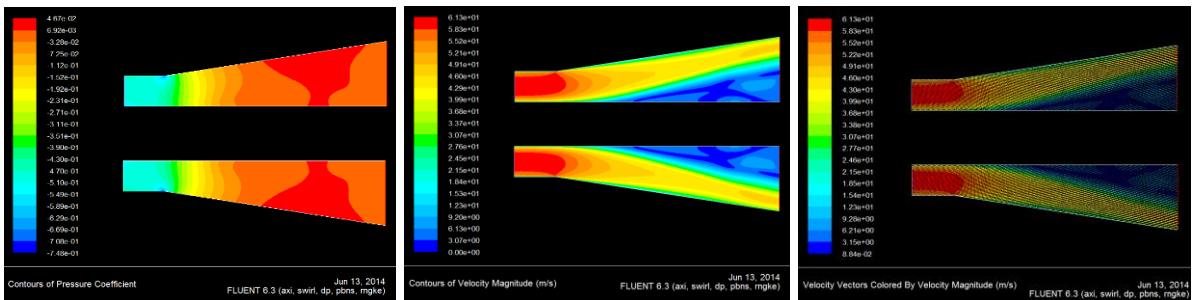
Pressure Coefficient Contours Velocity Magnitude Contours Velocity Vectors

Fig. 21 AR3, Casing Wall Angle=8°, Swirl Angle=0°, Velocity=60 m/s



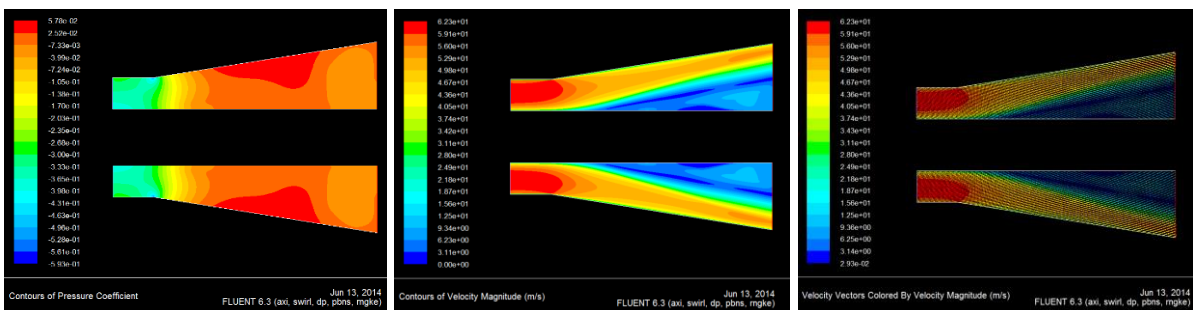
Pressure Coefficient Contours Velocity Magnitude Contours Velocity Vectors

Fig. 22 AR3, Casing Wall Angle=8°, Swirl Angle=7.5°, Velocity=60 m/s



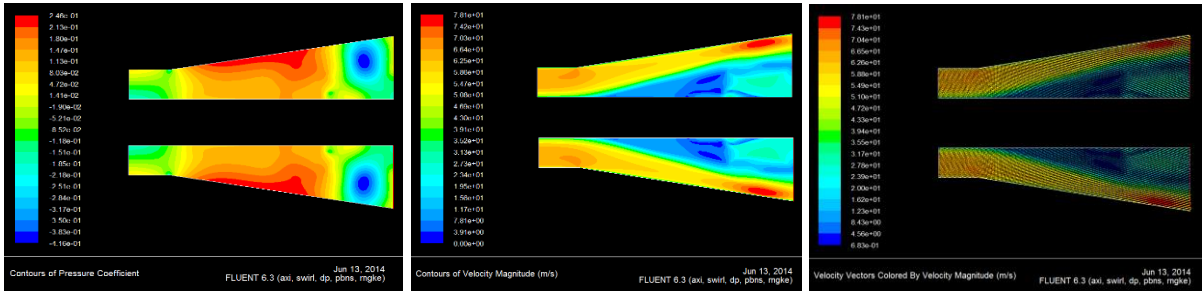
Pressure Coefficient Contours Velocity Magnitude Contours Velocity Vectors

Fig. 23 AR3, Casing Wall Angle=8°, Swirl Angle=12°, Velocity=60 m/s



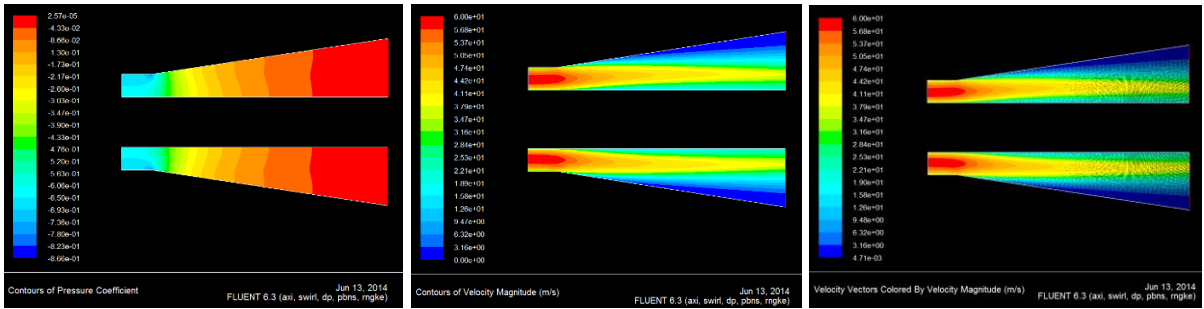
Pressure Coefficient Contours Velocity Magnitude Contours Velocity Vectors

Fig. 24 AR3, Casing Wall Angle=8°, Swirl Angle=17°, Velocity=60 m/s



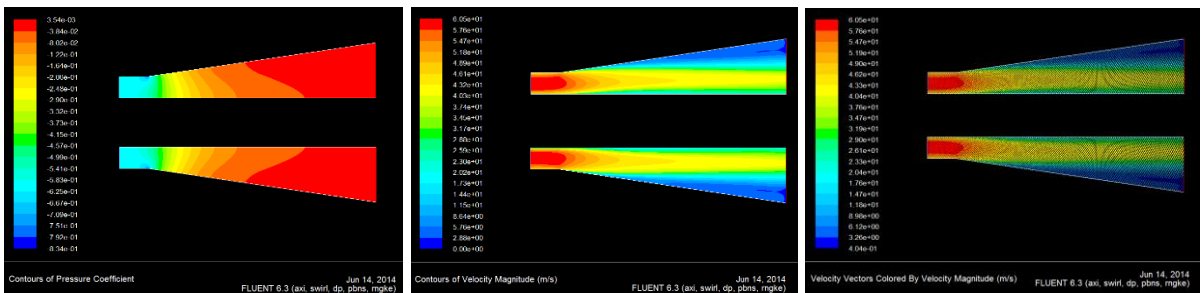
Pressure Coefficient Contours Velocity Magnitude Contours Velocity Vectors

Fig. 25 AR3, Casing Wall Angle=8°, Swirl Angle=25°, Velocity=60 m/s



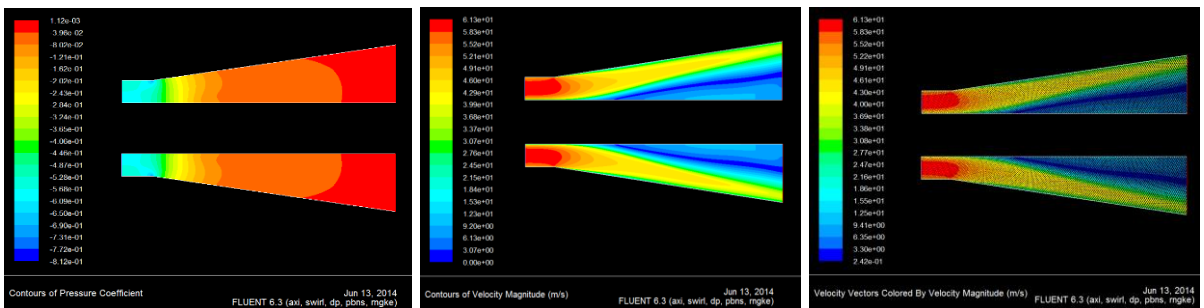
Pressure Coefficient Contours Velocity Magnitude Contours Velocity Vectors

Fig. 26 AR4, Casing Wall Angle=8°, Swirl Angle=0°, Velocity=60 m/s



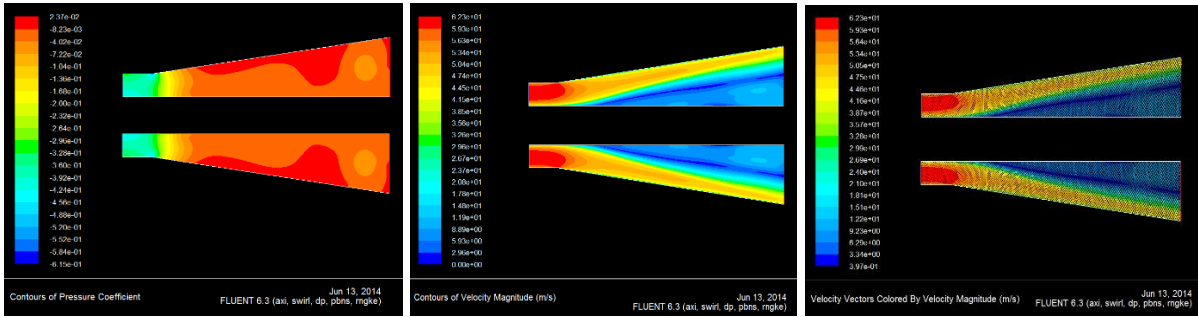
Pressure Coefficient Contours Velocity Magnitude Contours Velocity Vectors

Fig. 27 AR4, Casing Wall Angle=8°, Swirl Angle=7.5°, Velocity=60 m/s



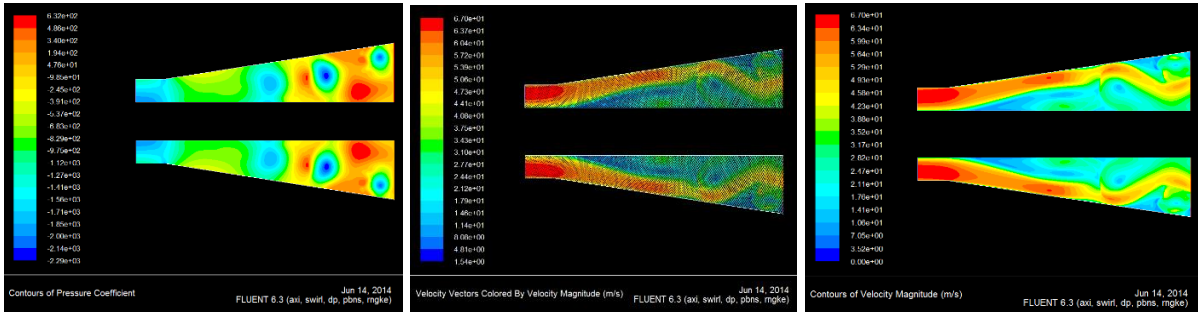
Pressure Coefficient Contours Velocity Magnitude Contours Velocity Vectors

Fig. 28 AR4, Casing Wall Angle=8°, Swirl Angle=12°, Velocity=60 m/s



Pressure Coefficient Contours Velocity Magnitude Contours Velocity Vectors

Fig. 29 AR4, Casing Wall Angle=8°, Swirl Angle=17°, Velocity=60 m/s



Pressure Coefficient Contours Velocity Magnitude Contours Velocity Vectors

Fig. 30 AR4, Casing Wall Angle=8°, Swirl Angle=25°, Velocity=60 m/s

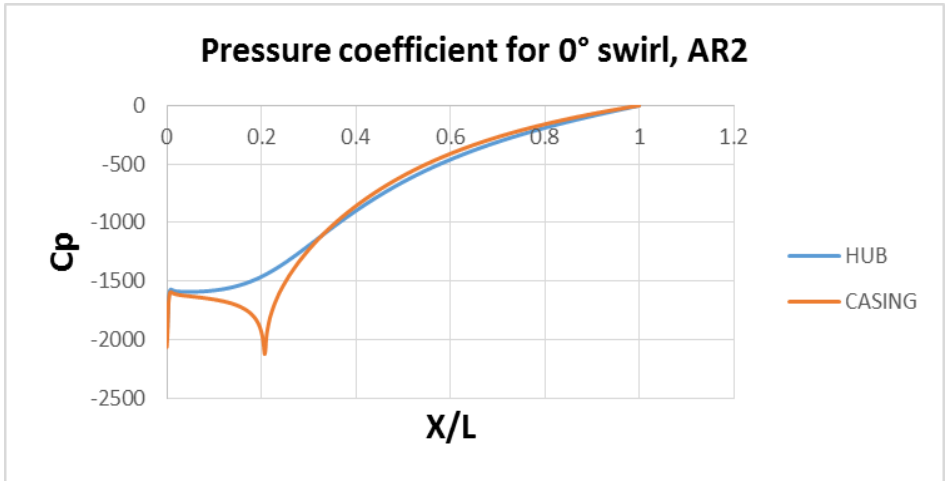


Fig.31 AR=2, Pressure coefficient, Casing wall angle=6°, Velocity=60m/s (0°)

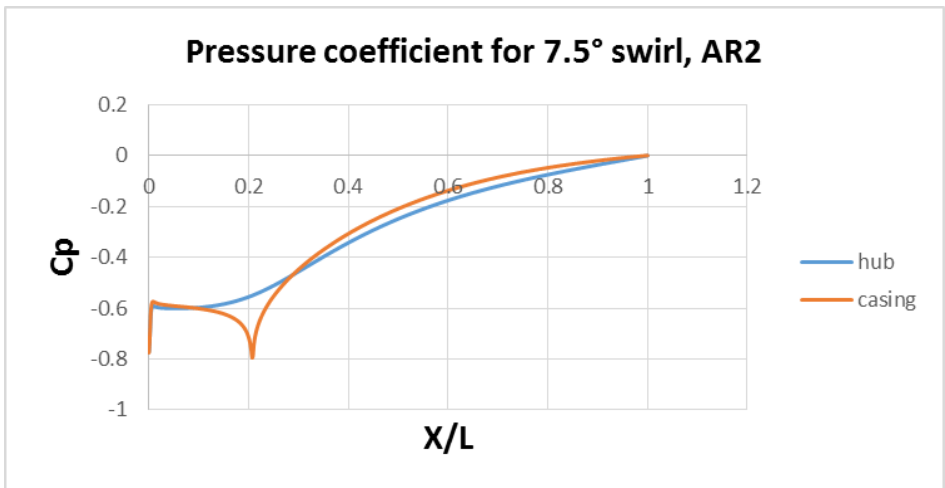


Fig.32 AR=2, Pressure coefficient, Casing wall angle=6°, Velocity=60m/s (7.5°)

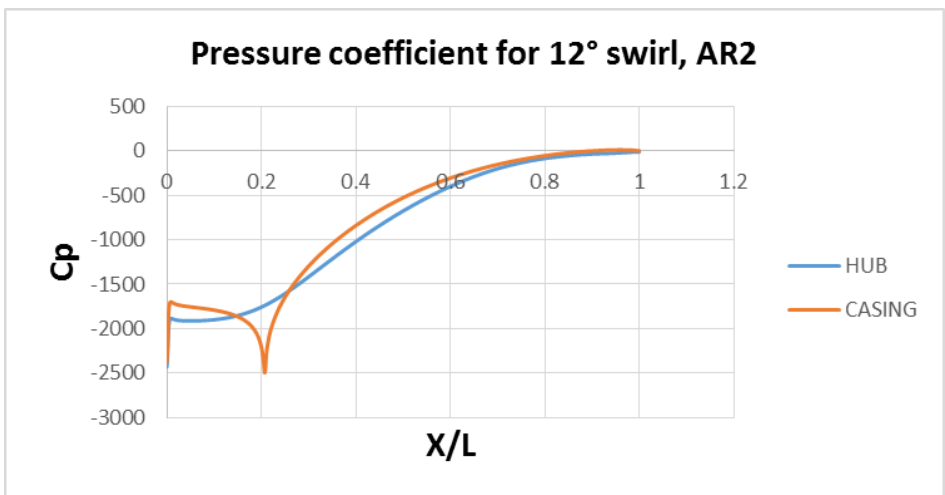


Fig.33 AR=2, Pressure coefficient, Casing wall angle=6°, Velocity=60m/s (12°)

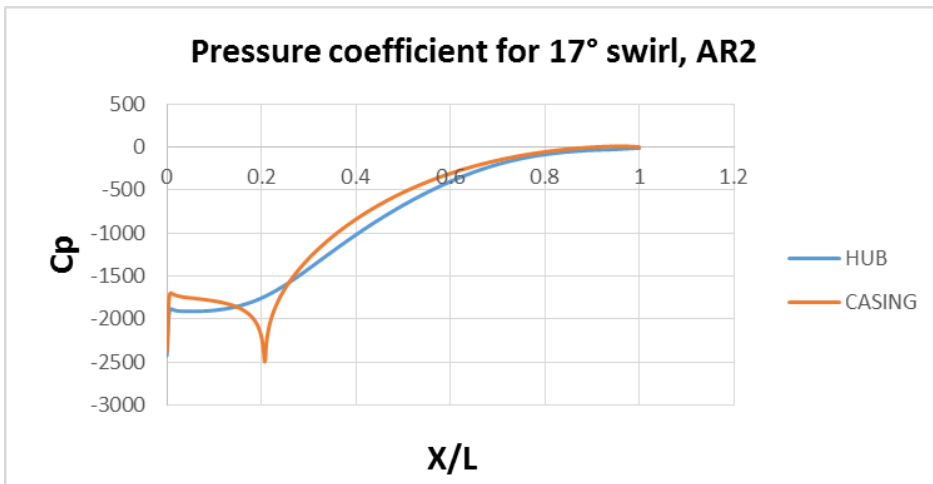


Fig.34 AR=2, Pressure coefficient, Casing wall angle=6°, Velocity=60m/s (17°)

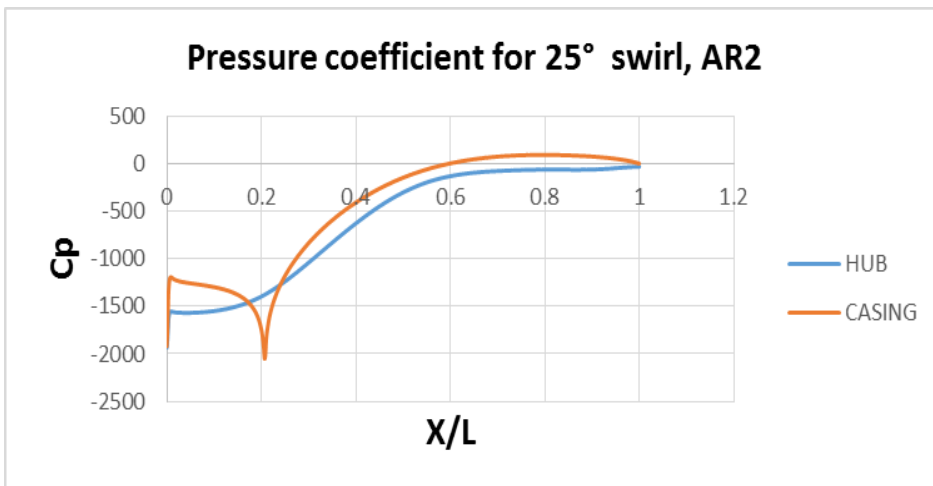


Fig.35 AR=2, Pressure coefficient, Casing wall angle=6°, Velocity=60m/s (25°)

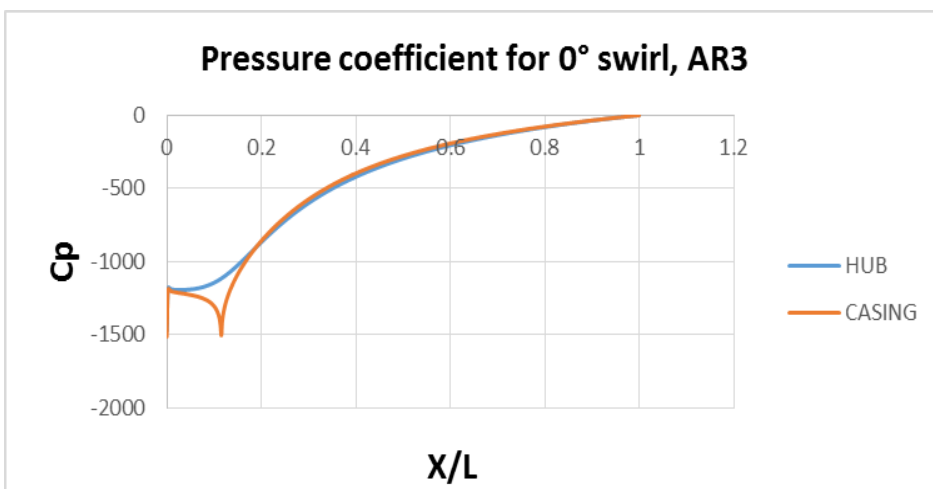


Fig.36 AR=3, Pressure coefficient, Casing wall angle=6°, Velocity=60m/s (0°)

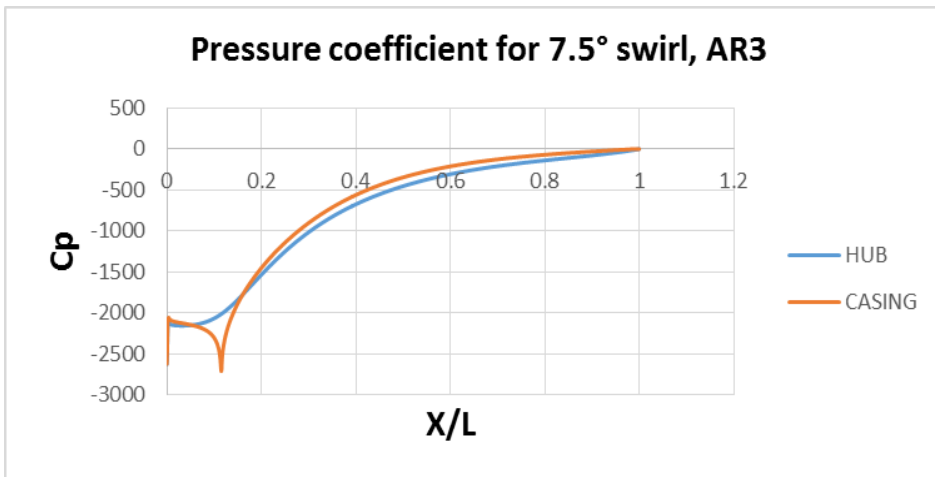


Fig.37 AR=3, Pressure coefficient, Casing wall angle=6°, Velocity=60m/s (7.5°)

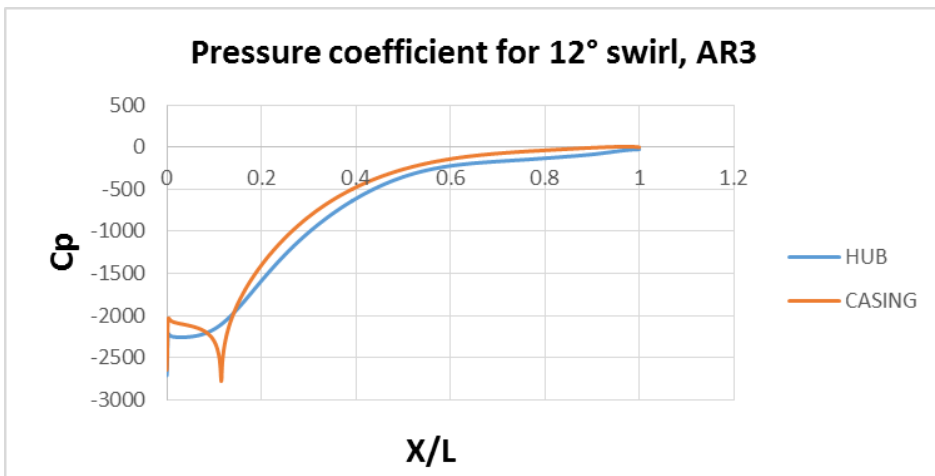


Fig.38 AR=3, Pressure coefficient, Casing wall angle=6°, Velocity=60m/s (12°)

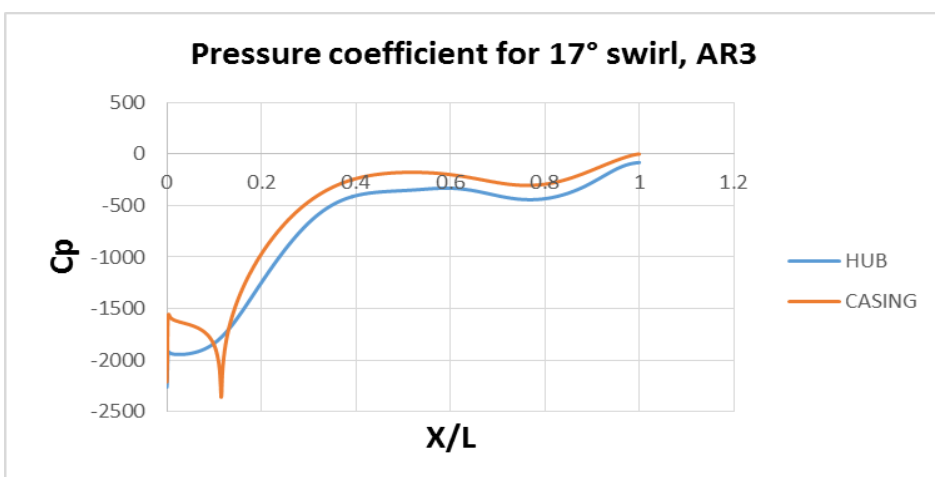


Fig.39 AR=3, Pressure coefficient, Casing wall angle=6°, Velocity=60m/s (17°)

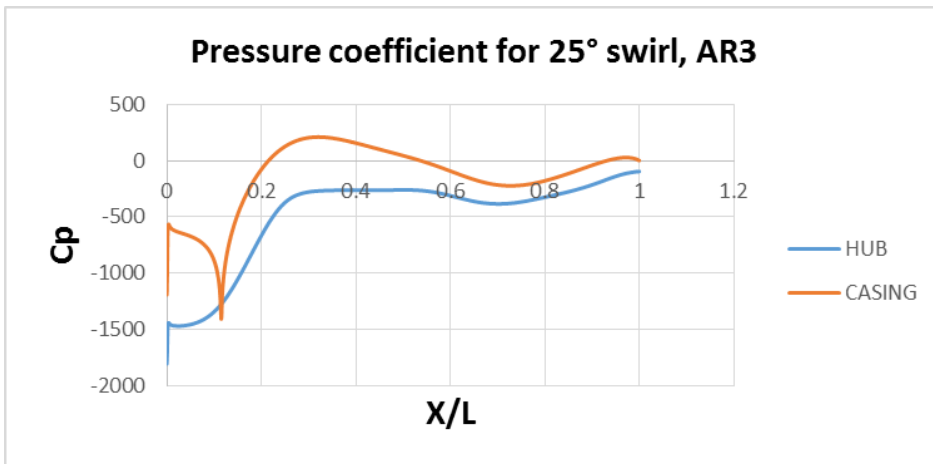


Fig.40 AR=3, Pressure coefficient, Casing wall angle=6°, Velocity=60m/s (25°)

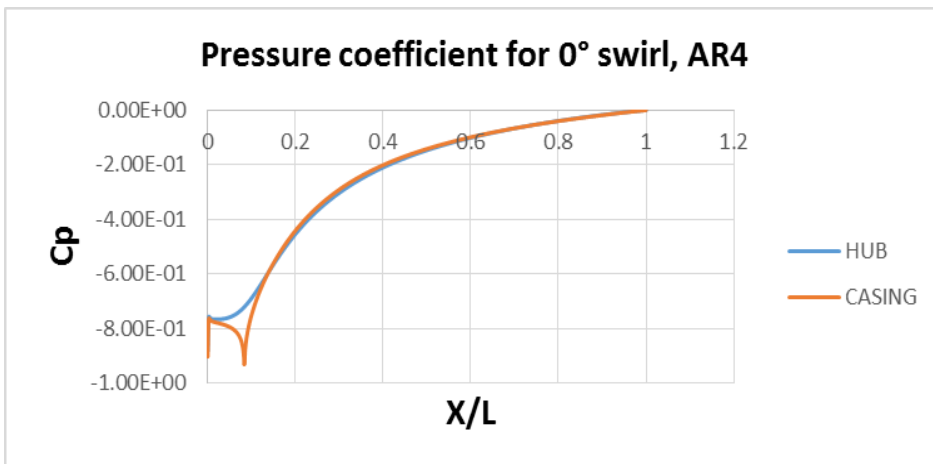


Fig.41 AR=4, Pressure coefficient, Casing wall angle=6°, Velocity=60m/s (0°)

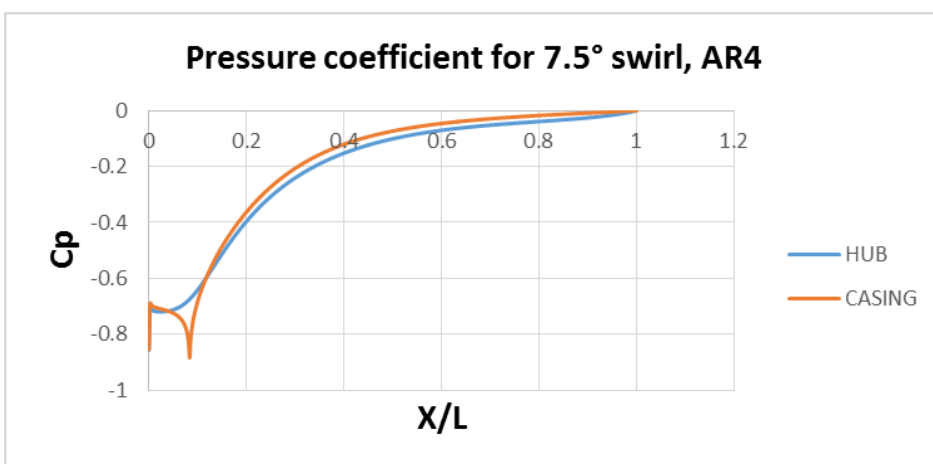


Fig.42 AR=4, Pressure coefficient, Casing wall angle=6°, Velocity=60m/s (7.5°)

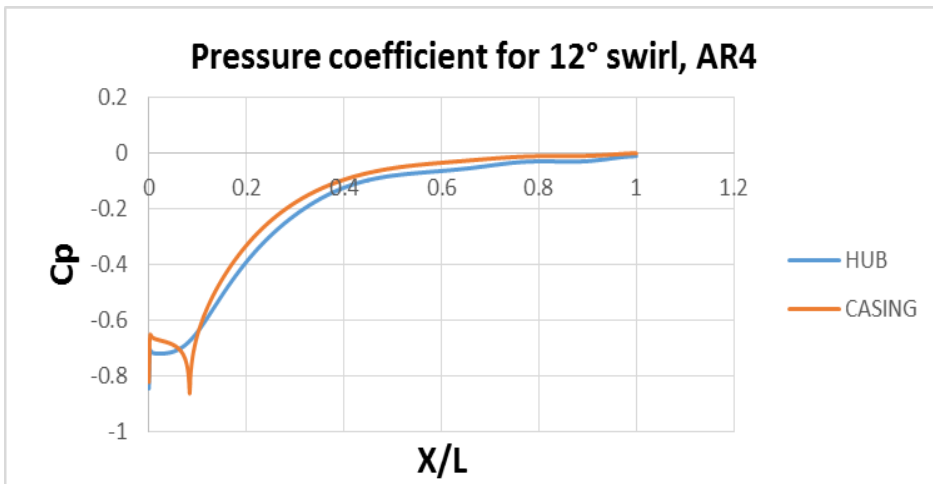


Fig.43 AR=4, Pressure coefficient, Casing wall angle=6°, Velocity=60m/s (12°)

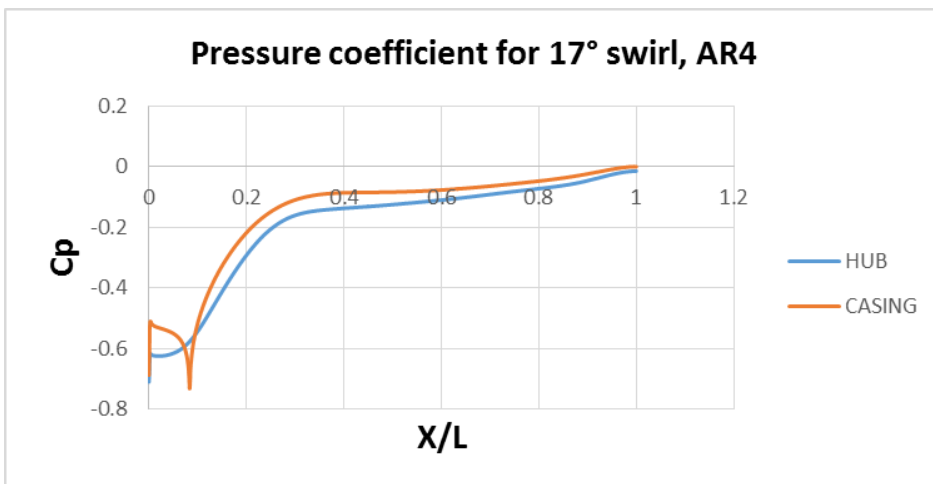


Fig.44 AR=4, Pressure coefficient, Casing wall angle=6°, Velocity=60m/s (17°)

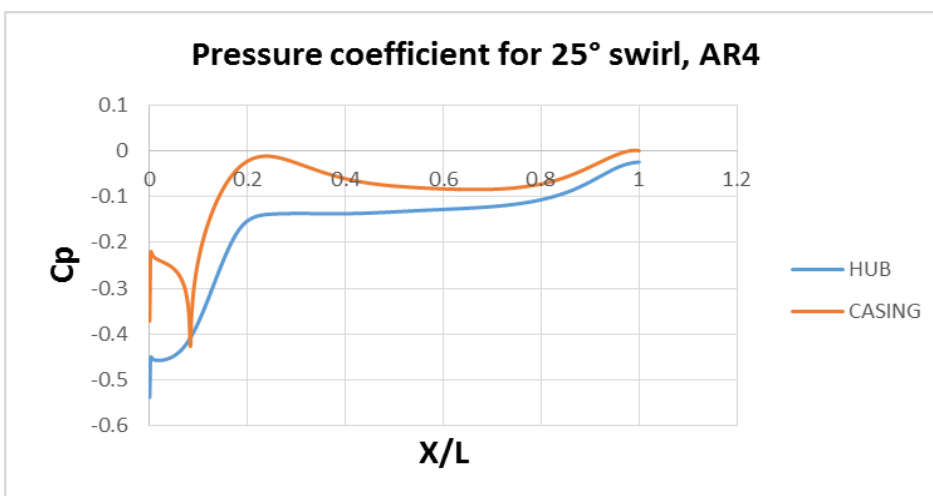


Fig.45 AR=4, Pressure coefficient, Casing wall angle=6°, Velocity=60m/s (25°)

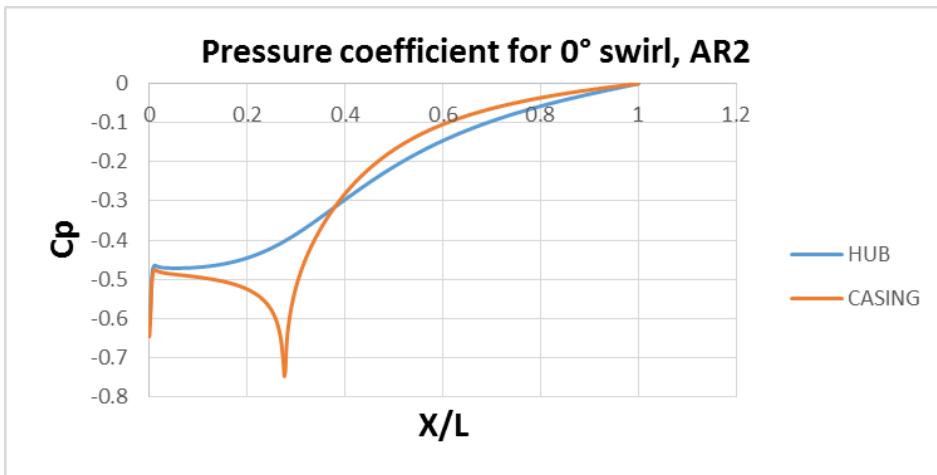


Fig.46 AR=2, Pressure coefficient, Casing wall angle=8°, Velocity=60m/s (0°)

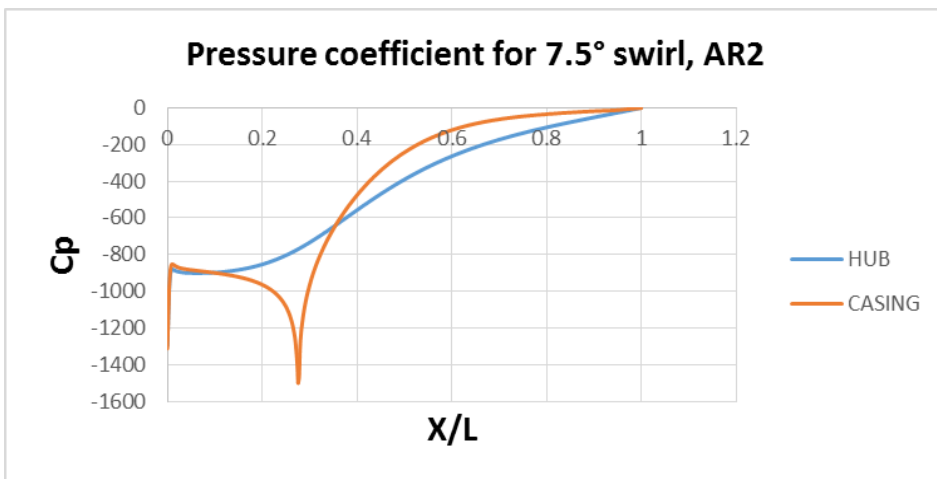


Fig.47 AR=2, Pressure coefficient, Casing wall angle=8°, Velocity=60m/s (7.5°)

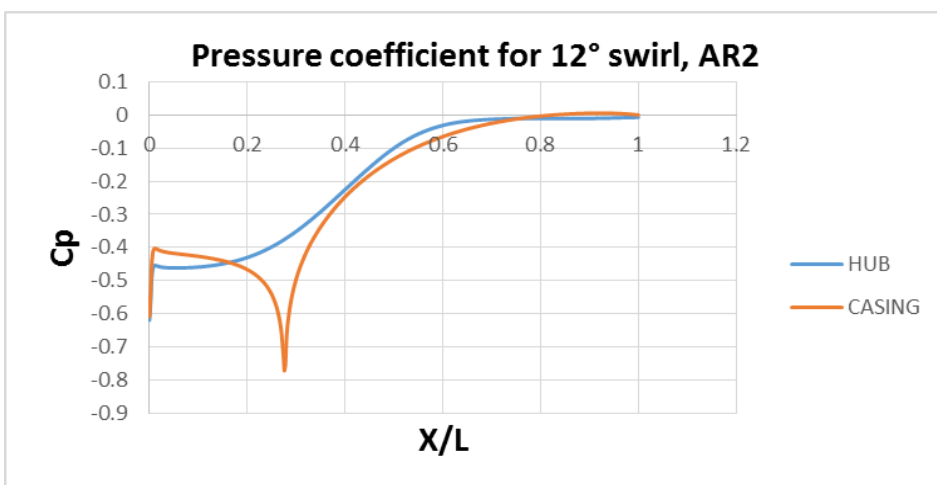


Fig.48 AR=2, Pressure coefficient, Casing wall angle=8°, Velocity=60m/s (12°)

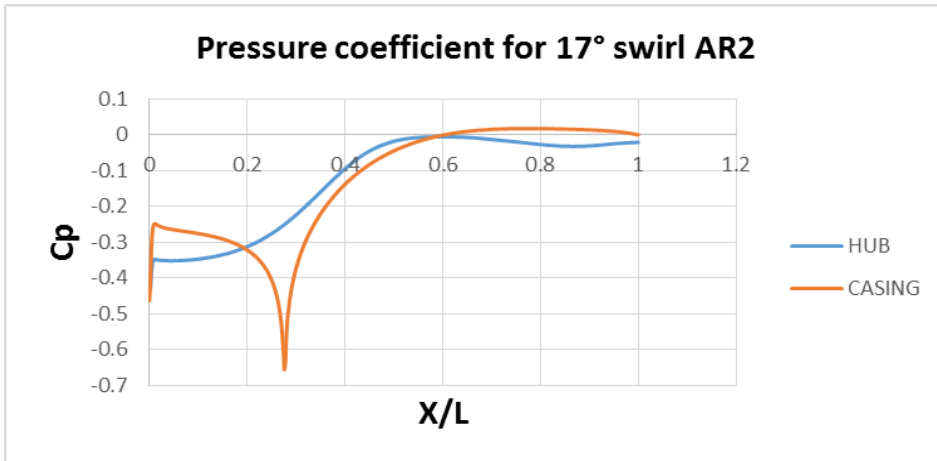


Fig.49 AR=2, Pressure coefficient, Casing wall angle=8°, Velocity=60m/s (17°)

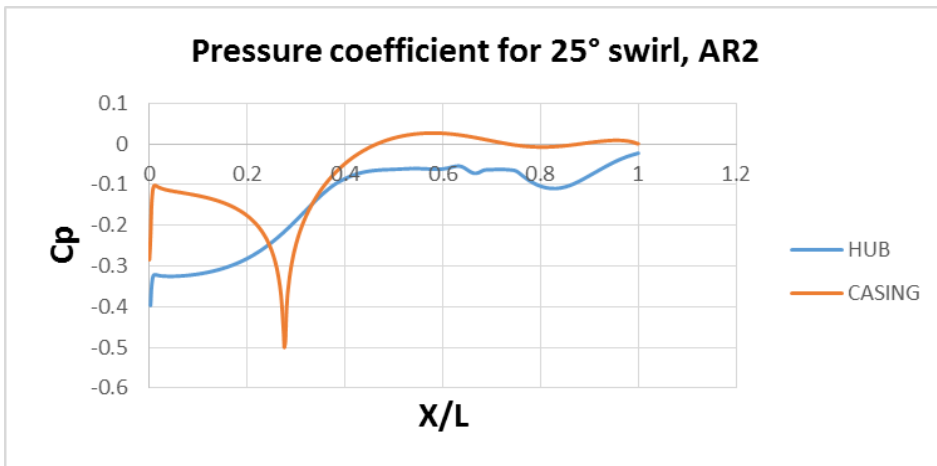


Fig.50 AR=2, Pressure coefficient, Casing wall angle=8°, Velocity=60m/s (25°)

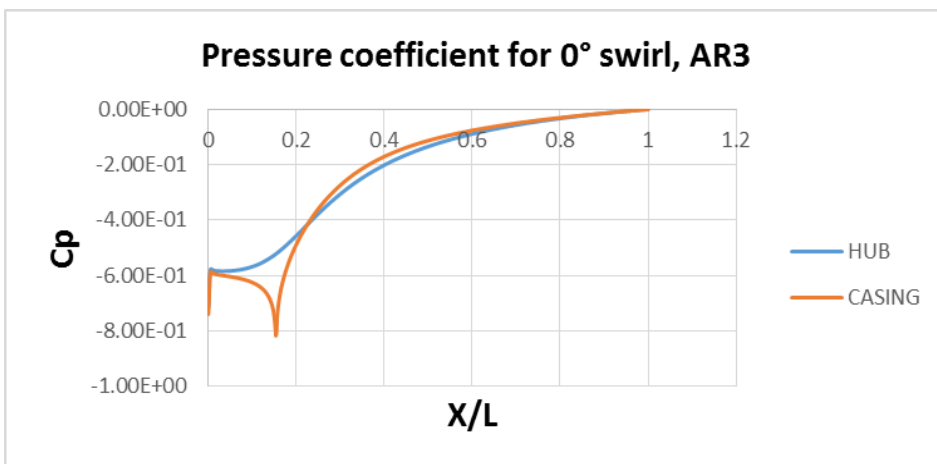


Fig.51 AR=3, Pressure coefficient, Casing wall angle=8°, Velocity=60m/s (0°)

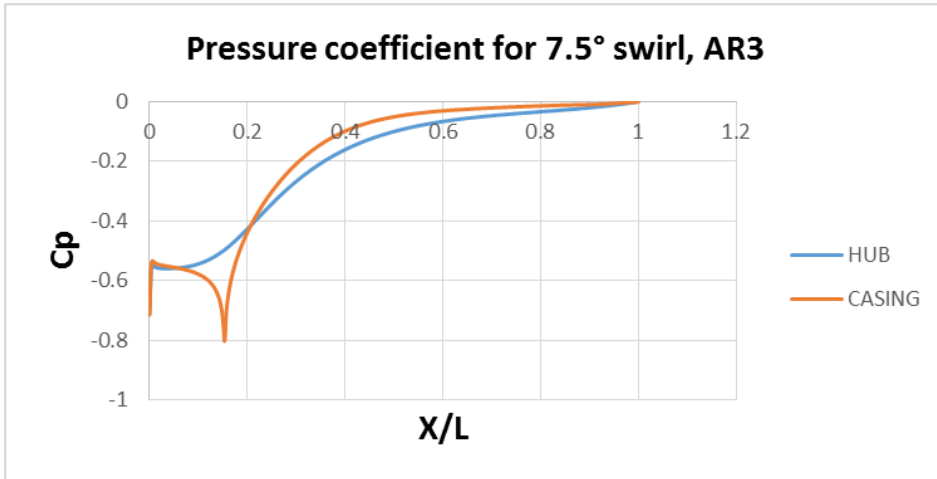


Fig.52 AR=3, Pressure coefficient, Casing wall angle=8°, Velocity=60m/s (7.5°)

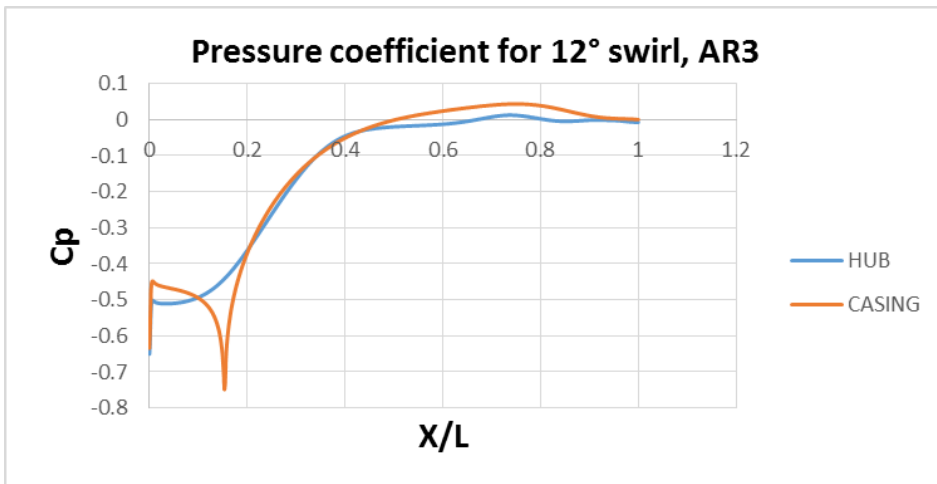


Fig.53 AR=3, Pressure coefficient, Casing wall angle=8°, Velocity=60m/s (12°)

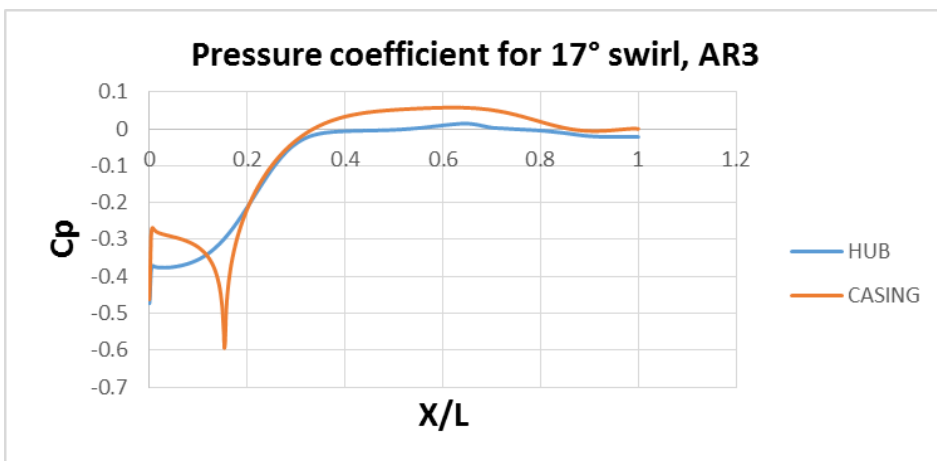


Fig.54 AR=3, Pressure coefficient, Casing wall angle=8°, Velocity=60m/s (17°)

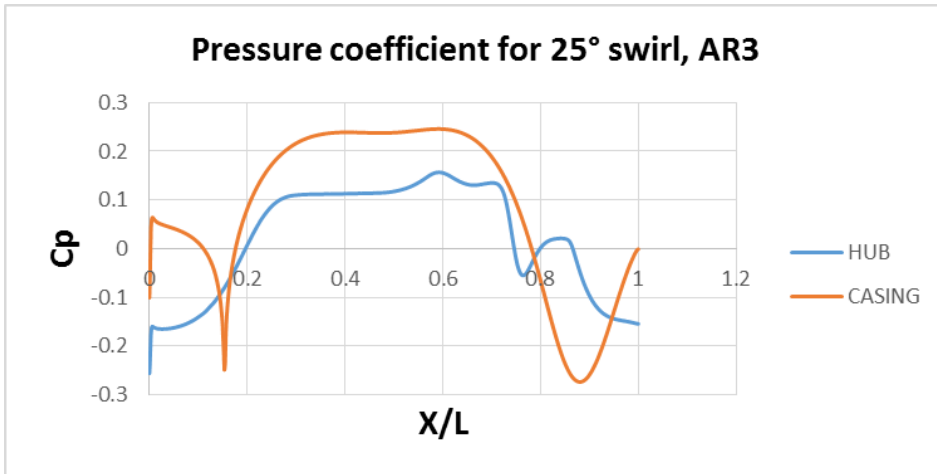


Fig.55 AR=3, Pressure coefficient, Casing wall angle=8°, Velocity=60m/s (25°)

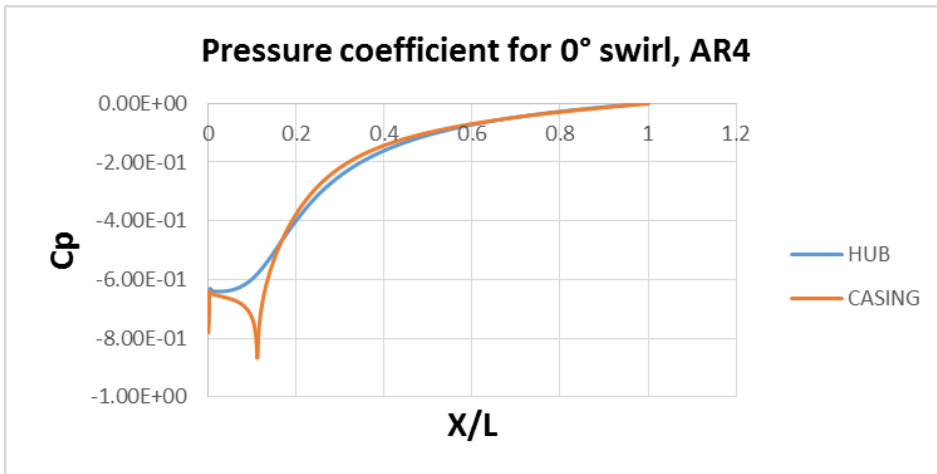


Fig.56 AR=4, Pressure coefficient, Casing wall angle=8°, Velocity=60m/s (0°)

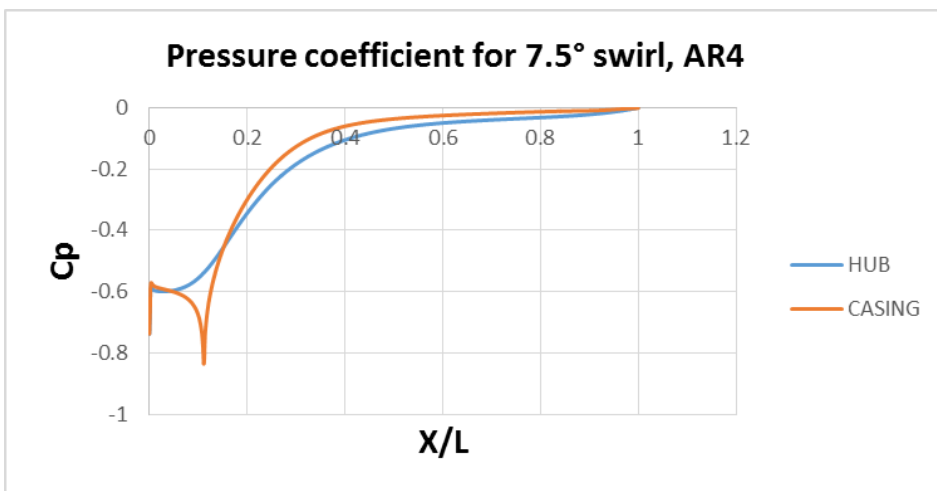


Fig.57 AR=4, Pressure coefficient, Casing wall angle=8°, Velocity=60m/s (7.5°)

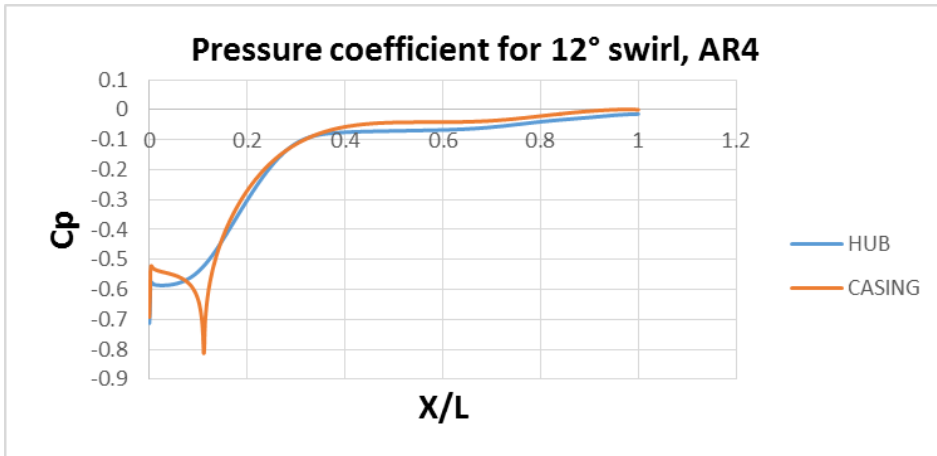


Fig.58 AR=4, Pressure coefficient, Casing wall angle=8°, Velocity=60m/s (12°)

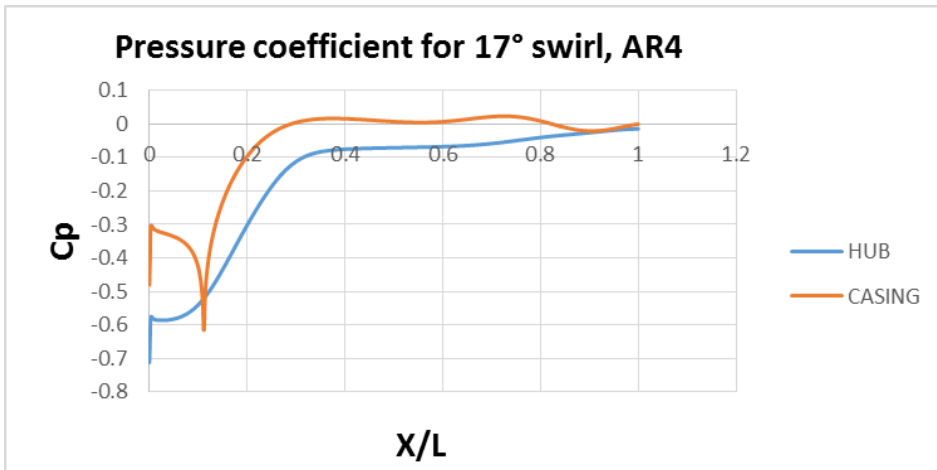


Fig.59 AR=4, Pressure coefficient, Casing wall angle=8°, Velocity=60m/s (17°)

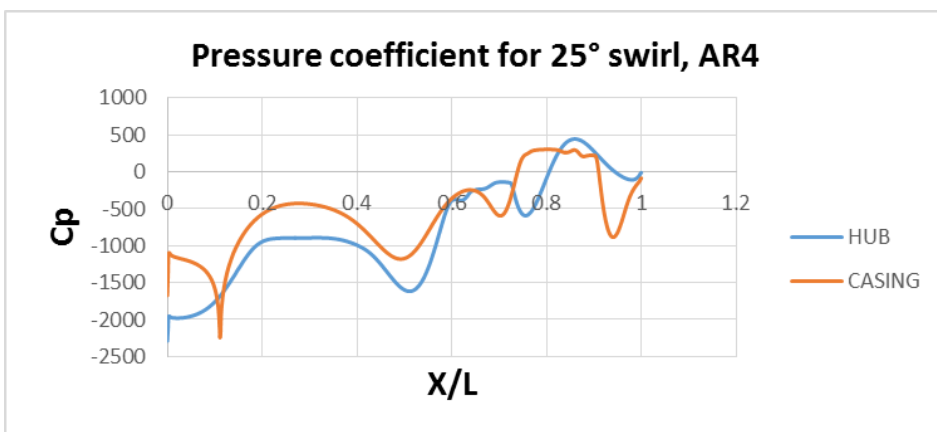


Fig.60 AR=4, Pressure coefficient, Casing wall angle=8°, Velocity=60m/s (25°)

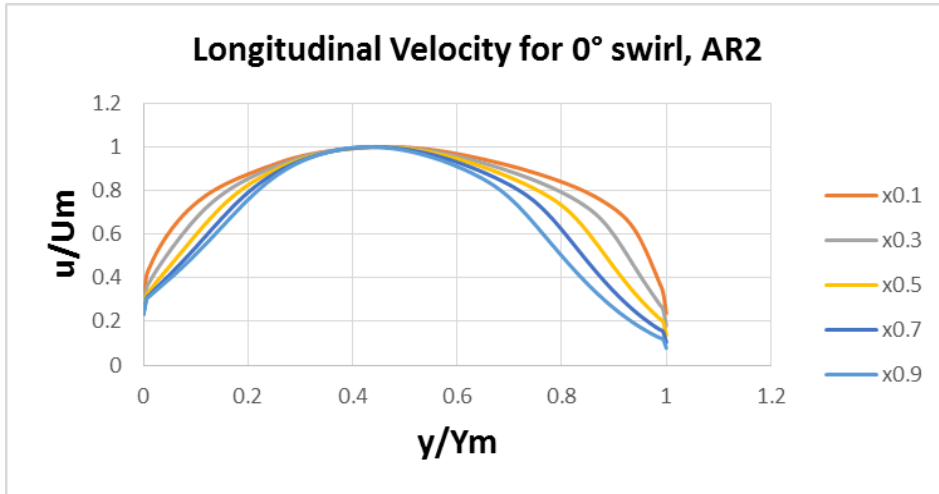


Fig.61 AR=2, Casing wall angle=6°, Velocity=60m/s (0°L)

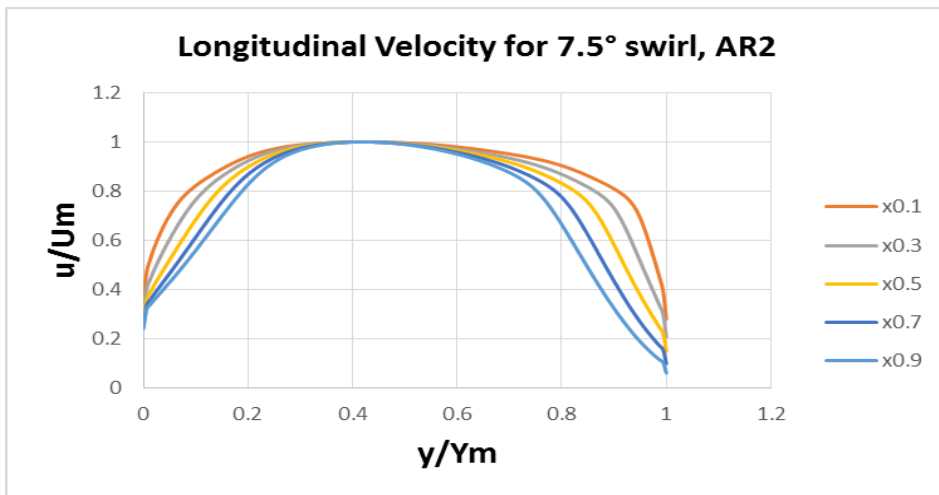


Fig.62 AR=2, Casing wall angle=6°, Velocity=60m/s (7.5°L)

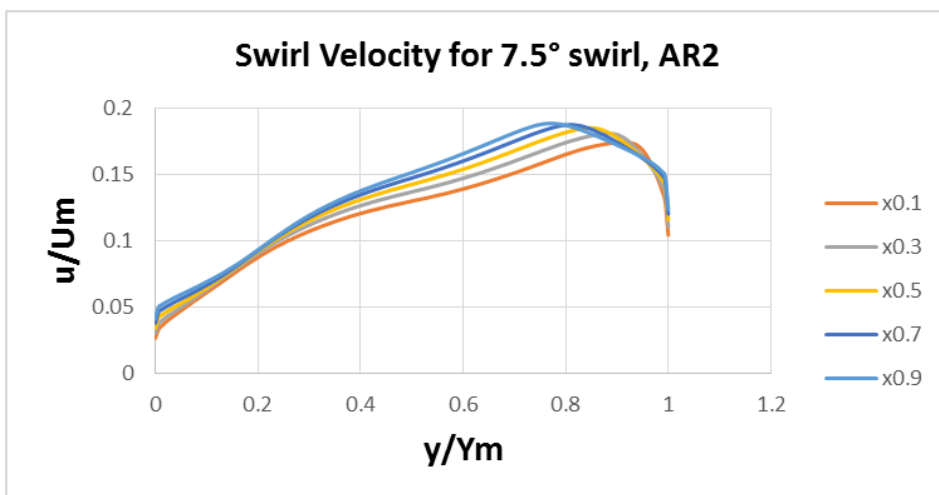


Fig.63 AR=2, Casing wall angle=6°, Velocity=60m/s (7.5°S)

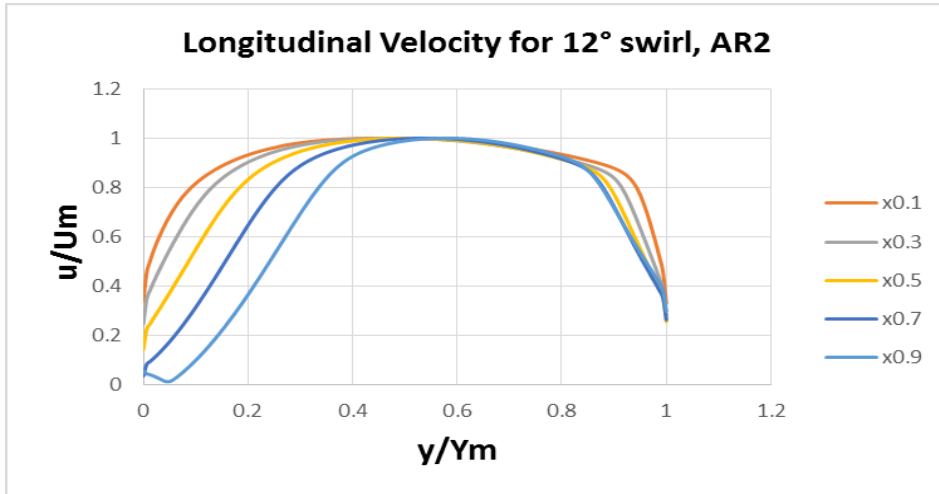


Fig.64 AR=2, Casing wall angle=6°, Velocity=60m/s (12°L)

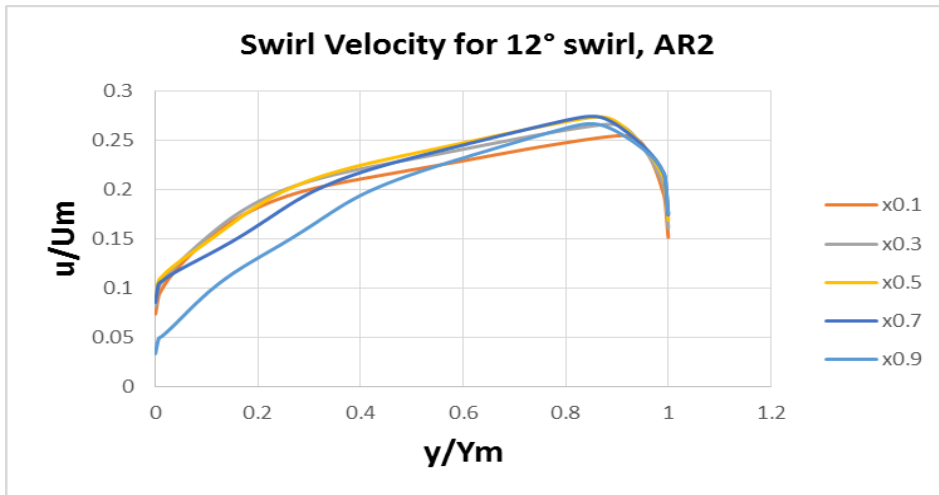


Fig.65 AR=2, Casing wall angle=6°, Velocity=60m/s (12°S)

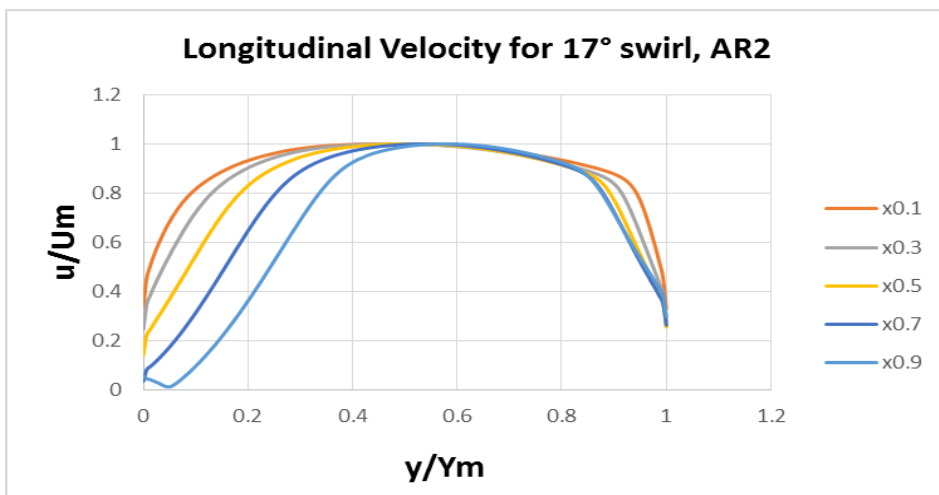


Fig.66 AR=2, Casing wall angle=6°, Velocity=60m/s (17°L)

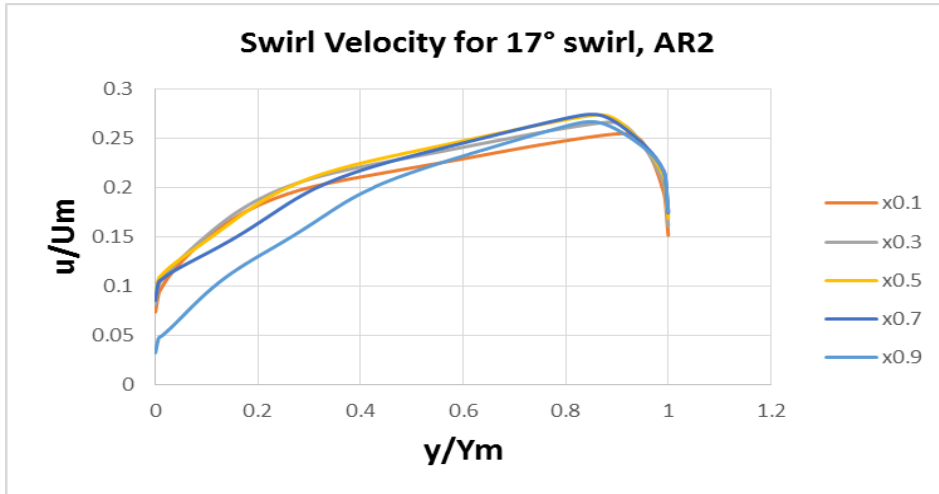


Fig.67 AR=2, Casing wall angle=6°, Velocity=60m/s (17°S)

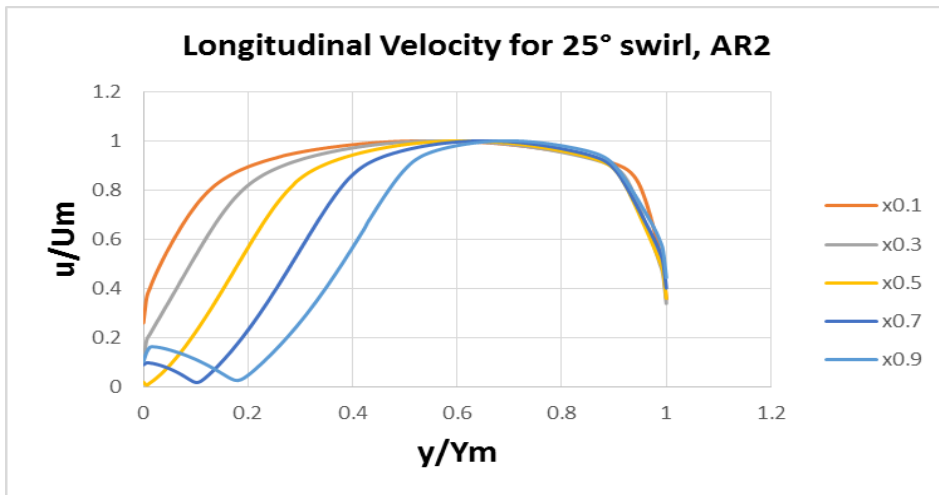


Fig.68 AR=2, Casing wall angle=6°, Velocity=60m/s (25°L)

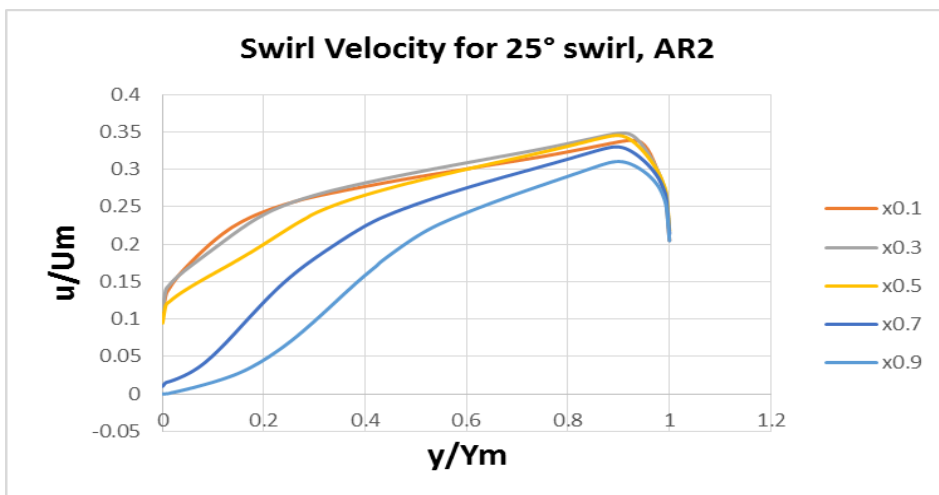


Fig.69 AR=2, Casing wall angle=6°, Velocity=60m/s (25°S)

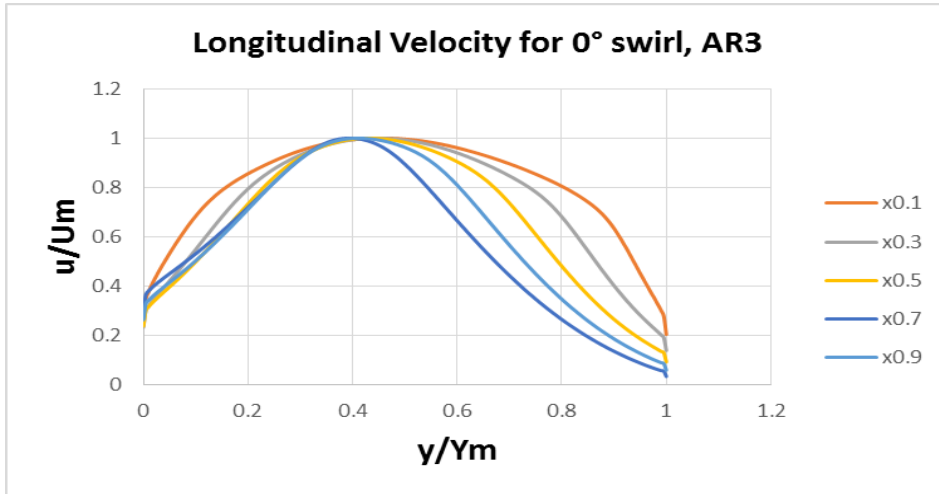


Fig.70 AR=3, Casing wall angle=6°, Velocity=60m/s (0°L)

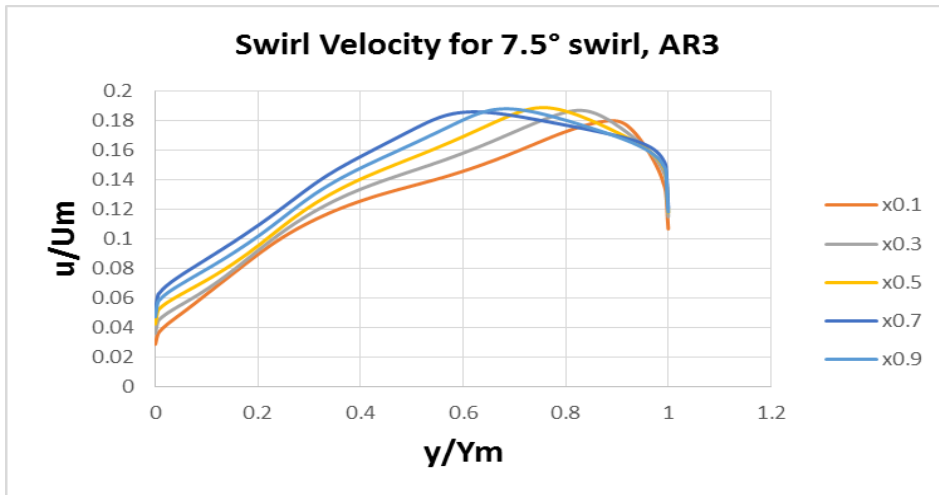


Fig.71 AR=3, Casing wall angle=6°, Velocity=60m/s (7.5°S)

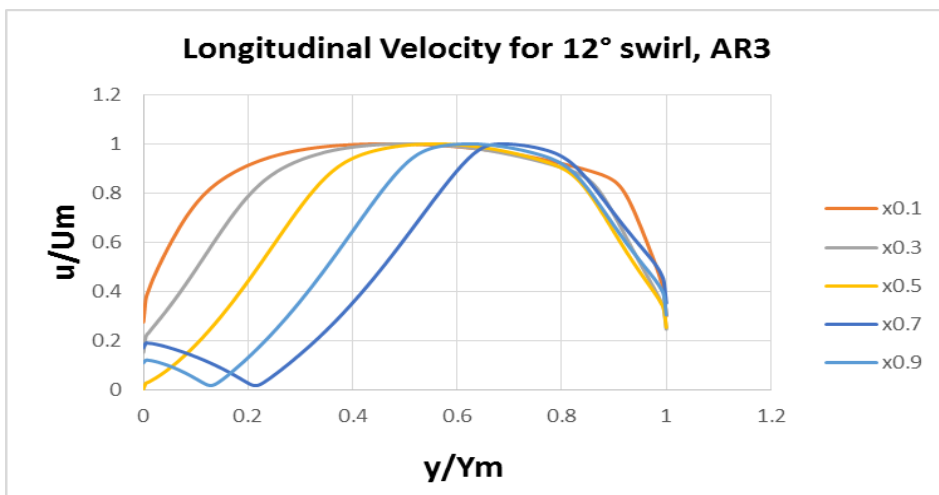


Fig.72 AR=2, Casing wall angle=6°, Velocity=60m/s (12°L)

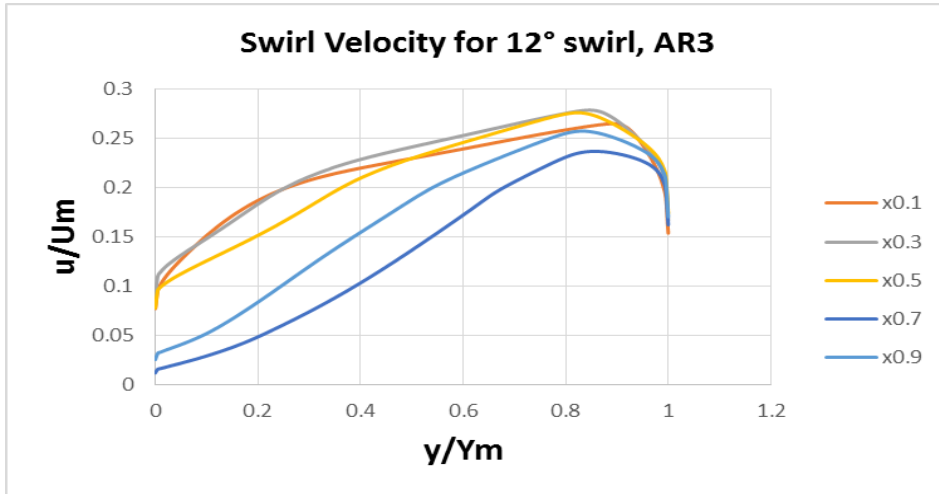


Fig.73 AR=3, Casing wall angle=6°, Velocity=60m/s (12°S)

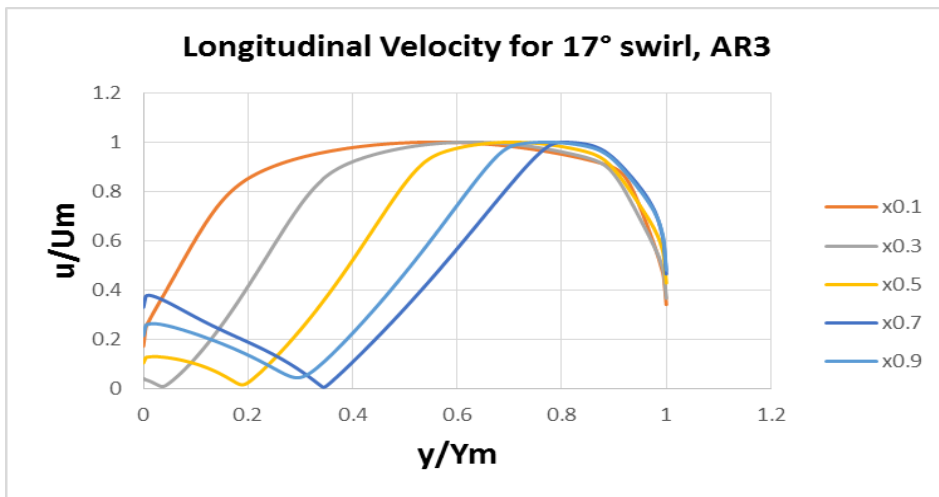


Fig.74 AR=3, Casing wall angle=6°, Velocity=60m/s (17°L)

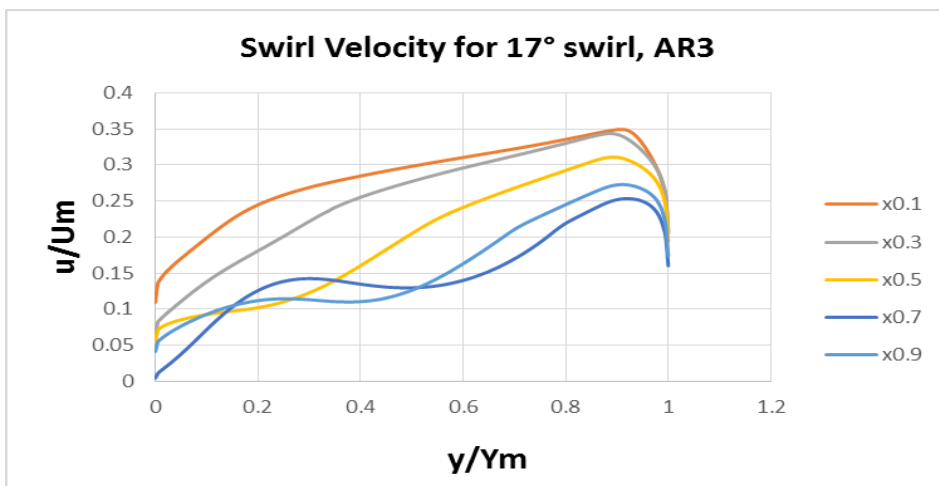


Fig.75 AR=3, Casing wall angle=6°, Velocity=60m/s (17°S)

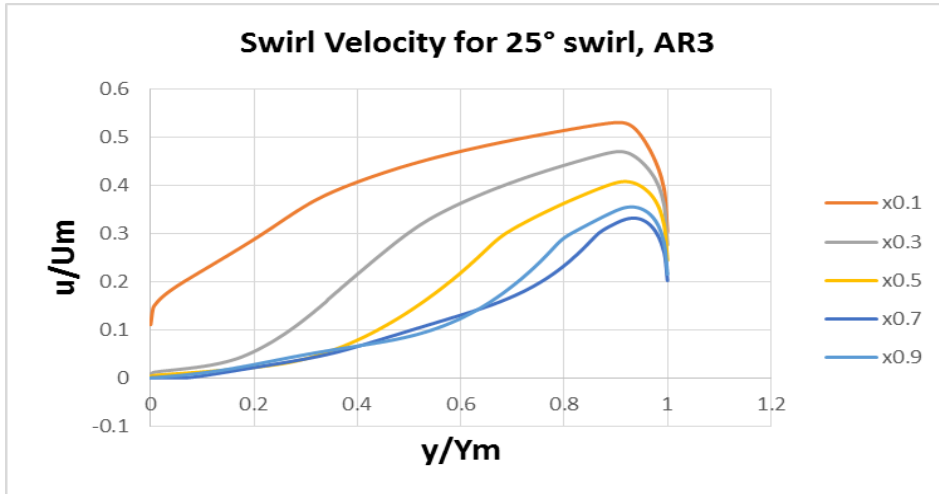


Fig.76 AR=3, Casing wall angle=6°, Velocity=60m/s (25°S)

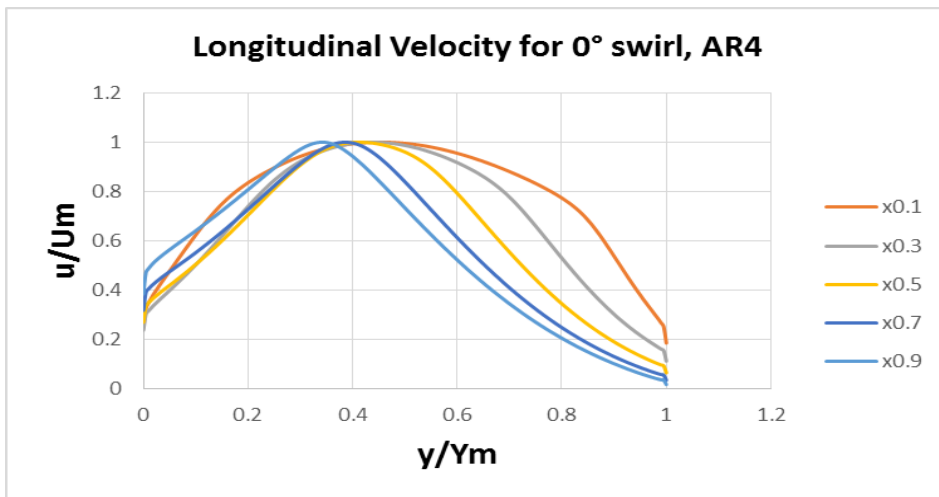


Fig.77 AR=4, Casing wall angle=6°, Velocity=60m/s (0°L)

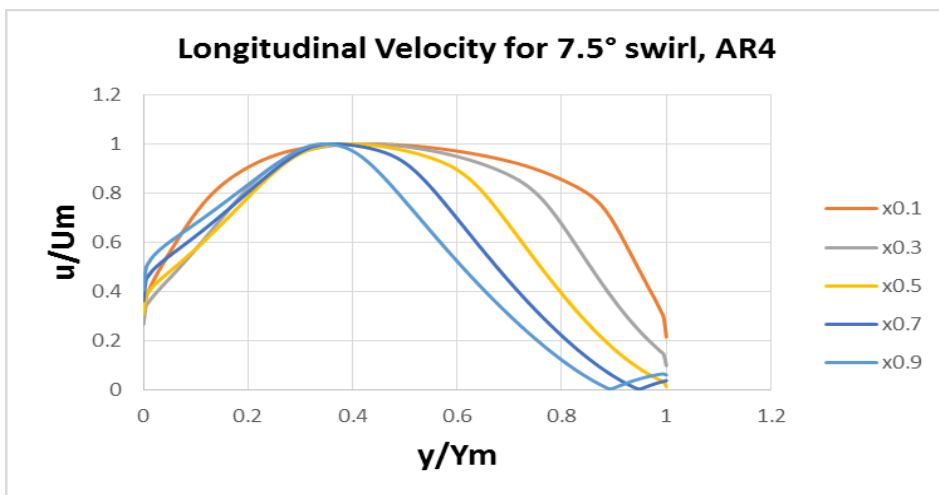


Fig.78 AR=4, Casing wall angle=6°, Velocity=60m/s (7.5°L)

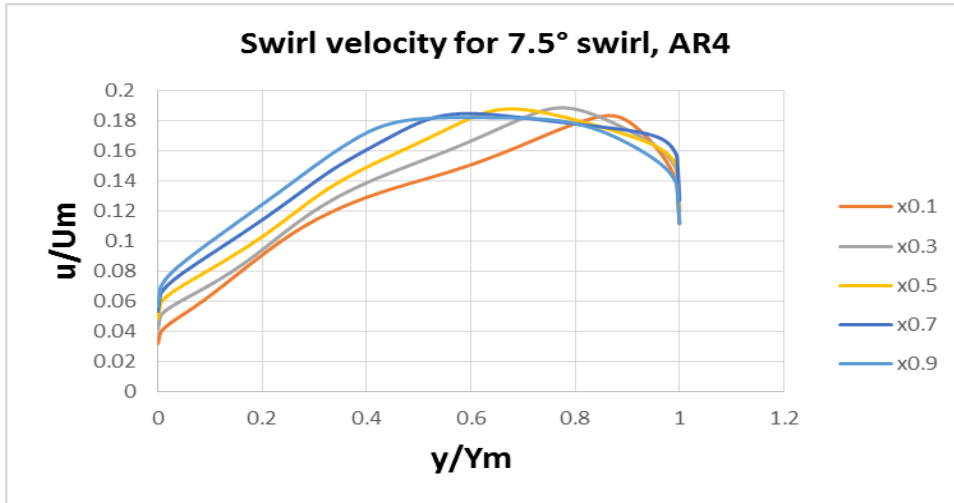


Fig.79 AR=4, Casing wall angle=6°, Velocity=60m/s (7.5°S)

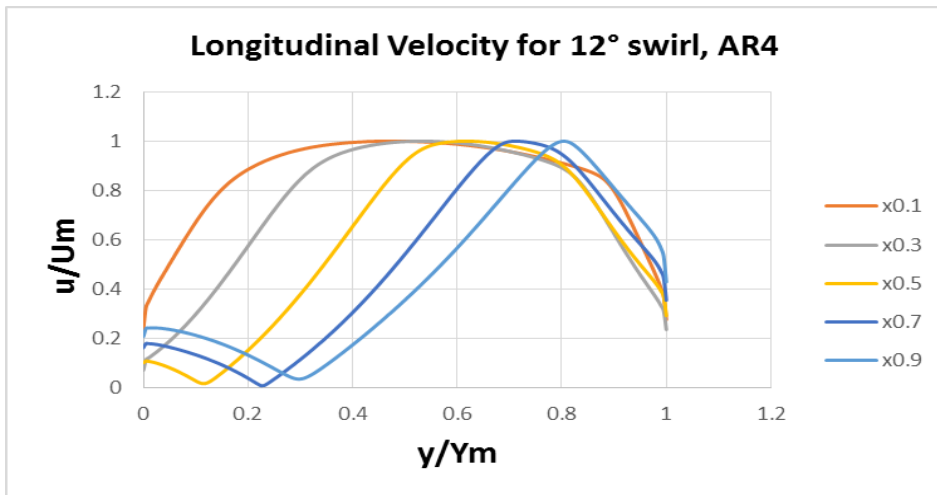


Fig.80 AR=4, Casing wall angle=6°, Velocity=60m/s (12°L)

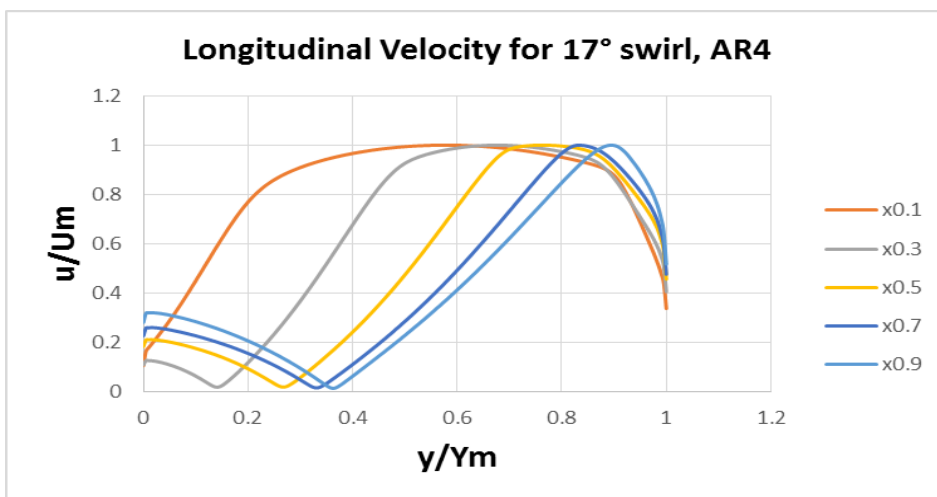


Fig.81 AR=4, Casing wall angle=6°, Velocity=60m/s (17°L)

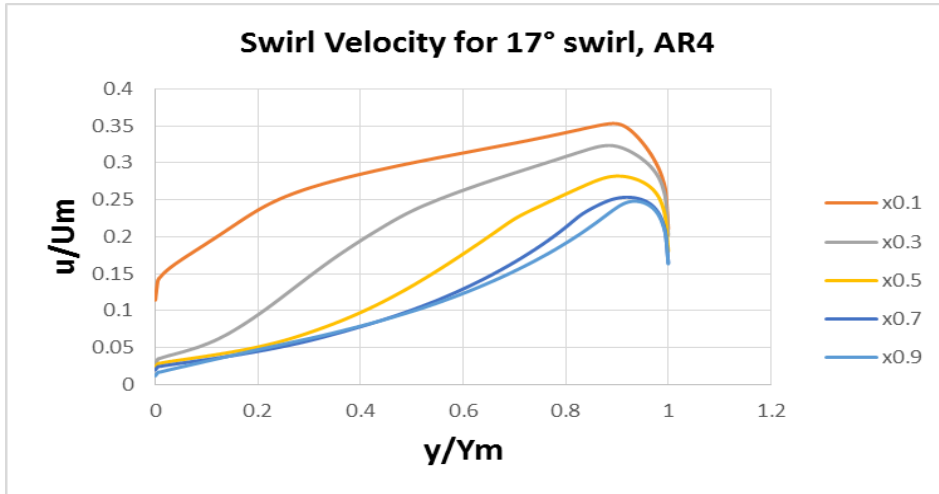


Fig.82 AR=4, Casing wall angle=6°, Velocity=60m/s (17°S)

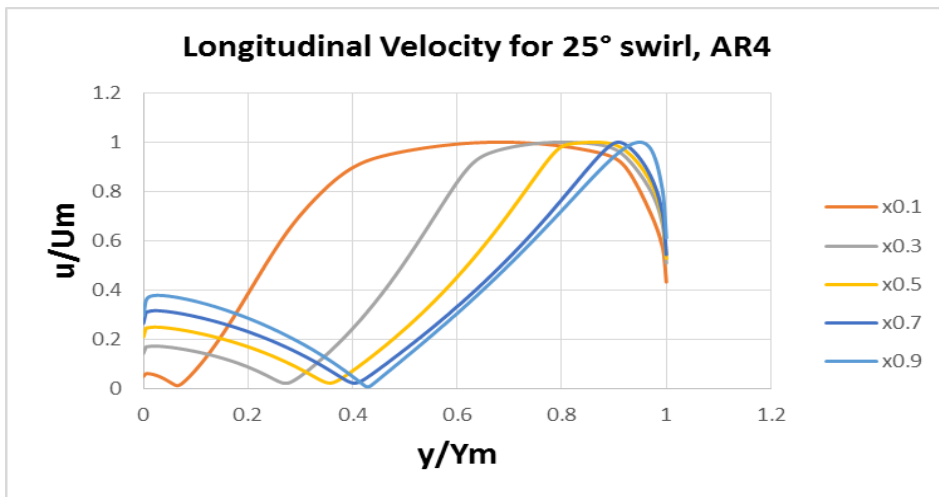


Fig.83 AR=4, Casing wall angle=6°, Velocity=60m/s (25°L)

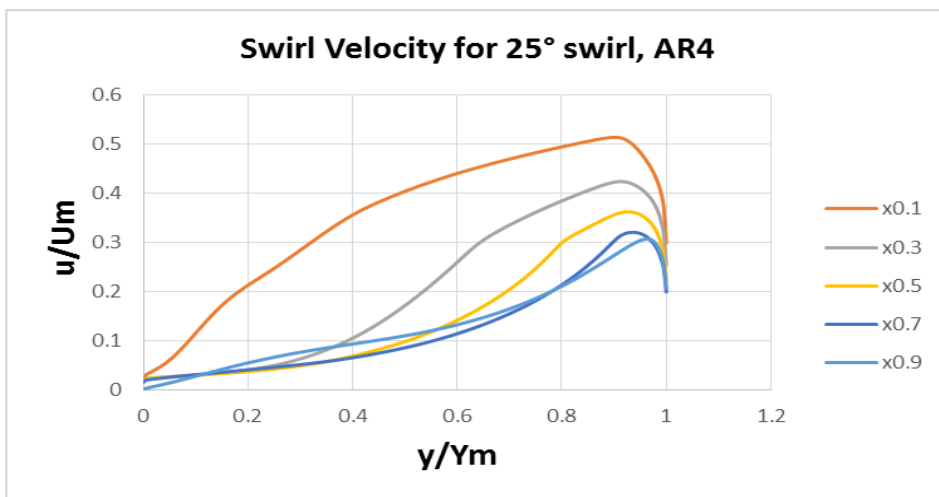


Fig.84 AR=4, Casing wall angle=6°, Velocity=60m/s (25°S)

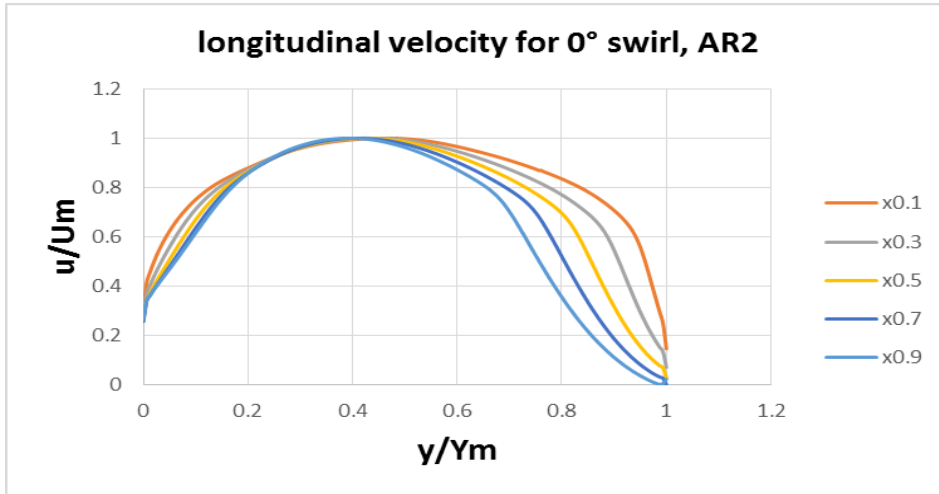


Fig.85 AR=2, Casing wall angle=8°, Velocity=60m/s (0°L)

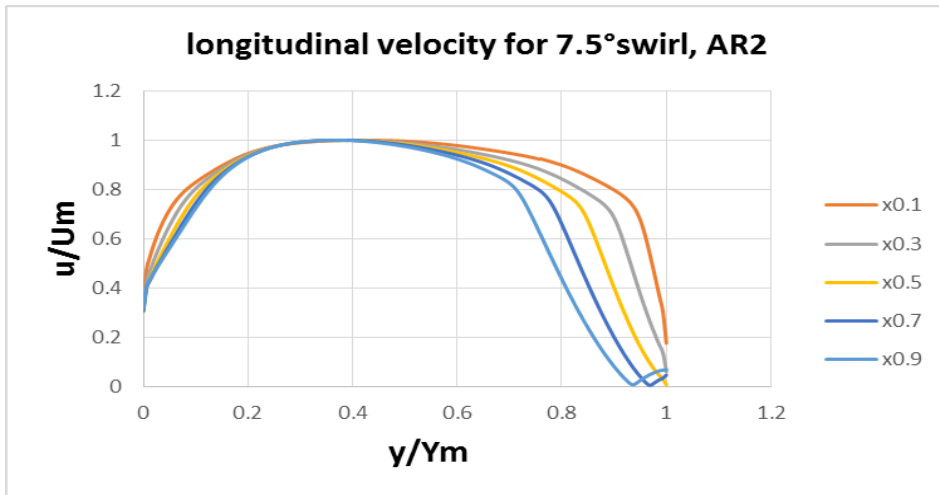


Fig.86 AR=2, Casing wall angle=8°, Velocity=60m/s (7.5°L)

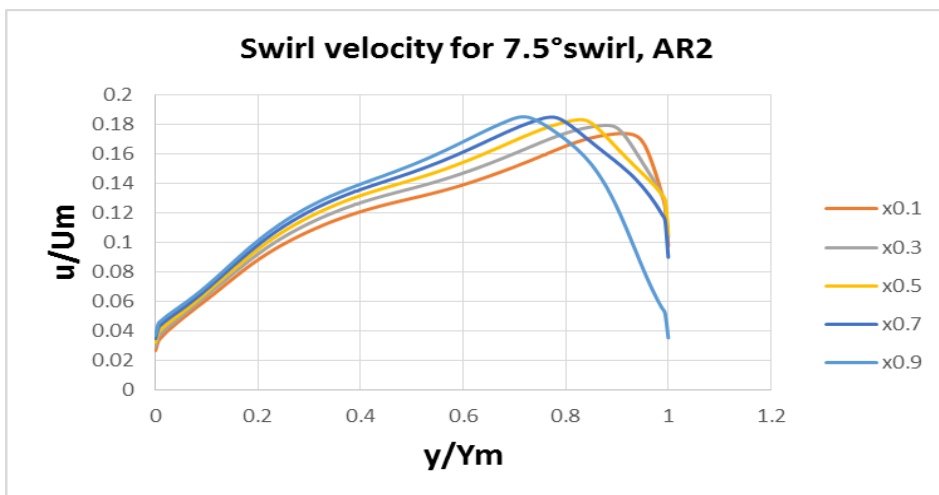


Fig.87 AR=2, Casing wall angle=8°, Velocity=60m/s (7.5°S)

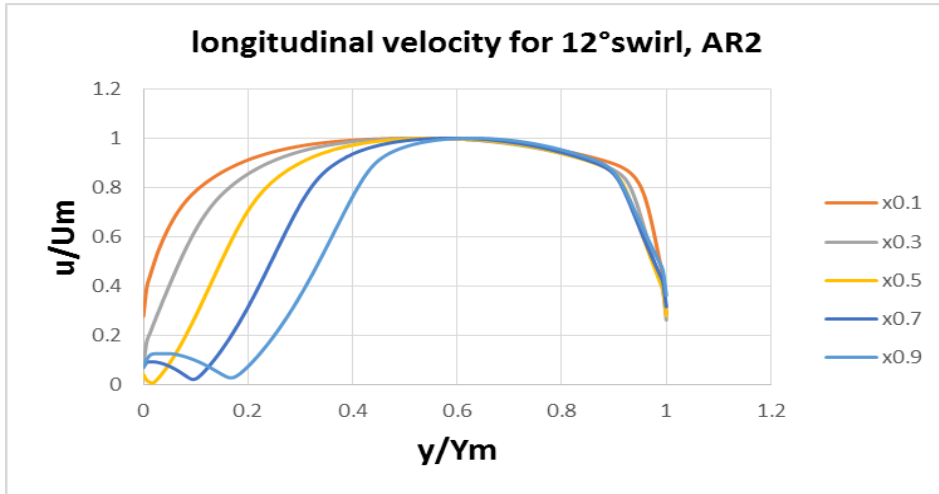


Fig.88 AR=2, Casing wall angle=8°, Velocity=60m/s (12°L)

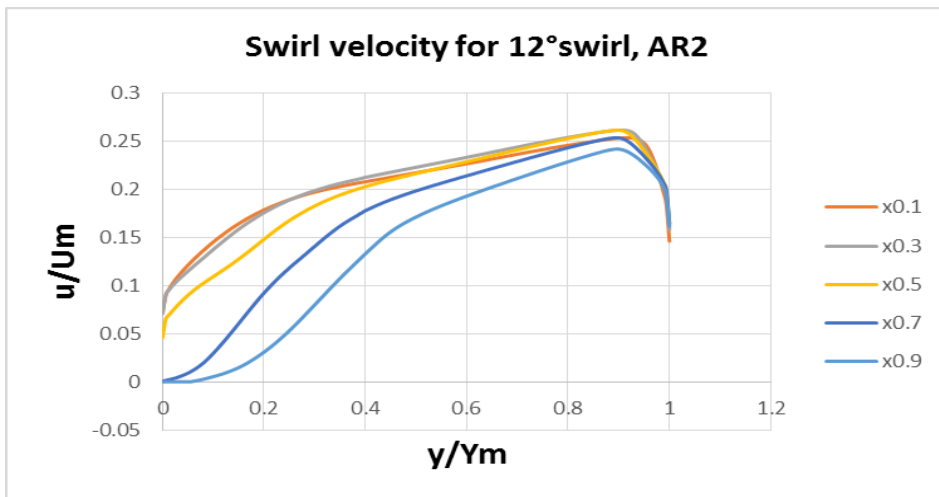


Fig.89 AR=2, Casing wall angle=8°, Velocity=60m/s (12°S)

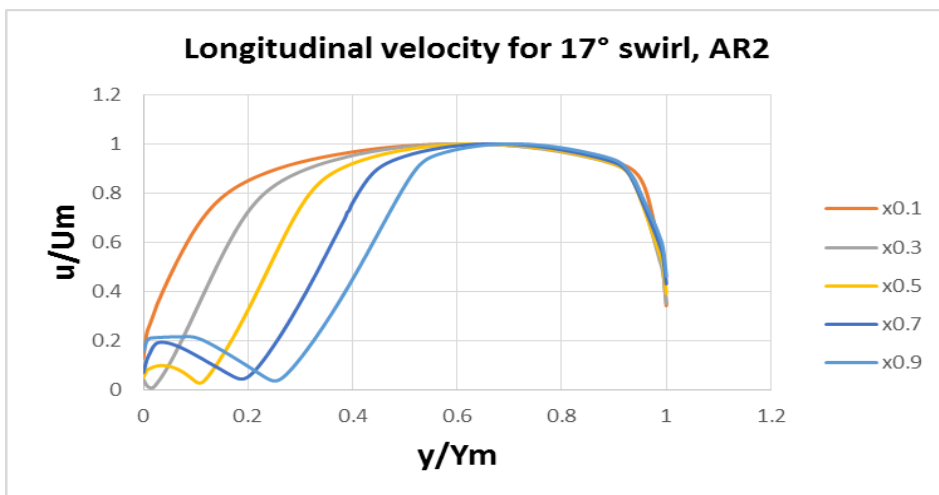


Fig.90 AR=2, Casing wall angle=8°, Velocity=60m/s (17°L)

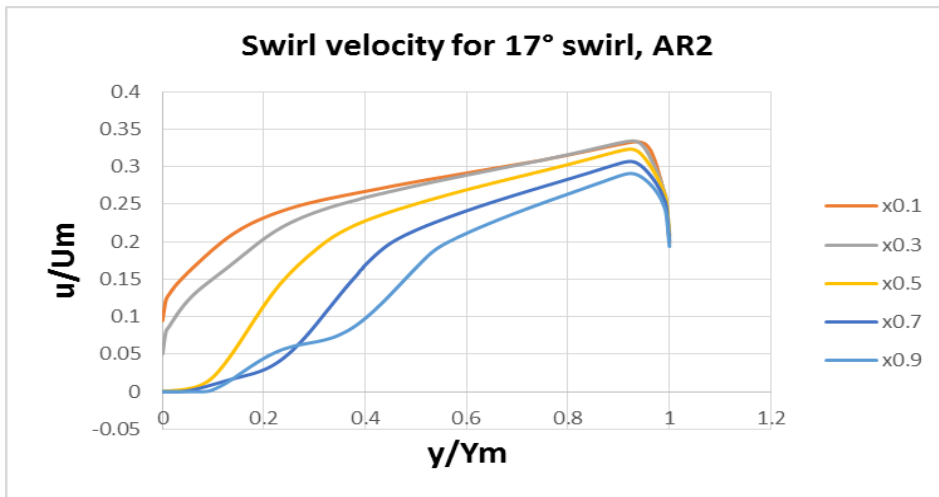


Fig.91 AR=2, Casing wall angle=8°, Velocity=60m/s (17°S)

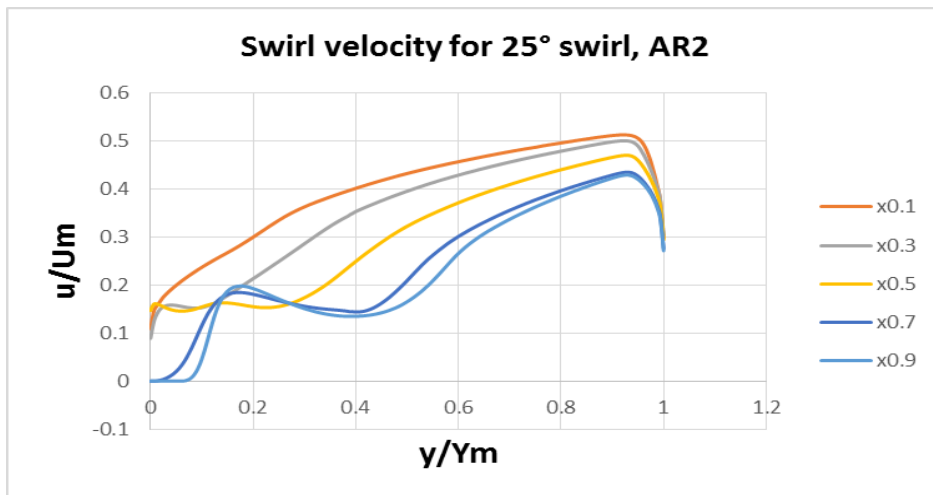


Fig.92 AR=2, Casing wall angle=8°, Velocity=60m/s (25°S)

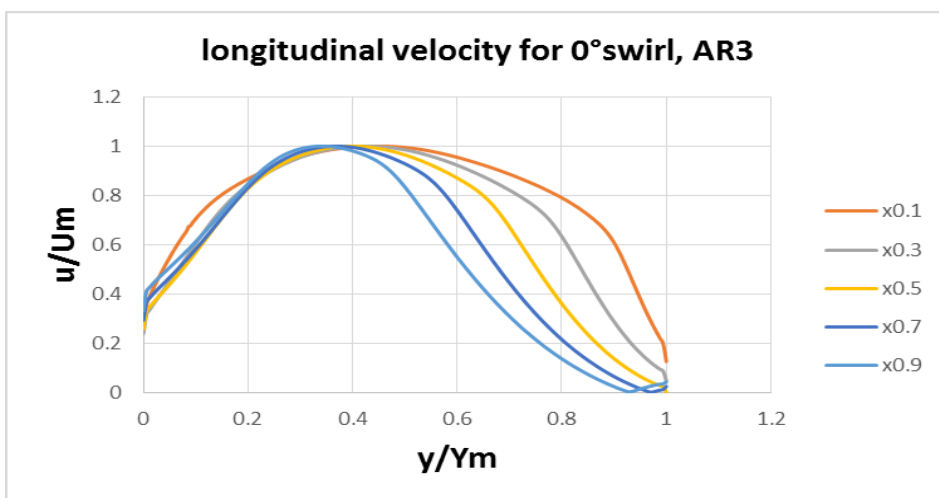


Fig.93 AR=3, Casing wall angle=8°, Velocity=60m/s (0°L)

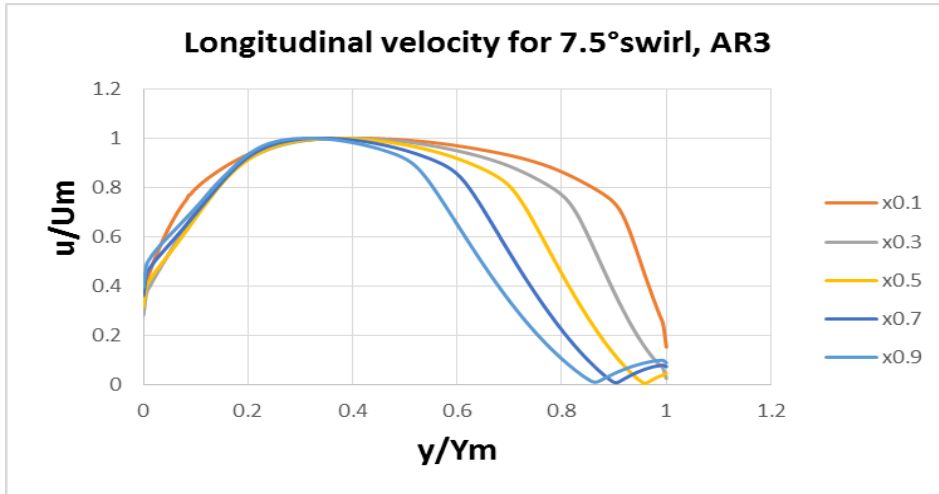


Fig.94 AR=3, Casing wall angle=8°, Velocity=60m/s (7.5°L)

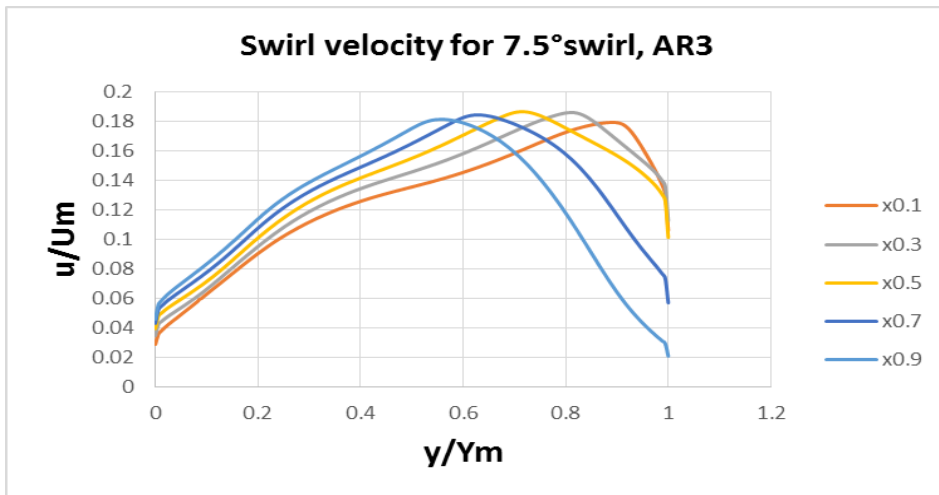


Fig.95 AR=3, Casing wall angle=8°, Velocity=60m/s (7.5°S)

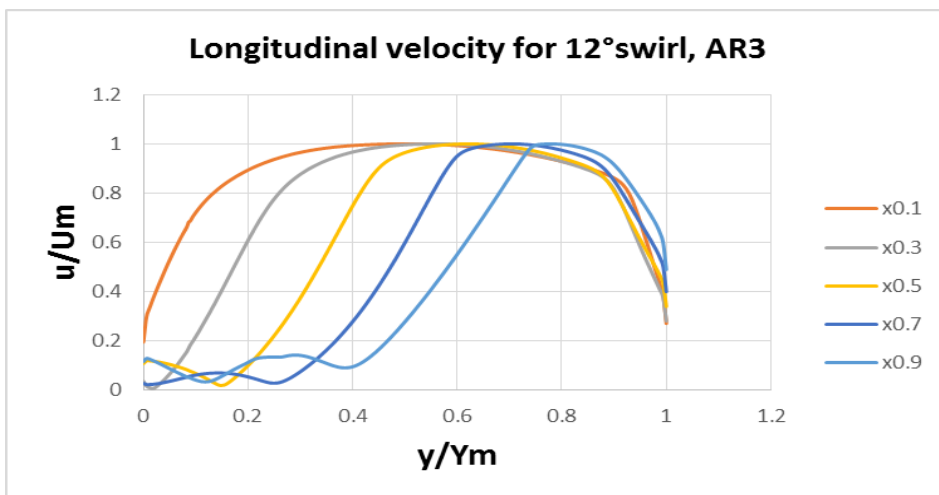


Fig.96 AR=3, Casing wall angle=8°, Velocity=60m/s (12°L)

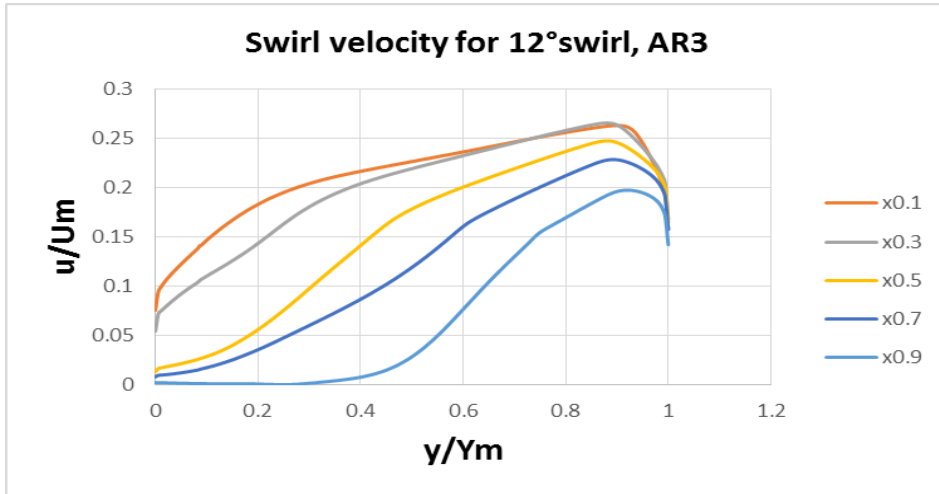


Fig.97 AR=3, Casing wall angle=8°, Velocity=60m/s (12°S)

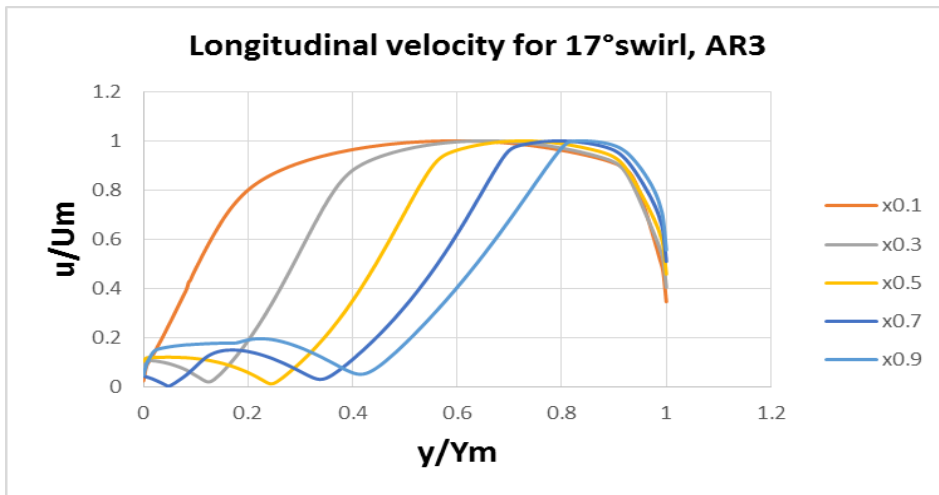


Fig.98 AR=3, Casing wall angle=8°, Velocity=60m/s (17°L)



Fig.99 AR=3, Casing wall angle=8°, Velocity=60m/s (17°S)

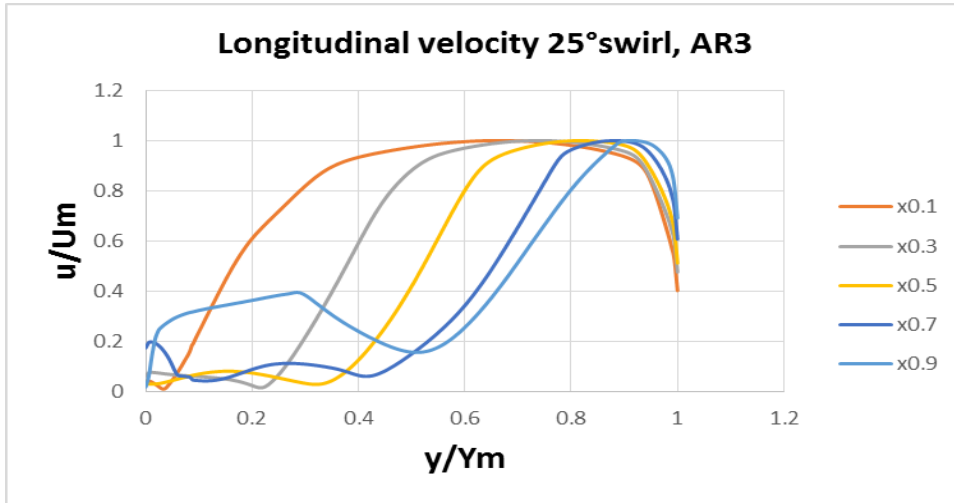


Fig.100 AR=3, Casing wall angle=8°, Velocity=60m/s (25°L)

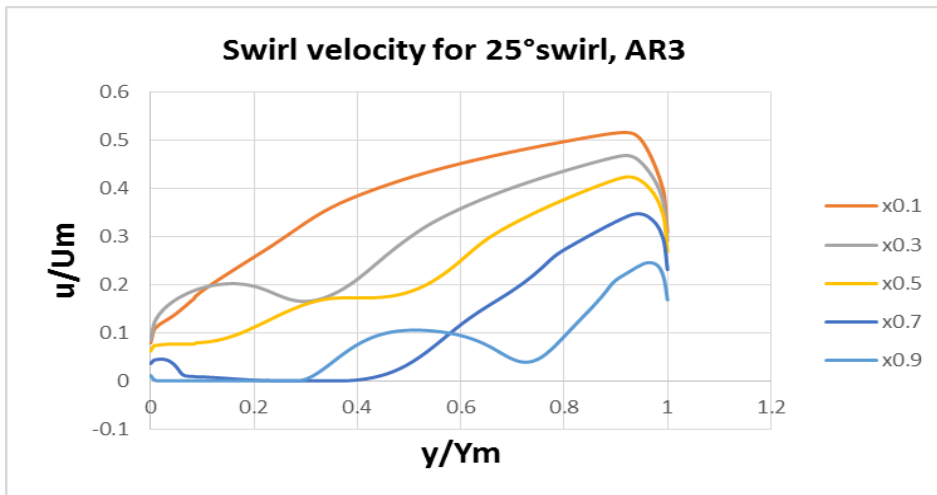


Fig.101 AR=3, Casing wall angle=8°, Velocity=60m/s (25°S)

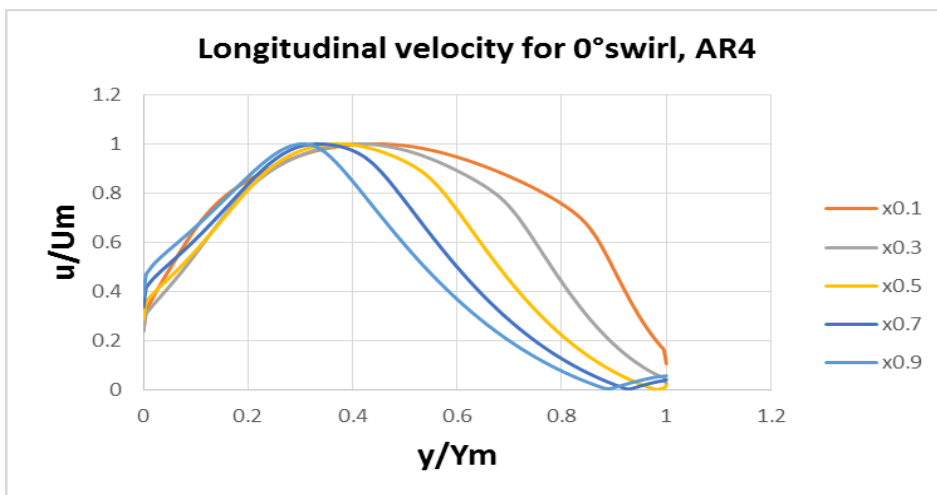


Fig.102 AR=4, Casing wall angle=8°, Velocity=60m/s (0°L)

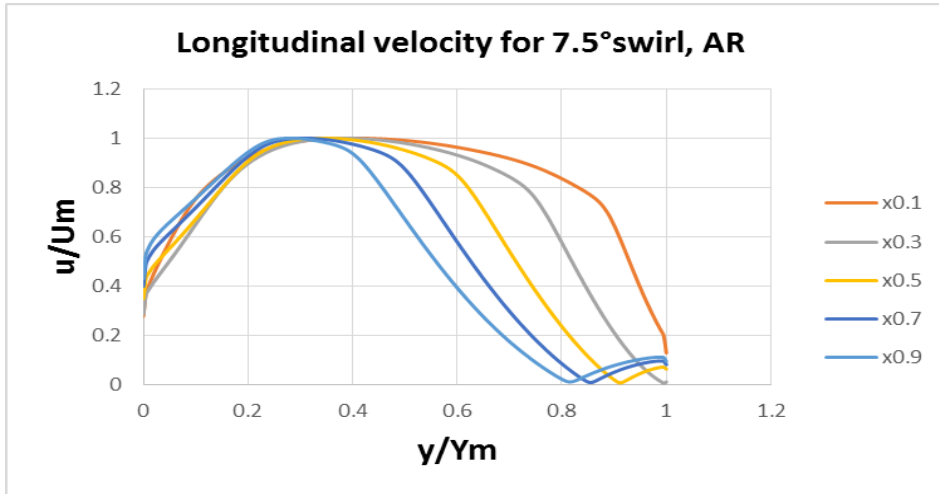


Fig.103 AR=4, Casing wall angle=8°, Velocity=60m/s (7.5°L)

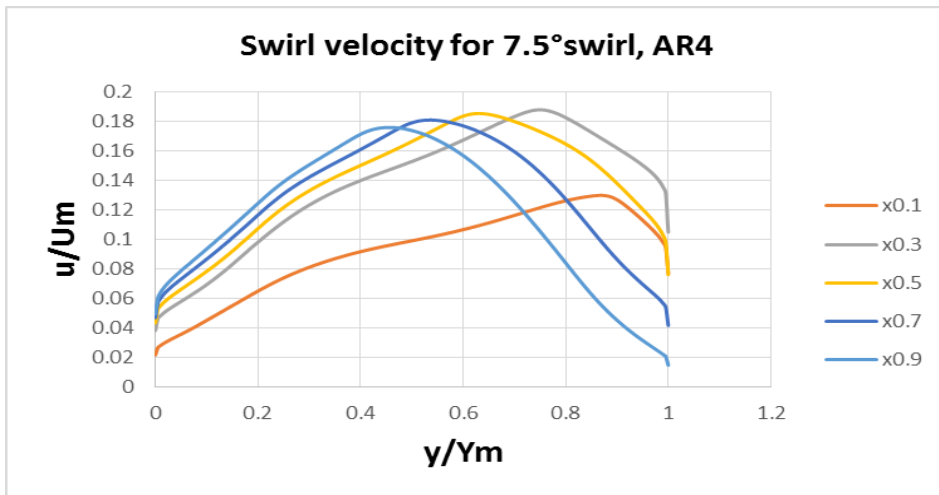


Fig.104 AR=4, Casing wall angle=8°, Velocity=60m/s (7.5°S)

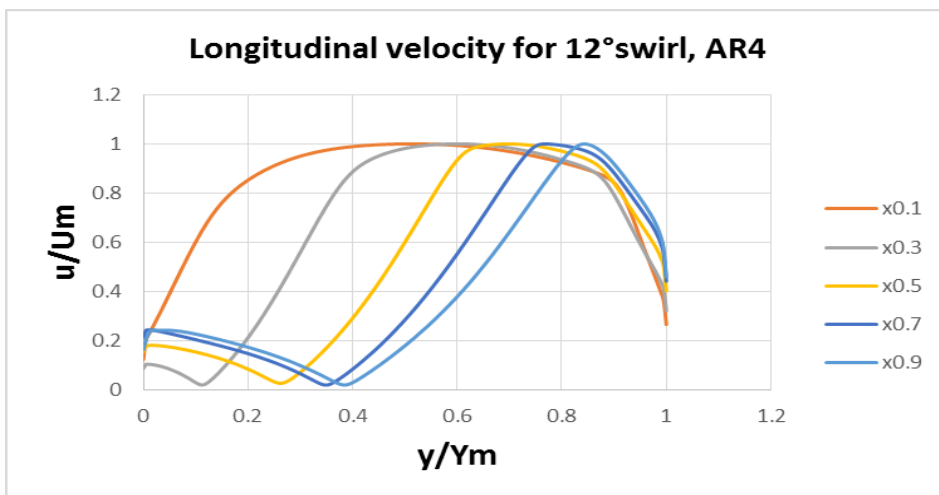


Fig.105 AR=4, Casing wall angle=8°, Velocity=60m/s (12°L)

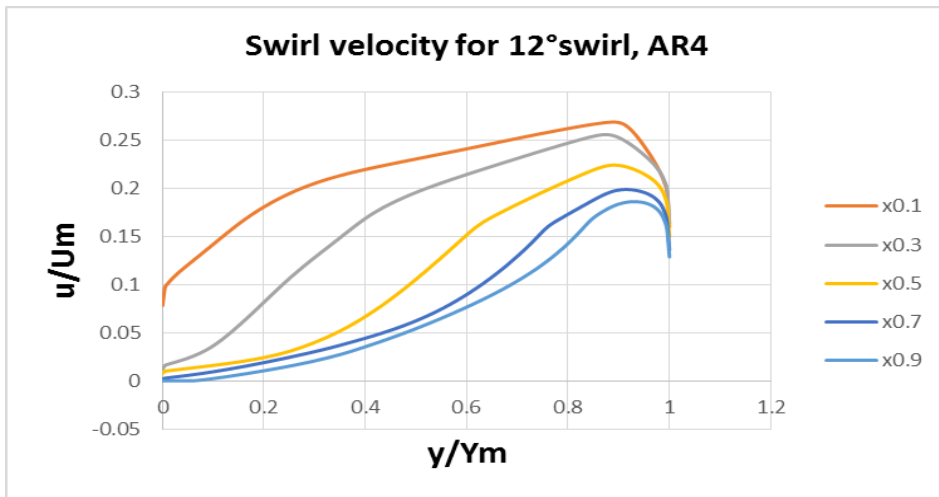


Fig.106 AR=4, Casing wall angle=8°, Velocity=60m/s (12°S)

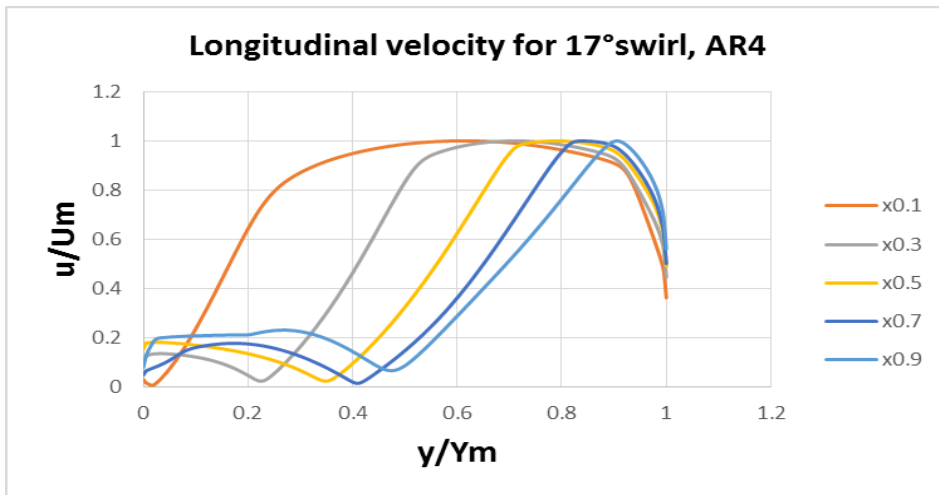


Fig.107 AR=4, Casing wall angle=8°, Velocity=60m/s (17°L)

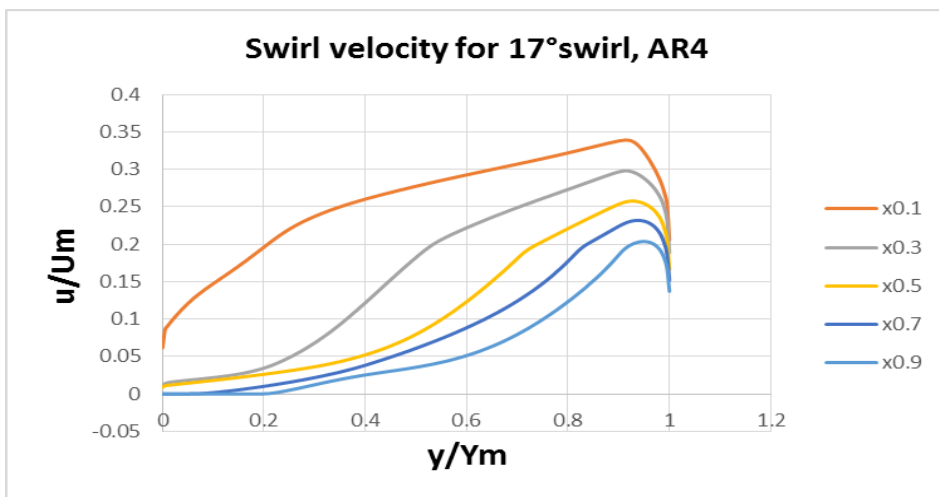


Fig.108 AR=4, Casing wall angle=8°, Velocity=60m/s (17°S)

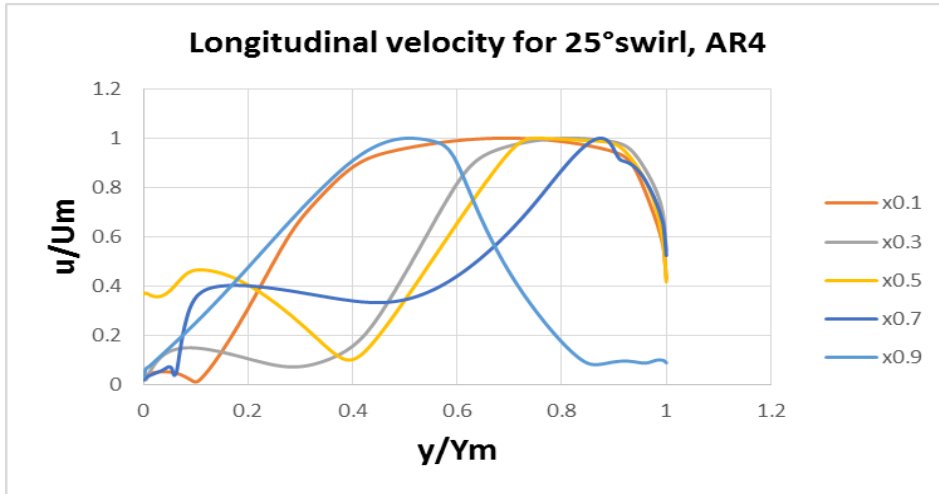


Fig.109 AR=4, Casing wall angle=8°, Velocity=60m/s (25°L)

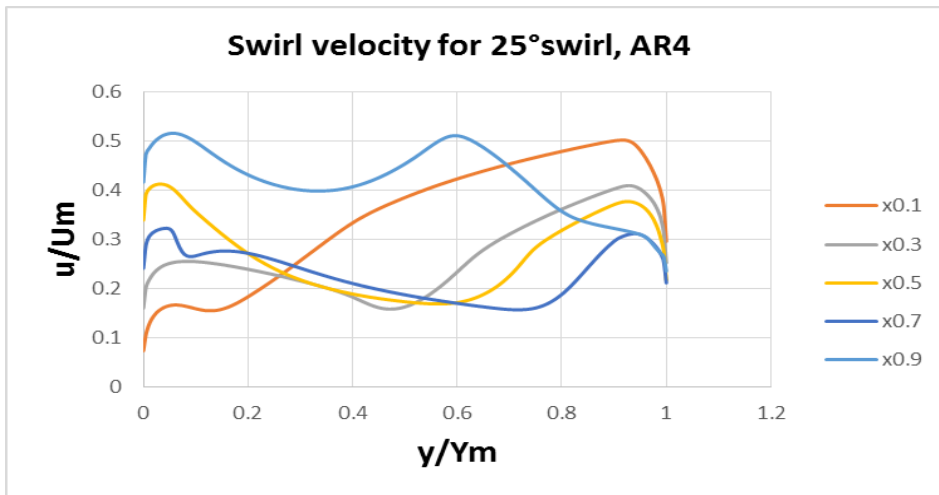


Fig.110 AR=4, Casing wall angle=8°, Velocity=60m/s (25°S)

Flow-Chart for CFD Modeling and Simulation

